PERFORMANCE EVALUATION OF ERBIUM DOPED FIBER AMPLIFIER (EDFA) FOR EFFICIENT DESIGN OF FIBER LASER

BY

MD. ZIAUL AMIN

A Thesis Presented to the

DEANSHIP OF GRADUATE STUDIES

KING FAHD UNIVERSITY OF PETROLEUM & MINERALS

DHAHRAN, SAUDI ARABIA

In Partial Fulfillment of the
Requirements for the Degree of

MASTER OF SCIENCE

In

ELECTRICAL ENGINEERING

SEPTEMBER, 2015

KING FAHD UNIVERSITY OF PETROLEUM & MINERALS

DHAHRAN- 31261, SAUDI ARABIA

DEANSHIP OF GRADUATE STUDIES

This thesis, written by **MD. ZIAUL AMIN** under the direction his thesis advisor and approved by his thesis committee, has been presented and accepted by the Dean of Graduate Studies, in partial fulfillment of the requirements for the degree of **MASTER OF SCIENCE IN ELECTRICAL ENGINEERING.**

K. Qureshi

Dr. Khurram Karim Qureshi
(Advisor)

Dr. Ali Ahmad Al- Shaikhi
Department Chairman

H. Masoudi 7/10/2015

Dr. Husain M. Masoudi
(Member)

Dr. Salam A. Zummo
Dean of Graduate Studies

Dr. Muhammad Baseer Haider
(Member)

7/10/15

Date

This thesis is dedicated to my parents

ACKNOWLEDGMENTS

First of all, I am grateful to Almighty Allah, the most Merciful, the most Gracious, for his guidance and protection throughout this study.

I would like to express my deepest gratitude to my thesis advisor, Dr. Khurram Karim Qureshi for his continuous support, encouragement, motivation, excellent guidance, and insightful suggestions. I would also like to thank my thesis committee members Dr. Husain M. Masoudi and Dr. Muhammad Baseer Haider for their excellent cooperation, and valuable suggestions. My sincere thanks also go to Dr. Ali Ahmad Al-Shaikhi, Chairman, Electrical Engineering Department, and all my Professors for their cordial support.

I am particularly indebted to King Fahd University of Petroleum and Minerals (KFUPM) for providing me the excellent research facilities. Moreover, I like to extend my appreciation to the Bangladeshi students and teacher's community for providing me the mental support and a homely environment throughout my study at KFUPM.

I am also indebted to Espinosa Jose and Irfan Ahmad for their cordial support in the laboratory work.

Finally, I would like to thank my parents, brother, sisters, and relatives for their love, prayers and support.

TABLE OF CONTENTS

LIST OF TABLES

LIST OF FIGURES

LIST OF ABBREVIATIONS

WDM : Wavelength Division Multiplexing

DWDM: Dense Wavelength Division Multiplexing

EDF: Erbium Doped Fiber

EDFA: Erbium Doped Fiber Amplifier

EDFAs: Erbium Doped Fiber Amplifiers

LASER: Light Amplification by Stimulated Emission of Radiation

EDFL: Erbium Doped Fiber Laser

EDFRL: Erbium Doped Fiber Ring Laser

PDL: Polarization Dependent Loss

PDG: Polarization Dependent Gain

SMF: Single Mode Fiber

HUC: Homogeneous Upconversion

IUC: Inhomogeneous Upconversion

PIQ: Pair-induced Quenching

NA: Numerical Aperture

CW: Continuous Wave

ESA: Excited State Absorption

KTP: Potassium Titanyl Phosphate

FFP: Fiber-Fabry Perot

ERMZI: Electro-optic Reflection Mach-Zehnder Interferometer

FSR: Free Spectral Range

WDC: Wavelength Dependent Coupler

FWHM: Full-Width at Half-Maximum

OSA: Optical Spectrum Analyzer

PPM: Parts Per Million

ACC: Automated Current Control

ASE: Amplified Spontaneous Emission

SOP: State of the Polarization

PC: Polarization Controller

GUI: Graphical User Interface]

ABSTRACT

Full Name : [MD. ZIAUL AMIN]

Thesis Title : [Performance Evaluation of Erbium Doped Fiber Amplifier (EDFA) for Efficient Design of Fiber Laser]

Major Field : [Electromagnetics]

Date of Degree : [September, 2015]

Fiber lasers have attracted considerable attention due to their potential applications in Wavelength Division Multiplexing (WDM) system, sensing, optical components testing and spectroscopy. In fact, fiber laser is a modified version of a fiber amplifier where a suitable feedback mechanism is applied to convert it into a fiber laser. Therefore, fiber amplifier performance analysis prior to designing fiber laser would be an efficient method. In this thesis, we have designed and simulated tunable erbium doped fiber ring laser (EDFRL) using OptiSystem (version 13) and VPIphotonicsComponetMaker (version 9.3). Before designing tunable erbium doped fiber ring laser, erbium doped fiber (EDF) performances have been analyzed in terms of doping radius, dopant ion concentrations, and ion-ion interaction. Then, detrimental ion-ion interaction effects are simulated by designing tunable erbium doped fiber ring laser. It is found that, ion-ion interaction process reduces the tunable range of erbium doped fiber ring laser. Also, erbium doped fiber performances have again been analyzed in terms of population inversion along the erbium doped fiber length using 1480 nm and 980 nm pumping wavelength with an aim to design a widely tunable erbium doped fiber ring laser. From the population inversion analysis, it was assumed that 1480 nm pumping wavelength and bidirectional pumping configuration would be suitable for wide band tunable erbium

doped fiber ring laser design. Following this, we have designed and simulated widely tunable erbium doped fiber ring laser based on active fiber length optimization with forward and bidirectional pumping configuration. Then, tuning range for the forward and bidirectional pumping configuration have been compared. Comparison results show that bidirectional pumping configuration provide the wider tuning range (1525-1645 nm) than the forward pumping case (1528-1620 nm). In addition, we have simulated the effects of intra-cavity loss, coupling ratio, and pumping power on the tuning range of erbium doped fiber ring laser. Finally, we have designed two experimental setups for erbium doped fiber ring laser using the existing lab equipment to investigate coupling ratio and intra-cavity loss effects on the tuning range]

ملخص الرسالة

الاسم الكامل: محمد ضياء الأمين

عنوان الرسالة : تقييم أداء ليف ليزري ممزوج بالإربيوم لتحقيق التصميم الأمثل لليف الليزري

التخصص: : الكهرومغناطيسية

تاريخ الدرجة العلمية : أيلول 2015

نظرا لتطبيقاتها المهمة في مجال تقسيم الأطوال الموجية والاستشعار و فحص الأجزاء البصرية و الطيفية فقد حظيت ألياف الليزر باهتمام بالغ من فرق البحوث المتنوعة. في الحقيقة يمكن النظر إلى الليف الليزري على أنه نسخة متطورة من المضخم الليفي غير أن الأول يحتوي على آلية تغذية راجعة مناسبة لتحويله إلى ما هو عليه. وبناء على ما تقدم، فإن دراسة سلوك المضخم الليفي يعد خطوة مناسبة قبل الشروع بتصميم الليف الليزري المرغوب.

في هذه الرسالة, قمنا بتصميم و محاكاة ليف ليزري حلقي قابل للمعايرة ممزوج بالإربيوم (EDFRL) باستخدام برنامج OptiSystem الاصدار 13 و برنامج VPIphotonicsComponetMaker الاصدار 9.3. لكن قبل هذا، فقد تمت دراسة أداء الليف المزوج بالاربيوم (EDF) بما يختص بقيمة نصف قطر المزج و تركيز أيون المزج و تفاعل الايونات مع بعضها البعض. و من ثم فقد تم عمل محاكاة رقمية لاثر هذه التفاعلات من خلال تصميم ليف ليزري حلقي قابل للمعايرة ممزوج بالإربيوم قابل للمعايرة. و قد وجد أن لهذه التفاعلات اثرا في تقليل مجال المعايرة الممكنة. اضافة الى ما قد سبق، فقد تم دراسة سلوك الليف المزوج بالاربيوم مجددا و لكن هذه المرة باعتبار معكوس الانتشار على طول الليف المزوج بالاربيوم باستخدام حزمتين ضوئيتين ضاغتتين بأطوال موجية مساوية ل 1480 nm و 980 nm بهدف تصميم ليف ليزري حلقي قابل للمعايرة ممزوج بالإربيوم قابل للمعايرة بشكل أكبر. من خلال تحليل أثر معكوس الانتشار، فقد تم التوصل الى ان استخدام حزمة ضوئية ضاغطة ثنائية الاتجاه و بطول موجي مساو ل. 1480 nm مناسب لتصميم ليف ليزري حلقي قابل للمعايرة ممزوج بالإربيوم قابل للمعايرة بشكل أكبر. تبعا لهذا، فقد قمنا أيضا بتصميم و محاكاة ليف ليزري حلقي قابل للمعايرة ممزوج بالإربيوم

قابل للمعايرة بشكل أكبر اعتمادا على طول الليف الانسب تحت تاثير الضخ الأحادي و الثنائي الاتجاه. و من ثم تم مقارنة مجال المعايرة الناتج عن كلا النوعين. و قد أثبتت المقارنة أن الضخ ثنائي الاتجاه يوفر مجالا أكبر للمعايرة و البالغ (1525-1645 nm) مقارنة بنظيره أحادي الاتجاه و الذي يبلغ المجال الناتج عنه (1528-1620 nm). بالاضافة الى ما سبق، فقد قمنا بمحاكاة أثر خسارة الفجوات الداخلية و نسبة الترابط و قوة الضخ و أثرها على مجال المعايرة الخاص ب. ليف ليزري حلقي قابل للمعايرة ممزوج بالإربيوم.

و ختاما، فقد قمنا ببناء منصتين للتجارب المتعلقة ب. ليف ليزري حلقي قابل للمعايرة ممزوج بالإربيوم اعتمادا على الادوات المتوفرة في المختبر و ذلك لاختبار أثر كل من خسارة الفجوات الداخلية و نسبة الترابط على مجال المعايرة.

درجة الماجستير في العلوم

جامعة الملك فهد للبترول و المعادن

الظهران, المملكة العربية السعودية

أيلول 2015

CHAPTER 1

INTRODUCTION

Rapidly increasing demand of telecommunication and internet services are acting as the major driving forces for widespread use of fiber optic technology. This technology has been developed from the vision of Kao, Hockham [1] and Werts [2]. Their vision was to transmit light through dielectric waveguides or optical fiber fabricated from silica glass. Initially, such systems were viewed as a replacement of coaxial cable or carrier transmission systems. However, it was impractical to replace low loss coaxial cable (i.e. 5 to 10 dB/km) by high loss (i.e. 1000 dB/km) optical fiber. Kao and his fellow workers realized that impurities in the fiber materials are responsible for the high fiber losses. The research works were going on to realize the practical fiber optic communication systems. In 1970, Kapron and his coworkers reported relatively low loss (20 dB/km) optical fiber [3]. Since then, optical fiber was considered as a practical transmission medium. Due to the continuous research efforts and products development, fiber optic communication is established today as one of the promising technologies for short and long haul data transmission. The progress of the fiber optic communication is divided into five generation [4],[5]. Each generation of fiber optic communication is described briefly in the following section:

Before the introduction of first generation optical fiber communication system some field trials had been done during the period 1977-1989. Following this, first generation optical

communication system was introduced commercially in 1980. This generation of optical communication system used multimode fiber as a transmission medium and GaAs semiconductor laser as an optical source, which was the only practical source available at that time. This generation lightwave system was operated near 0.8 μm wavelength region and it was capable of carrying data at the bit rate of 45-100 Mbps with repeater spacing up to 10 km [6].

Second generation fiber optic communication was developed early 1980 and operated in 1.3 μm wavelength region using InGaAsP semiconductor laser as the light source. The early system performance of this generation was limited by multimode fiber dispersion, and later on system performance was improved by using single mode fiber. Single mode fiber eliminated the intermodal fiber dispersion and improved the fiber loss performance by reducing internal Rayleigh scattering. By 1987, this generation was operated at the speed of 100 Mbps to 1.7 Gbps with repeater spacing up to 50 km.

Third generation optical fiber was operated at 1.55 μm wavelength region, which corresponds to the low loss (0.02 dB/km) window of the silica fiber. However, the chromatic dispersion of a standard single mode fiber is high for this wavelength region. Hence, to take the advantages of low loss window, a narrow linewidth laser is required to reduce the dispersion effects in this region. In another approach, a dispersion shifted fiber (DSF), whose chromatic dispersion is minimum at 1.55 μm wavelength region, is used to reduce the dispersion problem. This effect allows conventional laser with relatively large spectral width (i.e. several nm). This generation optical system can be operated at the speed of 10 Gbps with 100 km repeater spacing [7], [8].

In the fourth generation fiber optic communication system, optical amplifiers and wavelength division multiplexing (WDM) system are used to increase the repeater spacing and system capacity. These two improvements caused a revolution in doubling the data capacity in every six months starting from 1992 and reached 10 Tbps in 2001. In 2006, a bit rate of 14 Tbps was achieved using optical amplifier with repeater spacing up to 10,000 km [8].

The main goal of fifth generation fiber optic communication system is to increase data rate by using dense wavelength multiplexing (DWDM) and increasing wavelength range over which WDM system can operate. The other focus is to use solitons where the pulses maintain their shape by counteracting the negative effects of dispersion [7]. The progress of transmission capacity and their contributing technology is shown in Figure 1.1.

To satisfy the main goal of the fifth generation fiber optic communication, DWDM systems have been investigated to enlarge system capacity. However, the channel capacity in the DWDM systems is limited at C-band (1530-1565 nm) due to limited bandwidth available from the conventional erbium doped fiber amplifiers (EDFAs). Therefore, L-band (1570-1610 nm) erbium doped fiber amplifiers (EDFAs) have been investigated to enlarge the transmission bandwidth [10] [11], [12], [13].

At the same time, demand of widely tunable lasers covering (C+L) band is increased to test such wide band WDM devices. Another important application of these lasers is the inventory management of WDM system.

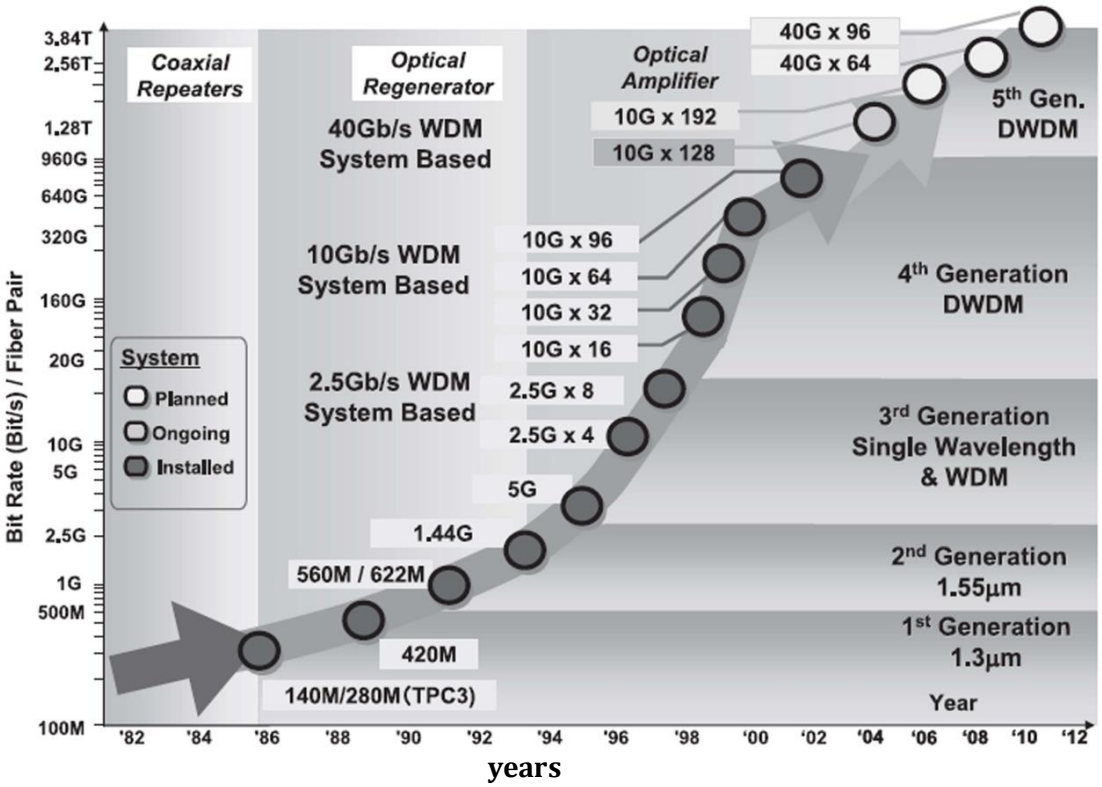

Figure 1.1: Progress of transmission capacity and applied technology [9].

Generally, a large number of lasers with different lasing wavelengths are used as a transmitter backup of the WDM systems. For the most secure WDM system a spare laser is kept for each channel wavelength. This is not a practical approach because of overwhelming cost and large inventory volume [14], [15]. Therefore, introduction of widely tunable laser can reduce the system cost and inventory substantially. These tunable light sources should provide wide tuning range, high output power, low coherent light to avoid interference, and unpolarized light to reduce polarization dependent loss (PDL) or gain (PDG). Though commercially available external cavity diode lasers can provide relatively wide tuning range (more than 200 nm) and high output power, however highly coherent and polarized light are the major limitations for the wideband WDM applications. On the other hand, erbium doped fiber laser can produce low

coherent light without any preferred polarization direction [16],[17]. Moreover, fiber laser has excellent fiber compatibility and produce low intensity noise (the details merits of fiber laser are given in section 1.1). In addition, tunable laser can be used in the sensing, optical metrology, biomedical light sources, and high resolution spectroscopy [18], [19], [20].

Considering the merits of fiber laser and low loss telecommunication window, we have focused our attention to design of tunable fiber laser using EDF. It is well known that fiber laser performances are greatly affected by the active gain media. Therefore, EDF performances have been evaluated before designing tunable EDFRL. Initially, EDF performances have been evaluated in terms of doping radius, dopant ion concentration, and ion-ion interaction by using OptiSystem (version 13) simulation tool. Following this, detrimental effects of ion-ion interaction effects on the tuning range of EDFRL are simulated by the same tool. Moreover, a widely tunable fiber laser is proposed based on the EDF length optimization and simulated using VPIphotonicsComponetMaker (version 9.3). Before that, we have evaluated the EDF performance in terms of population inversion by using different pumping configurations. It was predicted from the population inversion analysis that 1480 nm pumping wavelength with dual pumping configuration would provide the wider tuning range. With our predicted assumptions, we got 120 nm wide tuning range from our proposed EDFRL configuration. We also investigated the effects of coupling ratio, intra-cavity loss, and pump power on the tunability of EDFRL. Finally, we have designed two experimental setups with the existing lab equipment to observe the coupling ratio and intra-cavity loss effects on the tuning range.

1.1 Advantages of Fiber Laser

A fiber laser is a better option than the existing bulk and semiconductor diode laser because of its compatibility with the standard telecommunication fiber. Most of the advantages of the fiber lasers arise from the typical characteristics of single mode fiber (SMF) as compared with the bulk laser systems. The benefits of fiber laser in fiber optics technologies are briefly described in the following section [21], [22]:

Low Pump Power: As the gain media is large enough, the launched pump power will continue to propagate along the fiber until it is completely absorbed. For the fiber laser, pump intensity inside the fiber core is much higher as compared with bulk laser because of its smaller core size. If the fiber is chosen to be single transverse mode for both pump and signal wavelength, fiber structure provides good field overlap between the pump and signal lights, which is beneficial for achieving higher pumping efficiency. Therefore, lower pump power is required in the fiber laser systems than the bulk one.

Design Freedom: The lasing media length and pumping spot size are two important parameters in fiber laser design. The length of gain media can be selected depending on the doping ion concentrations for achieving the desired lasing efficiency. In addition, having decoupled the pumping intensity from the device length allows some weak absorption band to be used to excite lasing transitions.

High Output Power: The heat dissipating ability of fiber laser is more efficient than the bulk glass laser systems due to its large surface area to volume ratio. At the raised temperature, the fluorescence decreases in the bulk laser systems. However, it is rarely observed in the fiber laser systems [23]. As compared with the semiconductor laser, fiber

laser has high optical damage threshold [24]. Therefore high power laser, mode-locked and Q-switching, design using fiber gain media are more advantageous.

Wavelength Tunability: In case of fiber laser, wide tuning range can be achieved using tunable filter in the cavity. Tuning range more than 100 nm has been reported in the literature [25], [26]. On the other hand, it is difficult to get specific wavelength in the distributed feedback (DFB) diode laser due to substrate inconsistency and manufacturing tolerance.

Different Lasing Wavelength: Fiber lasers can offer different lasing wavelengths, which depend on the dopant rear earth ion in the core of the fiber. Fiber laser can produce wavelengths in 1.3 μm and 1.5 μm region, which are of great interest in the telecommunication industries. Moreover, it can produce lasing wavelengths in the important 2 and 3 micron spectral range. These spectral ranges have a considerable significance for the low loss mid-infrared communication systems.

Compact size: As the fiber can be bent and coiled to save space, the size of the fiber laser is smaller than the rod or gas laser of comparable power.

1.2 A Brief History of Fiber Laser

The field of fiber laser started in 1961, when E. Snitzer published his famous paper on laser oscillation in glass and then on the possibility of fiber laser operation [27], [28]. Few years later, Koester and Snitzer experimentally demonstrated an amplifier using the gain fiber. They also observed the laser oscillation in the same media [29]. This work was then followed by the other research groups to develop the fiber laser. In 1974, J. Stone

and C. A. Burrus developed Neodymium (Nd^{3+}) doped fiber laser, which was pumped by the diode laser [30]. However, that technique could not gain popularity among the researchers because the diode powers were low and their lifetimes were limited. Moreover, great success of other laser active media put a hold on fiber laser research in 1960s and 1970s. The fiber laser research again gained momentum in 1980s and 1990s due to the development of the reasonably powerful and reliable diode lasers and pump laser technology [31].

After the demonstration of a low threshold Neodymium (Nd^{3+}) based fiber laser at Southampton University by David. N. Payne and his co-authors, the rare earth doped fiber got significant attention as a lasing media. Since then, extensive research has been done for the further development of fiber laser technology using Nd^{3+} based fiber [32]–[35]. With the further advancement of diode pump laser technology and optical telecommunication system, researchers soon shifted their attention to the other rare earth doped (Erbium, Praseodymium, and Ytterbium) fiber as a gain medium. Among the fiber lasers, EDFL has drawn much attention due to its operating window and other potential applications. It can be operated in a broad operation range within 1550 nm window, which provides low attenuation for silica fiber.

1.3 Summary of Contribution

The main focus of this thesis is to design tunable fiber laser using erbium doped fiber (EDF). Before designing the tunable erbium doped fiber ring laser (EDFRL), erbium doped fiber performances have been evaluated to have some predictions of the design parameters. Therefore, this thesis is divided into two subsections: erbium doped fiber performance evaluation, and tunable erbium doped fiber ring laser design. In this thesis erbium doped fiber performances are presented in terms of doping radius, dopant ion concentration, and ion-ion interaction. Then detrimental effect of ion-ion interaction is evaluated by designing erbium doped fiber ring laser. Following this, erbium doped fiber performances have again been evaluated in terms of population inversion for designing widely tunable erbium doped fiber ring laser. The specific contributions of this thesis are given below:

- By analyzing pump signal absorption characteristics in the erbium doped fiber core and ion-ion interaction effects of erbium ion (Er^{3+}), we have shown that there is an optimal doping radius for which erbium doped fiber amplifier (EDFA) provides the best gain performances.

- We have simulated the effects of dopant ion concentration on the erbium doped fiber length determination. Following this, detrimental effects of ion-ion interaction on the erbium doped fiber amplifier gain performances are simulated.

- By analyzing the absorption characteristics of EDF, the detrimental effects of ion-ion interaction are also investigated in the tuning range analysis of erbium doped fiber ring laser.

- For designing widely tunable erbium doped fiber laser (EDFL), population inversion of the erbium doped fiber is analyzed to determine the pumping wavelength and configuration. It is found that bidirectional pumping configuration with 1480 nm pumping wavelength provides the wider tuning range for an optimized erbium doped fiber length.

- Then, tuning range variation due to coupling ratio, intra-cavity loss and pump power are investigated for the optimized erbium doped fiber length.

- Finally, tuning range variation due to coupling ratio and intra-cavity loss is investigated via experimental setups with the available lab equipment.

1.4 Organization of Thesis

This thesis is divided into two sections: EDF performance evaluation and tunable EDFL design. In first section of this thesis, EDF performances have been investigated in terms of doping radius, dopant ion concentrations, ion-ion interactions, pumping wavelength and, pumping configuration. The second section focuses on the design of tunable EDFRL. One tunable laser is designed for investigating the detrimental ion-ion interaction effects on the tuning range. Another tunable laser is designed based on length optimization and, pumping configuration for providing the wider tuning range.

To cover the above mentioned topics as precisely as possible, this thesis work is divided into five chapters. Introduction of thesis is presented in Chapter 1.

Chapter 2 describes the background theories relevant to this thesis. Firstly, we have started with the basic laser structure, light amplification mechanisms, and rate equations.

Following this, we have presented fiber resonator configurations, laser threshold and phase conditions. Then, we have described EDFL gain media characteristics. Later on doping radius and ion-ion interaction effects on the EDF performances are discussed.

First section of Chapter 3 presents the background literature review on EDF performance evaluation. Then background literature on tunable EDFL is presented in the last section of the Chapter 3.

In Chapter 4, we have presented different simulation models to investigate the EDF performances and tuning range of EDFRL. We also present experimental EDFRL configuration to investigate the tunability based on the available lab equipment.

Simulation and experimental results are presented and discussed in the initial part of Chapter 5. Finally, last section of Chapter 5 concludes this thesis.]

CHAPTER 2

BACKGROUND THEORY OF EDFL

The term "LASER" originated as an acronym for "Light Amplification by Stimulated Emission of Radiation". The laser makes use of the processes that increase or amplify light signals after those signals have been generated by the other means. The following three basic elements are required for the laser action [5], [36], [37]:

a. Gain or laser medium
b. Pumping system
c. Optical cavity or resonator

The gain medium is used to amplify the electromagnetic radiation. Resonator cavity is partly or completely filled with the gain medium for lasing operation.

Pumping system is used to supply the energy in the active medium to achieve population inversion condition, as explained in section 2.1. Different pumping mechanisms such as optical pumping with another laser or a lamp, pumping with a gas discharge, pumping with current through semiconductor, and chemical pumping are available in laser system.

Optical cavity or resonator is formed by arranging mirror or other reflective devices to circulate the light back and forth for the continued growth of optical beam. The combination of gain and feedback form an oscillator, which is conceptually quite similar to an electrical oscillator with a very high frequency. The most fundamental difference between the electrical and optical oscillators is the amplification process.

In the laser system, optical amplification occurs by stimulated emission, which was first proposed by Albert Einstein in 1917. The basic idea of stimulated emission can be understood by considering the light interaction with an atom.

Figure 2.1 illustrates a two energy state atomic system where an atom is in initially in the lower energy state. When a photon of right energy is incident on the atom, it may be excited to the higher energy state absorbing the incident photon. This process sometimes referred to as stimulated absorption. On the other hand, when the atom initially in the excited state it can decay back to lower energy state emitting a photon. The emission process can occur in two ways:

a. By spontaneous emission in which the excited atom decays back to the ground state in an entirely random manner.
b. By stimulated emission when a photon having energy equal to band gap energy of the two states interacts with the excited state atom causing it return to the lower energy state with creation of a second photon. The second photon is virtually identical to the photon which was incident on the atom.

In its simplest form, a laser consists of amplifying medium (where stimulated emission occurs), and a set of mirrors to feed the light into the amplifier for the continued growth of developing beam [31]. Therefore, practical realization of the laser is as an optical oscillator. The operation of the device can be described by the formation of an electromagnetic standing wave within a cavity which provides an output of monochromatic, highly coherent radiation. The basic laser structure is shown in Figure 2.2.

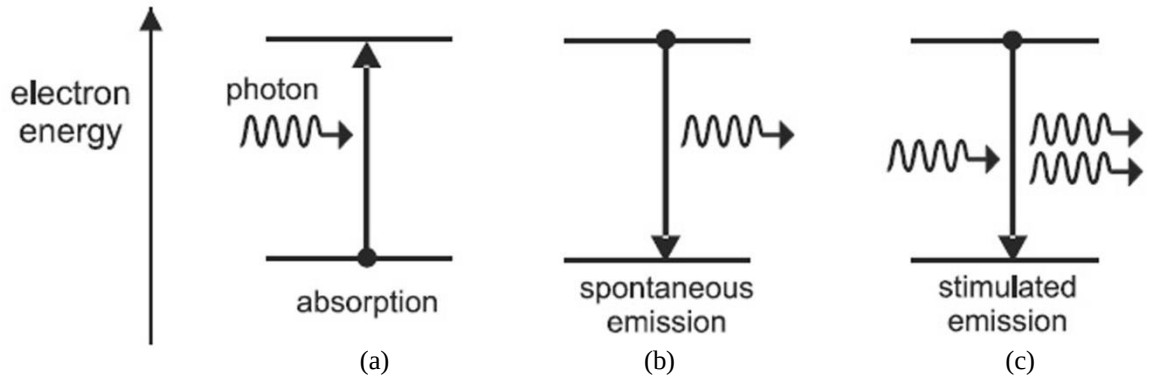

Figure 2.1: Energy state diagram showing: (a) absorption; (b) spontaneous emission; (c) stimulated emission.

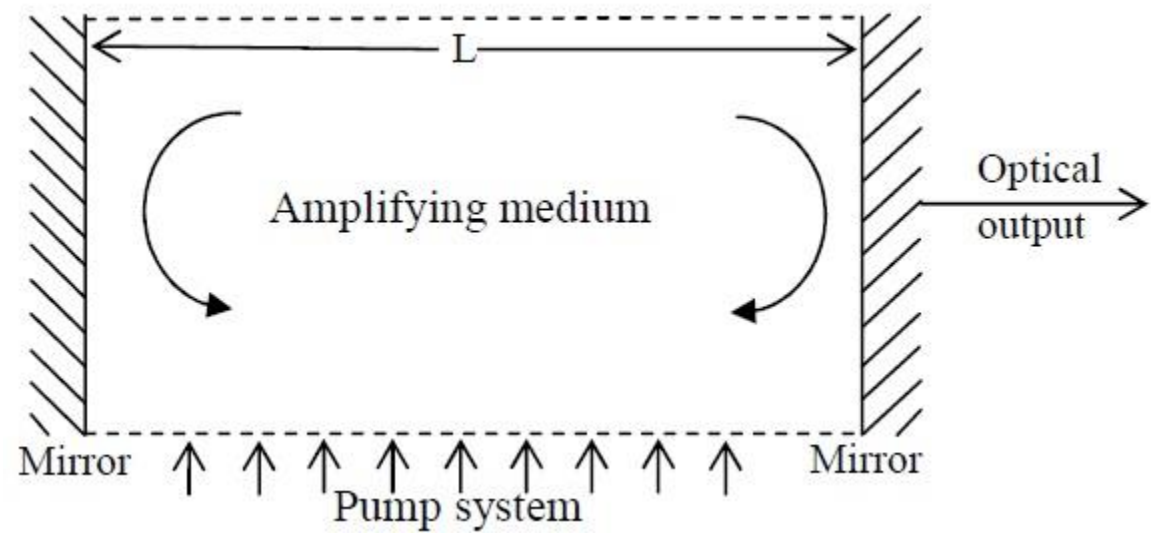

Figure 2.2: The basic laser structure [5].

A fiber laser is a variant of laser in which optical fiber doped with rare-earth elements (erbium, ytterbium, neodymium, dysprosium, praseodymium, and thulium) act as the gain medium. Fiber lasers are usually optically pumped, most commonly with laser diodes but in a few cases with the other fiber laser [38]. Pumping diode can be single one, an array, or many separate single diodes, each with a fiber pigtail to couple the pump energy in the doped fiber core via coupler. If pump energy is sufficiently high, population

inversion between two lasing level can be achieved, thus optical signal amplification can be provided from the lasing media. With suitable feedback mechanism, it is possible to obtain lasing oscillation leading to fiber laser. Two basic fiber laser resonators – linear Fabry Perot and ring configurations are shown in Figure 2.4, and Figure 2.5.

2.1 Population Inversion

Population inversion is a condition of a matter in which more electrons are in higher energy state than in a lower energy state. This mechanism plays an important role in laser physics because it provides a means of electromagnetic waves amplification and oscillation. The phenomenon of population inversion can be understood by knowing the basic statistics of the particles' distribution at thermal equilibrium. In the thermal equilibrium, the number of particles at two neighboring non-degenerated energy levels follows the Boltzmann distribution [31]:

$$N_2 = N_1 \exp\left(-\frac{E_2 - E_1}{k_B T}\right) = N_1 \exp\left(-\frac{h.v_0}{k_B T}\right) \tag{2.1}$$

Where $E_2 > E_1$ and v_0 is the resonant frequency of the transition between these two energy levels. Particles can either occupy the level 1 with population N_1 or level 2 with population N_2. Therefore, the total number of particle is:

$$N = N_1 + N_2 \tag{2.2}$$

In thermal equilibrium, higher energy level is less populated than the lower energy level. Therefore, the atomic system does not emit light and naturally relaxed. Though the number of electrons at higher energy level increases with the increasing temperature but never exceeds population of the lower level. According to the Boltzmann distribution as

given by (2.1), populations of both levels can be equal at infinite temperatures. However, to obtain the optical gain through the stimulated emission, non-equilibrium situation need to be achieved when the number of particles at higher level is greater than that at lower level. This non-equilibrium situation is required for optical amplification.

If the proper radiation frequency is interacted with the matter, the population of the different energy levels will vary. In the following section the laser rate equations will be described, which determine the rate at which the population of different energy levels change under the action of pump energy and in the presence of laser radiation.

2.2 Laser Rate Equations

2.2.1 The Two Level System

The two level system is shown in Figure 2.3, where E_1 and E_2 represents lower and higher energy states. The number of atoms per unit volume in lower and higher energy state can be given by N_1 and N_2, respectively. In the presence of radiation, an atom can be excited to the higher energy state E_2 at $\omega = \frac{E_2 - E_1}{h}$ frequency. This absorption rate is proportional to the number of atoms present in lower energy state E_1 and the energy density of the radiation at frequency, 'ω'.

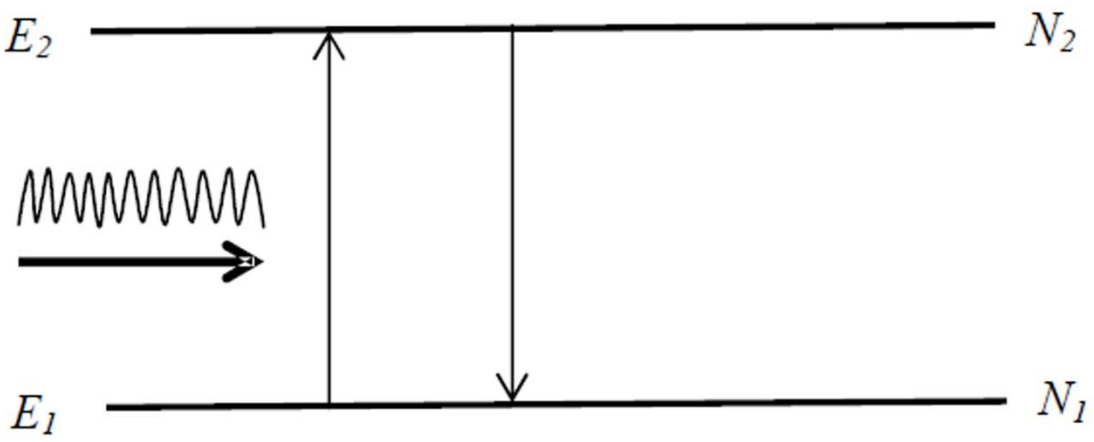

Figure 2.3: Two level system [39]

Let radiation with energy density u is incident on the system at frequency, 'ω'. By absorbing the radiation, atoms will be excited to the upper energy state [39]. The number of atoms excited to the upper state per unit volume can be given by:

$$\Gamma_{12} = \frac{\pi^2 c^3}{h\omega^3 t_{sp} {n_0}^3} u g(\omega) N_1 = W_{12} N_1 \tag{2.3}$$

Where

$$W_{12} = \frac{\pi^2 c^3}{h\omega^3 t_{sp} {n_0}^3} u g(\omega) \tag{2.4}$$

Where,

c, u , $g(\omega)$, t_{sp}, and n_0 represent velocity of light in the vacuum, energy density, line shape function, spontaneous life time, and refractive index of the medium respectively.

The stimulated emission per unit volume per unit time from level E_2 to E_1 is given by:

$$\Gamma_{21} = W_{21} N_2 = W_{12} N_2 \tag{2.5}$$

Here, absorption probability and stimulated emission probability is considered as the same. In addition to the above two transitions, some atoms will also go the lower energy

state by spontaneous emission. The number of atoms per unit time per unit volume will go to the lower energy state by spontaneous emission is given by:

$$T_{21}N_2 \tag{2.6}$$

Where

$$T_{21} = A_{21} + S_{21} \tag{2.7}$$

Here, A_{21} and S_{21} represents radiative and non-radiative transitions. The rate change of population of higher and lower energy levels can be written as:

$$\frac{\mathrm{dN_2}}{\mathrm{dt}} = \mathrm{W_{12}(N_1 - N_2) - T_{21}N_2} \tag{2.8}$$

$$\frac{dN_1}{dt} = -W_{12}(N_1 - N_2) + T_{21}N_2 \tag{2.9}$$

At steady state,

$$\frac{dN_1}{dt} = \frac{dN_2}{dt} = 0 \tag{2.10}$$

This gives

$$\frac{N_2}{N_1} = \frac{W_{12}}{W_{12} + T_{21}} \tag{2.11}$$

Since, both W_{12} and T_{21} are positive quantities, the above equation indicates that two level systems cannot provide population inversion by optical pumping.

2.2.2 The Three Level System

In three level laser system, as shown in Figure 2.7, lower energy atoms are elevated to the higher energy state 3 by using pumping energy. After reaching the excited state, the atoms must release some of its energy and drop to the desired lasing level [4], [31], [39] by non-radiative transitions. In three level system, level 2 (metastable level) and 1 (ground level) are referred to as upper and terminating laser level, respectively. In

metastable state (level 2), atoms stay longer time as compared to highest energy state (level 3). Therefore, atoms are accumulating in the upper lasing level. The laser terminating level is the ground level, which is always populated. Therefore, creating population inversion between the lasing levels is very strict in three level systems. More than half of the particles need to be excited to the upper laser level to create population inversion. To meet this condition much higher excitation energy is required. Moreover, special care needs to be taken so that reabsorption of amplified light can be eliminated. All this conditions increase the laser threshold and complicate the achievements of higher laser efficiency.

2.3 Fundamental Fiber Laser Resonators

The physics that is used for the fiber laser resonators is similar to the traditional laser resonators as explained in the first section of the chapter two. The main differences of fiber laser resonators from the traditional laser resonators are the intra-cavity optical components and gain medium geometry. Intra-cavity optical components of this resonator are related to the tolerance for optical damages and fiber coupling. An optical waveguide, which is significantly longer as compared to the traditional lasers, with small core diameter is used as a gain medium. There are two fundamental fiber laser resonator configurations are available [31],[40],[41]:

a. Standing wave Fabry-Perot resonator configuration
b. Travelling wave ring resonator configuration

2.3.1 Standing Wave Fabry-Perot Resonator Configuration

Standing wave Fabry-Perot resonator, as depicted in Figure 2.4, consists of two reflectors (usually mirror or fiber Bragg gratings or all fiber reflectors) set at the opposite ends of the optical cavity, gain medium (doped fiber), and other intra-cavity laser components to control temporal and spectral properties of the fiber laser. In this configuration, resonator modes are formed by the superposition of the two electromagnetic waves travelling in the opposite direction forming standing wave between the cavity reflectors. This standing wave nature is advantageous to the multi-wavelength lasing operation. However, the cavity gain and loss are counted twice because the electromagnetic waves travel twice during the each round trip with this configuration.

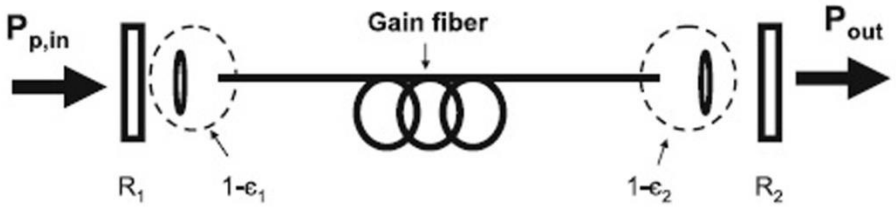

Figure 2.4: Standing wave Fabry-Perot resonator configuration [31].

Resonant frequencies of this resonator can be given by the following equation:

$$v = m\left(\frac{c}{2 \times n_0 \times L}\right) \tag{2.12}$$

Where,

m is an integer number

c is the velocity of light in vacuum

n_0 is the refractive index of the medium where the light is propagating

L is the cavity length

From (2.12), the frequency difference between two consequtive modes can be written by the following relation:

$$\Delta v = \frac{c}{2 \times n_0 \times L} \tag{2.13}$$

2.3.2 Travelling Wave Ring Type

The ring resonator, as shown in Figure 2.5, is another important type of fiber laser resonator, in which light travels along the ring configuration. This resonator can support counter propagating waves. However, it uses unidirectional propagation of light inside the laser cavity. Optical isolator is usually used for ensuring the unidirectional operation. In this configuration, the concept of cavity resonance frequency and cavity mode are not defined by the same wave as defined in standing wave Fabry-Perot configuration. Therefore, the resonator became travelling wave type. Here, gain and loss are counted once in each round trip time. This configuration is advantageous for single longitudinal and very narrow mode laser operation.

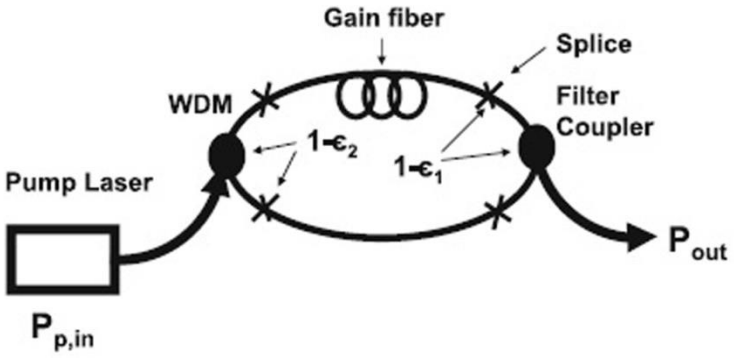

Figure 2.5: Travelling wave ring resonator [31].

To achieve the total phase shift of 2π in each round trip, the expression of resonant frequency can be written as:

$$\Delta v = m\frac{c}{n_0 \times L_{ring}} \tag{2.14}$$

Where, L_{ring} is the length of the close loop path.

2.4 Threshold Conditions for Laser Operation

Population inversion between the energy levels providing lasing transitions is a necessary condition to establish oscillation. However, this is not the sufficient condition for laser oscillations. In addition to the population inversion condition, a threshold gain within the gain medium must be attained to initiate laser oscillations. This threshold condition, when the gain of the amplifying media exactly balances the total losses, must be maintained for sustaining the laser operation [5].

For travelling wave ring resonator, the threshold value γ_{th} for the laser oscillation can be given by the following equation [40]:

$$\gamma_{th} = -\frac{\ln(R(1-L))}{l} \tag{2.15}$$

Where, R represents the effective fractional power reflectivity of the coupler.

L is the total lumped fractional intensity loss per round trip.

l is the total round trip distance, which is equal to total ring circumference.

The threshold condition for Fabry-Perot resonator configuration is given by the following equation:

$$\gamma_{th} = -\frac{\ln(R(1-L))}{2l} \tag{2.16}$$

Where, R is the fractional power reflectivity of the output mirror.

$2l$ is the round trip distance.

l is the distance between the mirrors, as shown in Figure 2.4.

2.5 Phase Conditions for Laser Operation

To satisfy the phase conditions for the laser operation, an integer number of resonating wavelengths must fit within one round trip of the laser's resonator cavity [40], [42]. The conceptual view of resonating modes that satisfy the phase conditions is depicted in Figure 2.6.

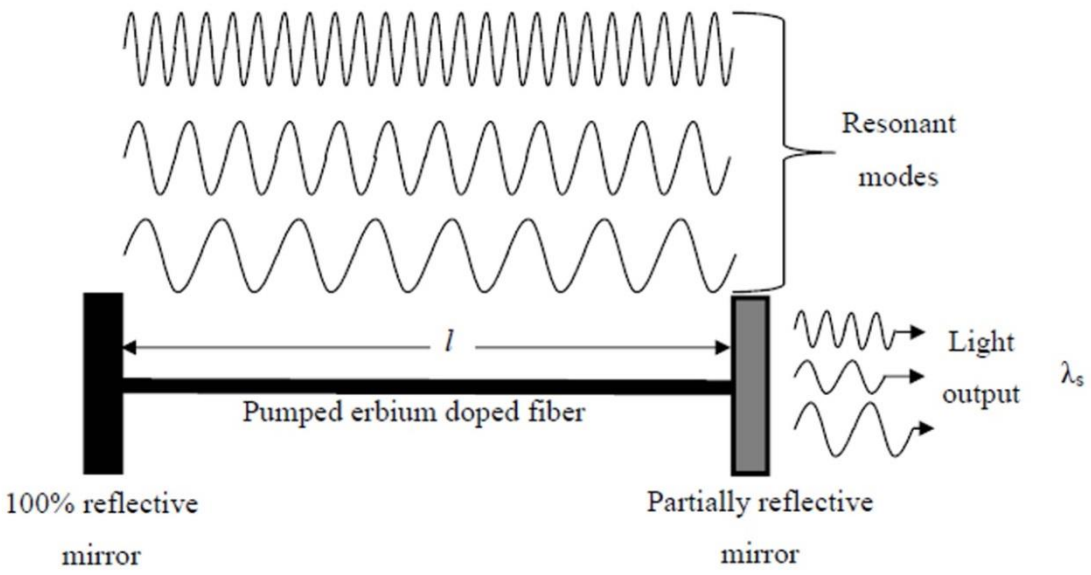

Figure 2.6: Conceptual view of the resonating modes that satisfy phase conditions in a Fabry-Perot resonator configuration [40].

Since the resonator length is very large as compared to the resonating wavelengths, there are many wavelengths which could satisfy the required phase conditions. The wavelengths which can satisfy the phase condition are commonly known as longitudinal

modes. For multimode Fabry-Perot laser, the frequency separation between two consecutive moods can be given by the following equation [43]:

$$df = \frac{\mathrm{c}}{2n_0 l} \tag{2.17}$$

Where,

c is the velocity of light in the vacuum.

n_0 represents refractive index of the fiber core.

l is the resonator cavity length as shown in Figure 2.6.

For the ring laser configuration, the frequency separation between the longitudinal modes is given by:

$$df = \frac{\mathrm{c}}{n_0 l} \tag{2.18}$$

Where, l represents total ring circumference.

2.6 EDFL Gain Medium

In EDFL, gain media is made by doping erbium ion (Er^{3+}) in the fiber core, where Er^{3+} acts as three level system, as shown in Figure 2.7. This simple model is capable of providing most important characteristics of the EDF, where excited state absorption is ignored, and it is assumed that transitions take place only between these three levels. In the case of EDF, the light is confined in the core of the fiber, which is very small. Therefore, very high light intensity can be obtained in the fiber core with relatively small pump powers. For the simplicity, it is assumed that the pump, signal intensities and erbium ion distributions are constant in the transverse direction over the effective cross-sectional area of the fiber.

Let N represents the total number of atoms per unit volume in the three level systems, and then it can be written as:

$$N = N_1 + N_2 + N_3 \tag{2.19}$$

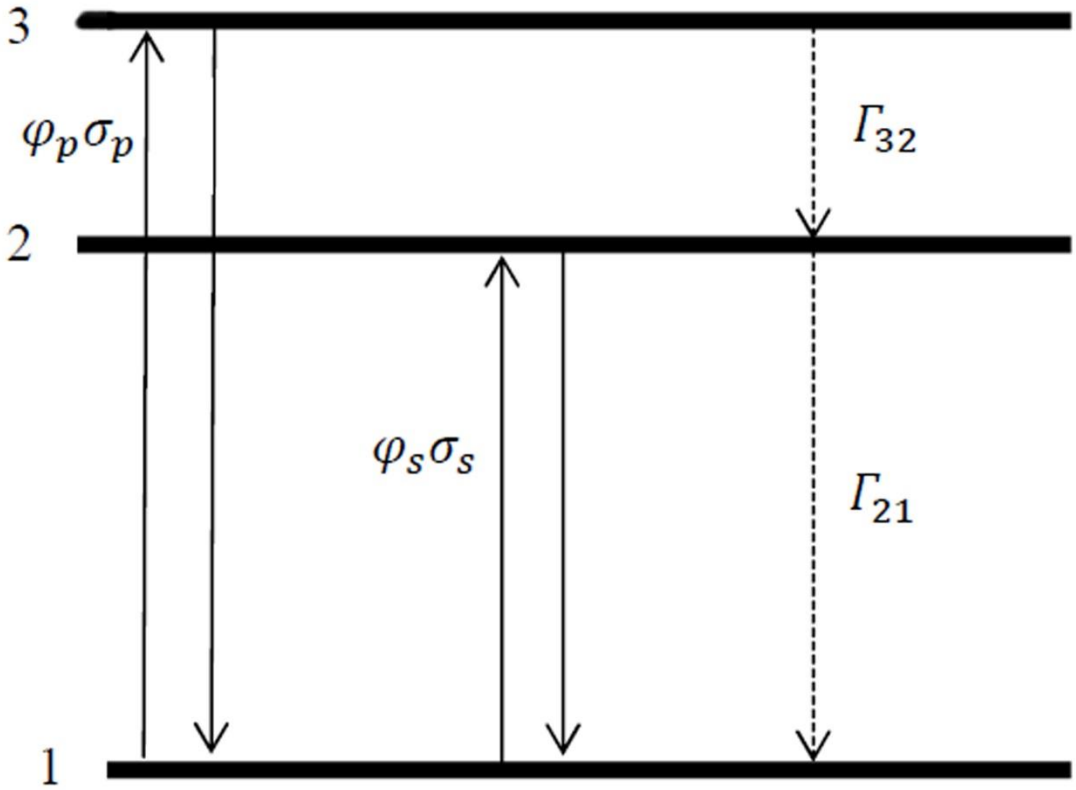

Figure 2.7 Three level system [44].

Now, the rate change of $\boldsymbol{N_3}$ can be expressed as [44]:

$$\frac{dN_3}{dt} = -\Gamma_{32}N_3 + (N_1 - N_3)\varphi_p\sigma_p \tag{2.20}$$

Where Γ_{32}, φ_p, and σ_p denote the transition probability between level 3 to 2, pump flux, and pump cross section respectively. Γ_{32} is the sum of radiative and non-radiative transition probability. Similarly, the following equations can be written for the rate change of N_2 and N_1:

$$\frac{dN_2}{dt} = -\Gamma_{21}N_2 + \Gamma_{32}N_3 - (N_2 - N_1)\varphi_s\sigma_s \tag{2.21}$$

$$\frac{dN_1}{dt} = \Gamma_{21}N_2 - (N_1 - N_3)\varphi_p\sigma_p + (N_2 - N_1)\varphi_s\sigma_s \tag{2.22}$$

Where Γ_{21}, φ_s and σ_s represent transition probability between the level 2 to level 1, signal flux, and signal cross section, respectively. For the erbium ion the transition between level 2 to 1 is due to the radiative transition and can be defined as $\Gamma_{21} = \frac{1}{\tau_2}$, where τ_2 is the lifetime of level 2.

At steady state,

$$\frac{dN_1}{dt} = \frac{dN_2}{dt} = \frac{dN_3}{dt} = 0 \tag{2.23}$$

Using (2.20), the population of level 3 can be written as:

$$N_3 = \frac{1}{1 + \Gamma_{32}/\varphi_p\sigma_p} N_1 \tag{2.24}$$

As Γ_{32} is large (decay rate is high from level 3 to 2) as compared with the pump rate ($\varphi_p\sigma_p$) into the level 3, hence N_3 is close to zero and population mostly reside in the level 1 and 2. By using (2.24) and (2.21), we can get the following expression:

$$N_2 = \frac{(\varphi_p\sigma_p/\Gamma_{32}) + \varphi_s\sigma_s}{\Gamma_{21} + \varphi_s\sigma_s} N_1 \tag{2.25}$$

The populations of level 1 (N_1) and level 2 (N_2) are then determined by using (2.19) to derive the population inversion ($N_1 - N_2$):

$$N_2 - N_1 = \frac{\varphi_p\sigma_p - \Gamma_{21}}{\Gamma_{21} + 2\varphi_s\sigma_s + \varphi_p\sigma_p} N \tag{2.26}$$

The condition for population inversions and thus for gain in level 2 to 1 transition is $N_2 \geq N_1$.

The threshold pump flux required to obtain the population inversion is given by:

$$\varphi_{th} = \frac{\Gamma_{21}}{\sigma_p} = \frac{1}{\tau_2 \sigma_p} \tag{2.27}$$

For a particular condition where the signal intensity is very small, and decay rate Γ_{32} is large as compared to the transition rate induced by the pump field, $\varphi_p \sigma_p$. Then the population inversion can be written as [44]:

$$\frac{N_2 - N_1}{N} = \frac{\varphi_p{}' - 1}{\varphi_p{}' + 1} \tag{2.28}$$

Where $\varphi_p{}' = \frac{\varphi_p}{\varphi_{th}}$ represent the normalized pump photon flux.

The fractional population inversion versus normalized photon flux curve is shown Figure 2.8. If the pump intensity is below the threshold value, the population inversion is negative and the signal experiences attenuation. On the other hand, the population inversion is positive i.e. the signal experiences gain when the pump intensity is above the threshold value. The pump intensity, in the units of energy per unit area per unit time, can be given by $I_p = h v_p \varphi_p$.Then the threshold intensity can be given by the following expression:

$$I_{th} = \frac{h v_p \Gamma_{21}}{\sigma_p} = \frac{h v_p}{\sigma_p \tau_2} \tag{2.29}$$

The photon absorbing ability of a medium is determined by the pump absorption cross section σ_p. The higher the value of the pump absorption cross section (σ_p), the higher the probability that pump photon is absorbed. This reduces the number of necessary pump photons to ensure that enough are absorbed to reach the threshold. Moreover, lesser

number of pump photons is required per unit time with longer metastable life time (τ_2). The metastable life time of the erbium in silica glass is about 10 ms, which is helpful in reaching the threshold with low pump power.

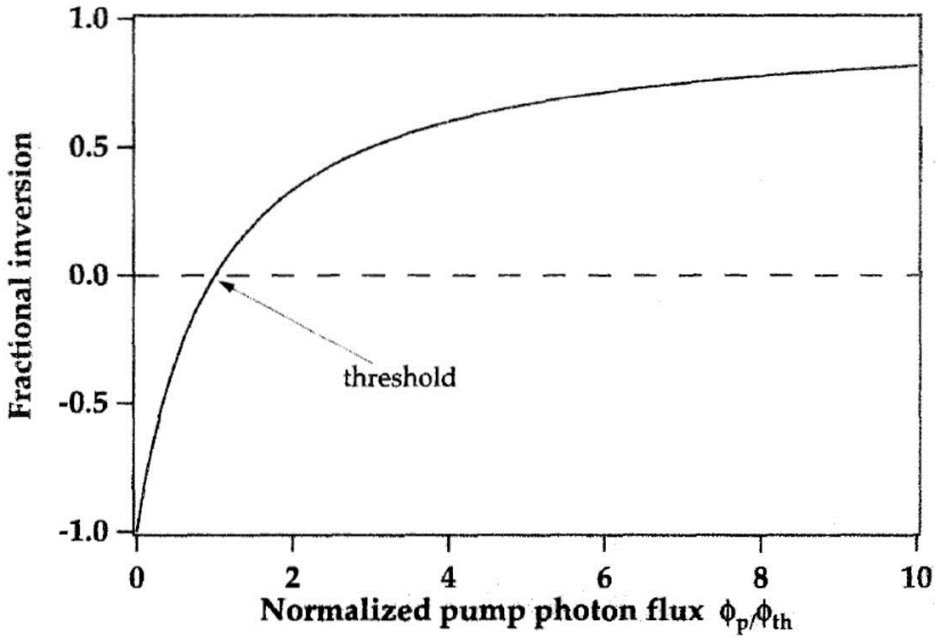

Figure 2.8: Fractional population inversion in three level system [44].

2.7 EDF Performance Analysis Based on Doping Radius

Depending on the thresold intensity, the erbium doped fiber (EDF) can be divided into two sub-regions such as amplifying and absorbing region, as shown in Figure 2.9. The amplification region is the specific area of the EDF where the pump intensity is above the thresold, while in the absoprtion region the pump intesity is below the thresold and the input signal is absorbed. This phenomenon can be explained by the pump envelope in the fiber core. Usually, optical pump intensity propagates through fiber core as a fundamental mode.

In the step index fiber, the intensity distribution of the fundamental mode is given by $P_p(z)\psi_{01}(\lambda_p, r)$, where P_p and ψ_{01} represent pump power and envelope of LP_{01}mode. The envelope of this mode is almost Gaussian and given by [45]:

$$\psi_{01}((\lambda_p, r) = \begin{cases} {J_0}^2\left(\frac{u_p r}{b}\right) & r \le b \\ \frac{{J_0}^2(u_p)}{{K_0}^2(w_p)} {K_0}^2\left(\frac{w_p r}{b}\right) & r \ge b \end{cases} \tag{2.30}$$

Where $J_0$and K_0 denote Bessel and modified Bessel functions, respectively; u_p and w_p are the transverse propagation constant of the LP_{01}mode; b is the core radius of the step index fiber.

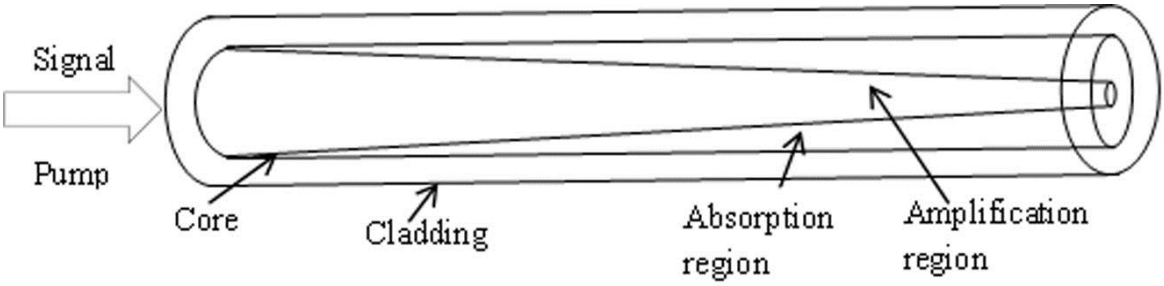

Figure 2.9: Absorption and amplifying region of the EDFA [46].

If the unifrom pump intensity was propagated through the fiber core, after certain distance pump intensity would go below the thresold. But this is not the case in EDF because the pump intensity is nearly Gaussian. In the EDF, the pump intensity is gradually absorbed and after certain distance it goes below the thresold near core cladding interface while at the sametime it exceeds the thresold value near the center of the core. After this length the absorption region increase gradually, while amplification region become smaller with the increasing propagation distance.

2.8 Er^{3+}- Er^{3+} Interaction Effects on EDFL Gain Media

In the last two decades, study of EDFs has become enormously extensive due to its increasing need in telecom related devices. Therefore, interest in the basic studies of EDFs has increased significantly. Among the basic studies, dopant concentrations have attracted significant attention during 1990s [47] - [48] to the recent days [49]-[50]. Different research groups have been investigating the effects of high concentration dopant ions in EDFs.

It has been clearly revealed that high concentration of dopant ions have deteriorating effect on the efficiency of EDFA. This performance degradation occurs due to the ion-ion interactions among the neighboring ions, which reduce the excited state populations. This performance degradation can be minimized by increasing the distance between the interacting neighboring ions. This can be achieved by using low concentration of dopant ions in a long fiber. Nevertheless, the EDFs can also be used in fiber lasers, which have the potential to become compact integrated sources of ultra-fast fiber optic communication systems. For compact integrated sources highly doped fibers are used to reduce the total cavity length and dispersion introduced by the amplifying fibers [51].

The EDF performance degradation is modeled in two ways: Homogeneous Upconversion (HUC) and Inhomogeneous Upconversion (IUC) [52]. In HUC model, it is assumed that Er^{3+} ions are homogenously distributed in the fiber core and their energies are transferred from one ion to its neighbor through the HUC factor. In IUC model, the average distance between neighboring Er^{3+} ions is considered to be very small. Therefore, some ions tend to cluster in pairs following a rapid cross relaxation process.

2.9 Upconversion Model

Nonradiative energy transfer due to electric multipolar interaction is responsible for the upconversion process. This process starts from the metastable state $^4I_{13/2}$ with two erbium ions as shown in Figure 2.10. In this state the energy is transferred from the donor to the acceptor atom. As a result donor atom nonradiativly decay to the state $^4I_{15/2}$ and acceptor atom is excited to the state $^4I_{9/2}$. Excited atoms then rapidly decay back to the metastable state $^4I_{13/2}$. For long range dipole-dipole interactions, it is commonly assumed that interaction rate is inversely proportional to the R^6, where R represents the separation between the interacting ions [48],[51].

In the glass lattice, which is formed with silica tetrahedron $(SiO_4)_2$, silicon is found in four fold coordination. Two dimensional representation of the glass lattice, which is shown in the Figure 2.11, corresponds to three fold silicon configuration. Figure 2.11 also shows that Er^{3+} ions shared limited number of non-bridging oxygen, which decreases the erbium ions solubility in the host matrix. If the distance between erbium ions is decreased by the residual interaction such as local charge compensations, they tend to cluster together. Incident photons excite these ions; and they start to interact with each other. Due to this interaction they transfer and exchange the energy with each other, which reduce the excited state populations [51][53].

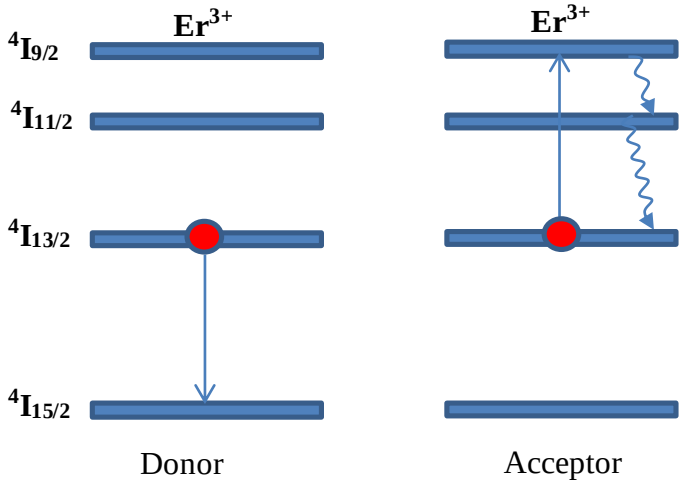

Figure 2.10: Energy level diagram of Er^{3+} and upconversion process [51].

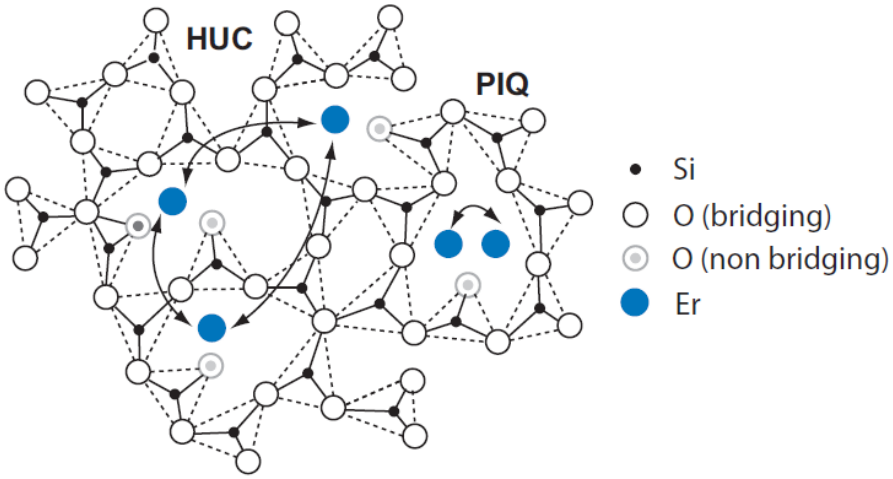

Figure 2.11: Homogeneous and inhomogeneous upconversion in two dimensional erbium doped silica glass model [54].

The separation of the ions determines the interaction rate. As the separation between the clustered ions is comparable with the erbium ion diameter (about 0.2 nm); therefore, inhomogeneous (interaction between ion pairs) upconversion is more rapid than their homogenous counterpart. The time scale for inhomogeneous upconversion is in submicroseconds and for the homogenous upconversion it is in milliseconds [55] .

2.9.1 Inhomogeneous Upconversion

In IUC model, erbium ions are described by a two level system approximation. In this model, the ions exist as two distinct species: single ions (do not interact with each other) and clustered ions. In each cluster, ions can exist only in two energy levels: state 1 and state 2. In state 1, all ions reside in the ground state. In state 2, only one ion per cluster resides in the excited state. If more than one ion is excited to the upper level in the cluster, the ions start transferring energy to each other. The upconversion process continues till one ion in the cluster occupy the metastable excited state [51].

Actually, cluster in the EDFs can be of different sizes, however sometimes equal size clusters are assumed for theoretical studies. If the total concentration of the erbium ions are N_t the clustered ions concentrations can be given as:

$$N_c = mkN_t \tag{2.31}$$

Where, *k* and *mk* represent the relative number of clusters and percentage of ions in the clusters, respectively.

Therefore, single ion concentrations can be given as:

$$N_s = (1 - mk)N_t \tag{2.32}$$

For example when $m = 2$ then $2kN_t$ ions resides in kN_t pairs.The rate equation describing the single ions residing in EDFs is given by [56], [51], [57]:

$$\frac{dN_{s2}}{dt} = -\frac{dN_{s1}}{dt} = -(A_{21} + W_{21})N_{s2} + (R + W_{12})N_{s1} \tag{2.33}$$

Where A_{21} represent spontaneous emission rate, and N_{si} (i = 1, 2) is the concentration of single ions in state i.

$$N_s = N_{s1} + N_{s2} \tag{2.34}$$

Absorption and emission rates of the signal are defined as:

$$W_{12} = \int_0^{\infty} \frac{\sigma_{as}(v) P_s(v) \Gamma_s(v)}{hv\pi b^2} dv \tag{2.35}$$

$$W_{21} = \int_0^{\infty} \frac{\sigma_{es}(v) P_s(v) \Gamma_s(v)}{hv\pi b^2}\ dv \tag{2.36}$$

At 980 nm, the pump rate is given by:

$$R = \int_0^{\infty} \frac{\sigma_{ap}(v) P_p(v) \Gamma_p(v)}{hv\pi b^2} dv \tag{2.37}$$

Where, hv represents the photon energy, b is the transverse radius of the uniformly distributed erbium doped region, $P_p$and P_s are the pump and signal power respectively, σ_{as} and σ_{es} are the absorption and emission cross sections for the signal power, respectively. And σ_{ap} is the absorption cross section at pump power and Γ_s and Γ_p are the overlap integrals.

2.9.2 Homogenous Upconversion

The homogeneous upconversion model is based on the two or three particles cooperative interactions between homogenously distributed ions. This upconversion occurs on nanometer distance scales between the dopant erbium ions, which are homogeneously distributed in the host glass matrix [51], [54].

In this model, the ions are represented by one rate equation for single ions with an additional upconversion term. For two-particle homogeneous upconversion model, the term $-k_2(N_{s2})^2$ needs to be added to the right side of (2.33). Where the added term represents the same cooperative process as introduced for the clustered ions, but the

distance between the homogeneously distributed ions is much larger than clustered ions, and k_2 coefficient indicates the effective interaction rate.

For three particle homogenous upconversion model, the term $-k_3(N_{s2})^2$ needs to be added to the right side of (2.33). This term represents that three particles are involved in the energy transferring process. This transferring process is quite less probable than the two particles one.

CHAPTER 3

LITERATURE REVIEW

3.1 Background Review on EDFA Performance Analysis

Fiber amplifier performance is determined by number of parameters such as dopant ions distribution, dopant ions concentration, numerical aperture (NA), cutoff wavelength, pump wavelength, host glass, and amplifier configuration. Two pump bands (980 nm and 1480 nm) have already been selected for efficient EDFA performances, which are free from excited state absorption (ESA) [58],[59].

By increasing the pump power conversion efficiency, EDFA performance can be improved. This can be done by reducing the doping radius of EDF. The confinement of the dopant ions near the core area increases interaction between the pump energy and the dopant ions, which in turn increase the efficiency of EDFA. J. R. Armitage has shown theoretically that confining the dopant ions near the core increases the pump conversion efficiency, which consequently increase the EDFA performance [60]. By decreasing the ions distribution profile width, the dopant ions are removed from those parts of the core where the pump intensity is rather low, i.e. where the dopants ions are not pumped very efficiently. On the other hand, dopant ions residing around the core region can interact with the highest pump intensity, and use the pump power efficiently.

In another paper, B. J. Ainslie and his co-authors have described the fabrication of erbium doped fibers in which erbium ions are confined around the core of Al_2O_3-P_2O_5-

SiO_2 glass fiber. They demonstrated the improved pumping efficiency with their proposed ions distribution technique, which is helpful in designing fiber based amplifiers and lasers [61].

M. Ohashi theoretically determined the optimum fiber parameters for an EDFA pumped at 1480 nm using rate equation of three level laser system. He showed that signal gain can be improved by decreasing the doping radius [62]. He also showed that cutoff wavelength increases as doping radius decreases.

However, confining the erbium ions in a relatively small volume will introduce troublesome clustering effects, which will degrade the EDFA performance. This happens via the rapid energy transfer within a fraction of clustered ions. Therefore, determination of optimal doping radius is needed for which detrimental ion-ion interaction is not that significant but pump power conversion efficiency is relatively high. In the following section, we have presented existing literatures based on dopant ions concentration, and detrimental ion-ion interaction on the EDFA performances.

Effect of dopant ions concentration on the EDFA performance has been investigated by the different research groups. High gain coefficient and high conversion efficiency have been reported using only low erbium ion concentration [63]–[65]. The gain efficiency decreases when the dopant ions concentration is greater than 100 ppm for germano-silicate and 1000 ppm for germano-alumino-silicate fibers due to ion-ion interaction.

M. Shimizu and his co-workers demonstrated that increasing erbium ions concentration deteriorates the EDFA performances for silica glass fiber, even when the erbium concentration was less than 1000 ppm [66]. This happens due to the cooperative ion-ion

interaction. To investigate the cooperative ion interaction, several theoretical models have been proposed. They are based on the inhomogeneous upconversion due to pair induced quenching [67], [68][69] or homogenous upconversion [22],[67],[70] in two or three particle cooperative energy transfer process.

H. Masuda *et al.* proposed a model of gain degradation for the high concentration erbium doped fiber amplifier pumped at 980 nm and 1480 nm introducing inhomogeneous cooperative upconversion. In this model, they explained an experimental result of low gain with high Er^{3+} concentration. They also found that maximum energy conversion efficiency is higher in the counter propagating scheme than the co-propagating one [69].

Pair-induced quenching (PIQ), which increase with the dopant concentration, effects in EDFA performances have been modeled by J. Nilsson and his co-authors. They showed that shorter length fiber requires higher pump power to achieve the desire gain. Moreover, they also found that there is a lower length limit of EDF which can be pumped by the realistic pump power to obtain the desired performance [71].

Blixt *et al.* examined the upconversion effects on the amplification performance of EDFA. They used eight different fibers with dopant concentration less than 1000 ppm to observe the upconversion effect as a function of erbium concentration. They reported that upconversion drastically reduces amplification for the erbium concentrations in the range of 70-840 ppm [48].

Another research group led by R. S. Quimby developed a technique to determine the degree of clustering. They did this by measuring the pump power dependence of the upconverted green fluorescence of erbium ions pumped at 980 nm. They reported that

degree of clustering in EDF is greater for higher dopant ion concentration. They also found that addition of aluminum to the glass of the fiber reduce the clustering effects [72].

The EDFA performance dependence on the erbium ion concentration is experimentally and theoretically studied by P. Myslinski and his co-workers [51]. It is found that the quantum efficiency of the amplifier is strongly dependent on the erbium ion concentration, the signal wavelength, the relative propagation direction of the pump and signal power. The dependence is fully explained by the presence of an upconversion mechanism between ions residing in pairs or larger clusters. They also suggested that performance degradation for the other sources such as back ground loss, excited state absorption and homogenous upconversions are negligible.

In addition to the erbium ions concentration, several other parameters such as relative index difference, pumping wavelength, numerical aperture have been investigated to increase the gain coefficient of EDFA [73]-[74]. EDF with high numerical aperture (NA) has small spot size, hence efficient pumping can be realized. This helps in achieving high gain coefficient from the EDFA.

3.2 Background Review on Tunable EDFL

The advent of long wavelength band (L-band) EDFA has doubled the transmission capacity of the WDM system. To test such wideband devices and many other optical component requires widely tunable laser which can cover both C and L band. Moreover, these widely tunable lasers can also be used in the inventory management of the WDM transmission system [14]. Usually, a large number of fixed wavelength lasers are used as

a transmitter back up, which increase the complexity, and cost of the system. Therefore, availability of the low cost widely tunable lasers can reduce the inventory substantially. There are several existing techniques to develop widely tunable lasers but EDFL has attracted considerable attention due to the advantages over semiconductor lasers.

First, continuous wave (CW) tunable fiber laser using erbium ion was reported by Reekie and his co-workers in 1986 [75]. A holographic diffraction grating having 600 lines/ mm blazed at $\lambda = 1.6$ μm was used to provide wavelength selective feedback. This wavelength selective feedback mechanism increases the intra-cavity loss, which subsequently increases the threshold value of lasing.

R. J. Mears and his co-authors reported tunable CW and Q-switched erbium doped fiber laser for the first time at room temperature [76].

First diode laser pumped Er^{3+} doped fiber laser operating around 1.6 μm was reported by L. Reekie *et al.* [77]. They used CW GaAlAs diode laser for pumping and got output power of 130 μW with a lasing threshold of 3 mW. In this paper, they showed the wavelength tuning possibility by varying the fiber length in the cavity. Finally, they demonstrated the wavelength tunability up to 15 nm (1550 nm to 1565 nm) by simply changing the fiber length in the cavity. For that experiment they used dye laser operating at 808 nm as a pump source. This configuration suffers from excess loss in the cavity due to the introduction of a diffraction grating resulting in a high threshold value (30 mw).

A research group led by P.L Scrivener demonstrated a tunable EDFL using a tunable ring resonator configuration with low threshold value (10 mw) as compared to holographic diffraction grating type. The ring resonator is made by splicing the EDF between selected

ports of the coupler as shown in Figure 3.1. This ring laser is lased at the wavelength for which the coupling coefficient is optimized. The coupling coefficient can be wavelength dependent in the polished fiber coupler with variable core separation, which enables tunablity [78]. This ring laser is pumped at 532 nm wavelength, which obtained from second harmonic generation in KTP (Potassium titanyl phosphate) crystal pumped with Nd-YAG laser, and exhibits discrete tuning bands within 70 nm wavelength region.

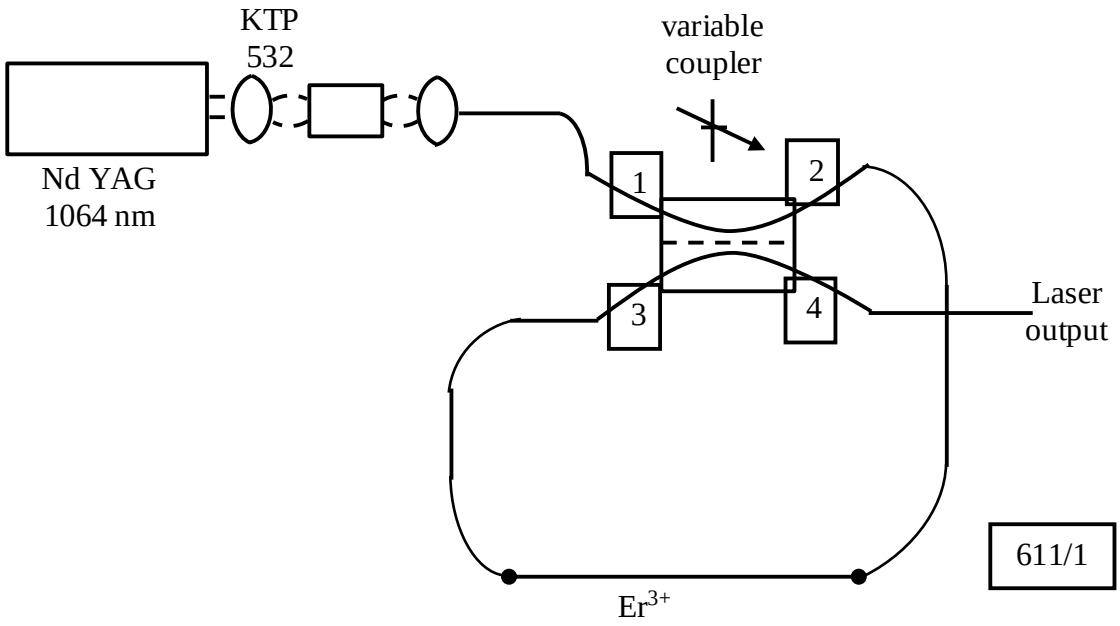

Figure 3.1: Tunable EDFL with wavelength dependent coupling [78].

C. Y Chen and his coauthors obtained (1522-1567 nm) 45 nm of continuous tuning range from an EDFRL. In the experimental setup, as shown in Figure 3.2, they used Al co-doped EDF as gain medium, second harmonic of Nd: YAG laser as pump source, and inline etalon as tuning element. A dichroic beam splitter was used to combining pump light at 532 nm and infrared signal into the EDF. The inline etalon, tuning element, had free spectral range of 55 nm and finesse of 200 near 1540 nm. Now, it has been

established that 980 nm, and 1480 nm pumping wavelength is the suitable source for EDFL design.

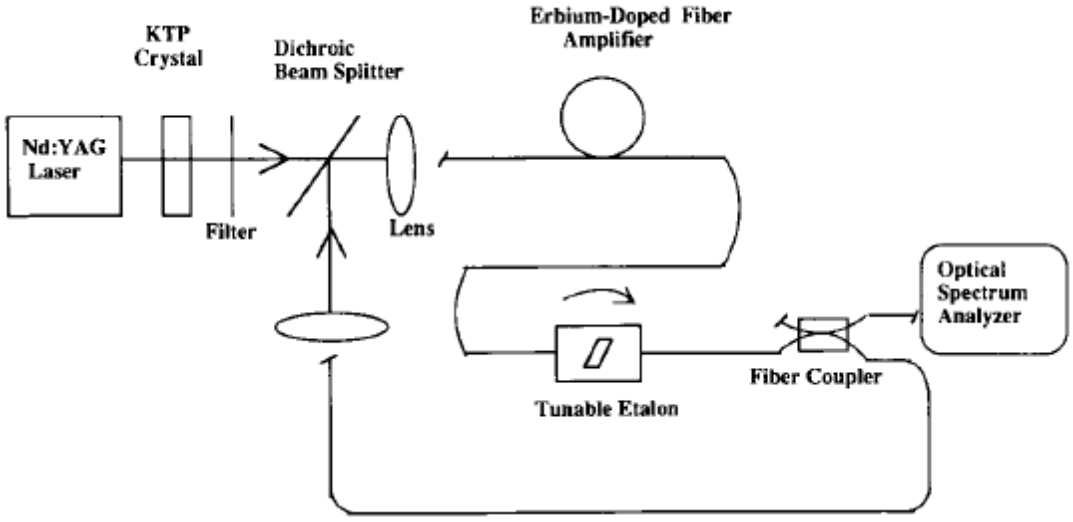

Figure 3.2: EDFRL using inline etalon for tuning [79].

In another report, J. L. Zyskind *et al.* demonstrated diode pumped, electronically tunable all optical fiber laser, as shown in Figure 3.3. They used EDF as a gain media and Fiber-Fabry Perot (FFP) etalon, which is polarization independent and electronically tunable filter, as a tuning element. This tuning element cannot be used in a standing wave resonator because it reflects wavelengths outsides FFP pass band and acts as a resonator for these wavelengths. In the ring resonator, these unwanted lasing are avoided by using optical isolator. Using this configuration, the output wavelengths is tuned form 1525 nm to 1586 nm with a variation in power less than 3.5 dB [80].

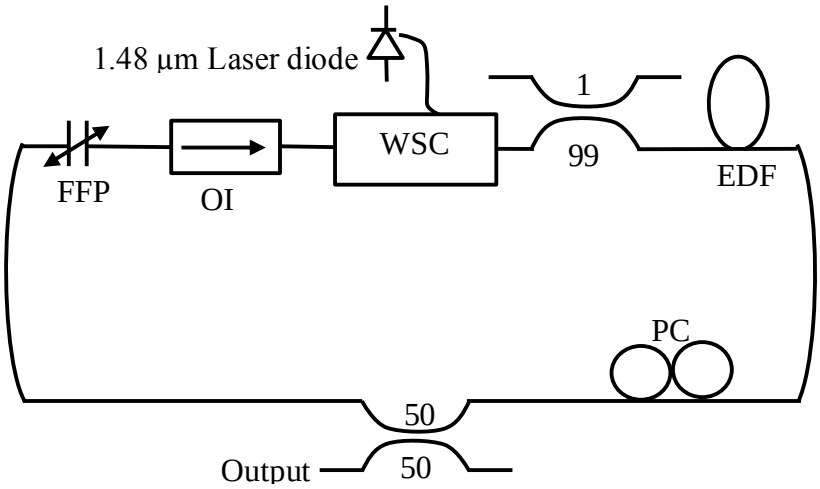

Figure 3.3: Tunable diode pumped EDFL using Fiber-Fabry Perot (FFP) etalon filter [80].

Fiber-birefringence tuning technique in erbium doped fiber laser was proposed by Paul D. Humphrey and John E. Bowers, as depicted in Figure 3.4. In this paper, they have shown that output wavelength is a monotonic function of the position of the halfwave fiber coils for the optimum positing of the quarterwave coils.

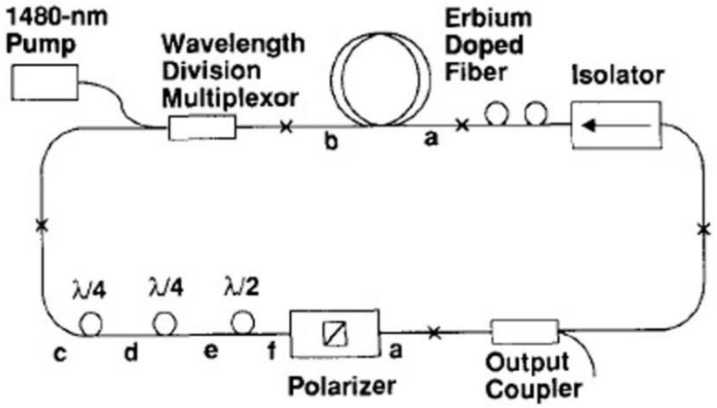

Figure 3.4: Tunable EDFL using fiber-birefringence [81].

The optimum positing of the quarter-wave coils was determined through a process of trial and error, which was not a very efficient method. In this technique, the wavelength was tuned over the range 33 nm (1533 nm- 1566 nm) by rotating half-wave coils [81].

Yew Tai Chieng and R. A Minasian proposed a intracavity tuning mechanism using electro-optic reflection Mach-Zehnder interferometer (ERMZI), as shown in Figure 3.5. In this scheme, EDF acts as a gain media and is optically pumped via the WDM coupler. ERMZI transmitivity characteristics, which is wave length dependent, ensure the wavelength tunablity. ERMZI allows to pass the desired wavelength with minimum attenuation and blocks the unwanted wavelength. High speed and broad range tuning (39 nm) were achieved by this technique [82].

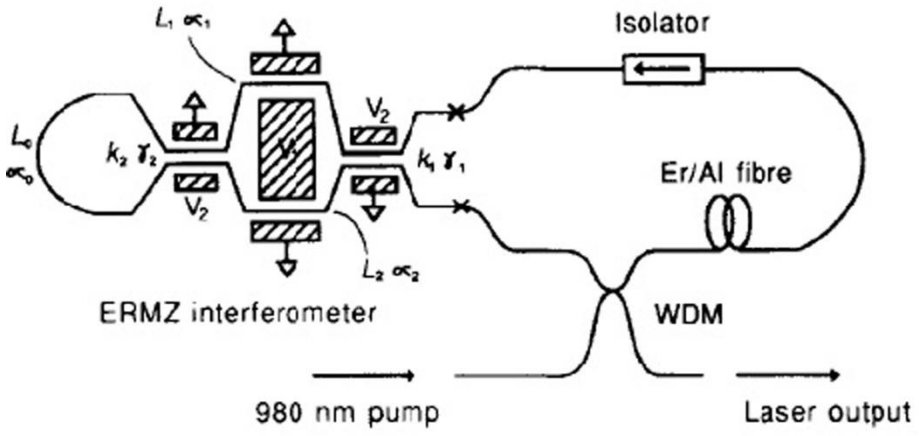

Figure 3.5: Tunable EDFL using ERMZI [82].

A widely tunable EDF ring laser, as shown in Figure 3.6, covering both conventional band (C-band) and long wavelength band (L-band) was demonstrated by Shinji Yamashita and Masato Nishihara. They used 50-200 m long EDF as gain medium and two FFP filters: FFP#1 and FFP#2 as tuning filter. FFP#1 has the free spectral range (FSR) of 41.89 nm (5.18 THz) and the finesse of 114, and FFP#2 has the FSR of 101.78 nm (12.7 THz) and the finesse of 211. They optimized the EDF length to obtain maximum 80 nm tuning range. They achieved this tuning range by using 50 m long EDF and FFP#2. While for the same EDF length FFP#1 provided only 35 nm tuning [16].

Though, they got wide tuning range (80 nm) with their proposed experimental setup but they did not mention about the pumping wavelength and direction effects on the tuning range.

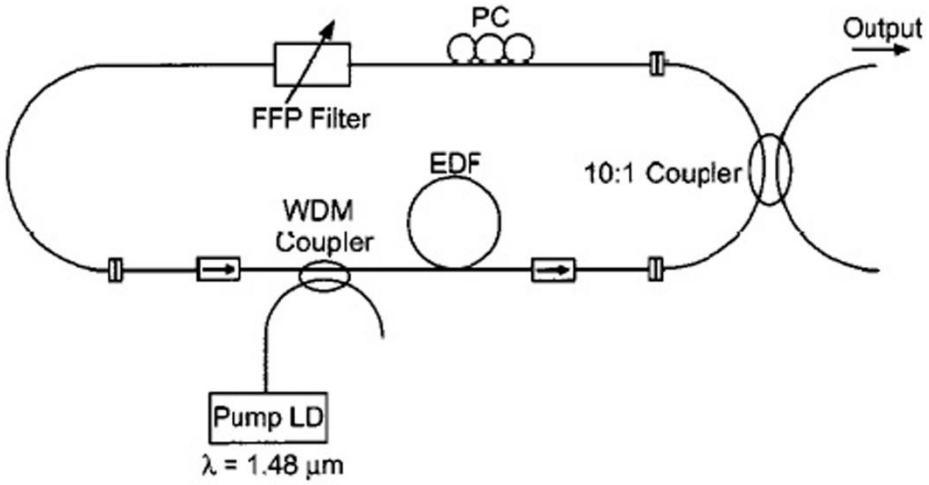

Figure 3.6: Widely tunable EDFL using length optimization [16].

Antoine Bellemare and his coworker used a numerical model to analyze the impact of various laser variables such as cavity loss, EDF length, pump power, and lasing wavelength [83]. They also developed experimental setups to compare the numerical data with experimental data. They found a good agreement between numerical data and experimental data. The experimental setup is shown in Figure 3.7, which is backwardly pumped through wavelength dependent coupler (WDC) by a 180 mW diode laser emitting at 980 nm. In their investigations, they used an EDF, which was co-doped with Ge-Al, with absorption coefficent of α (1530 nm) = 4.76 dB/m, α (980 nm) = 4.08 dB/m, doping concentration of 680 ppm, core diameter of 3.4 μm, cutoff wavelength of 835 nm, and NA 0.186. They used a multilayer thin-film interference bandpass filter, which has 0.15 nm full-width at half-maximum (FWHM) at normal incidence. A polarization controller is used to ensure linear polarization state of light; and a fiber optic spliter is

used to take 10% light from the cavity as output. In this paper, they showed that 30% less pump power is required with 1480 nm pumping than 980 nm to obtain the same output power. However, the did not mention the effects of pumping configuration on the tuning range.

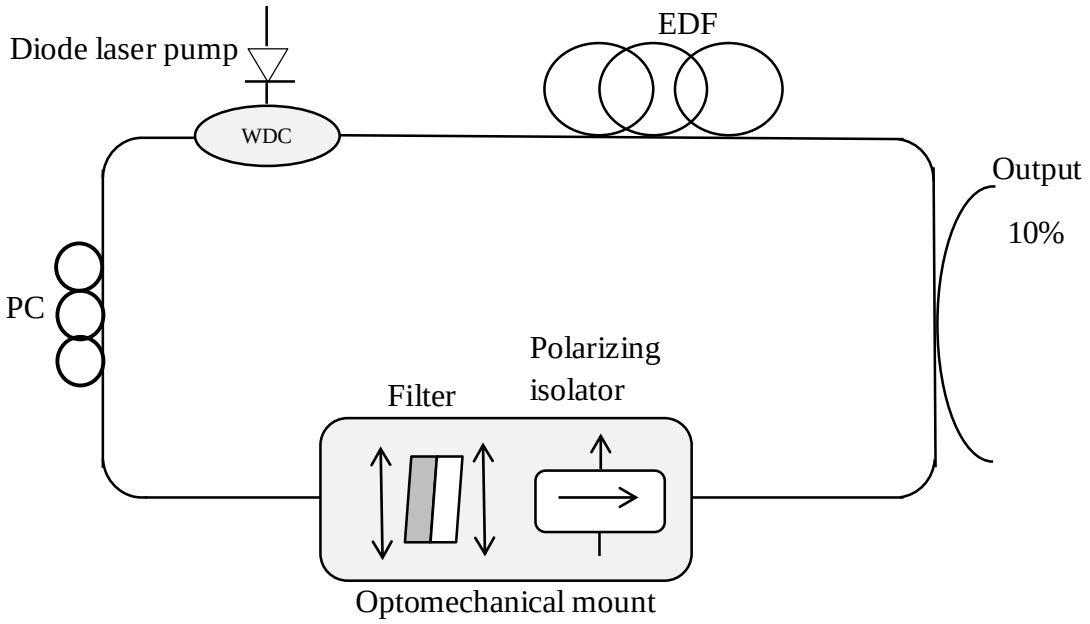

Figure 3.7: Experimental setup of broadly tunable EDFRL [83].

By using the combination of 1480 nm pump laser diode and high concentration EDF, a high power EDFRL with wide tuning range (over 100 nm) was reported by X. Dong and his co-authors [84]. They also investigated the effects of EDF length, output coupling ratio, and pump power on the laser performance. They showed that EDF length and output coupling ratio have the significant effects on the tuning range and output power. Their experimental data show that tunable range shift from C band to L band with the increase of EDF length. The experimental setup used for their demonstration is shown in the Figure 3.8. For the gain media they used high concentration EDF with absorption coefficient of α (1480 nm) = 7 dB/m, and α (1532 nm) = 15 dB/m. A laser diode with maximum pump power of 136 mW is coupled to the ring cavity via 1480/1550 micro-

optic WDM coupler. For the wavelength tuning a tunable narrow band-pass fiber Fabry-Perot (FFP) filter with bandwidth of 0.2 nm and FSR of 28 nm and six optical band-pass filters (BPFs) with 20 nm bandwidth with different wavelength ranges was used in their experimental setup. An isolator and a polarization controller are used for unidirectional operation and adjusting polarization state of the light.

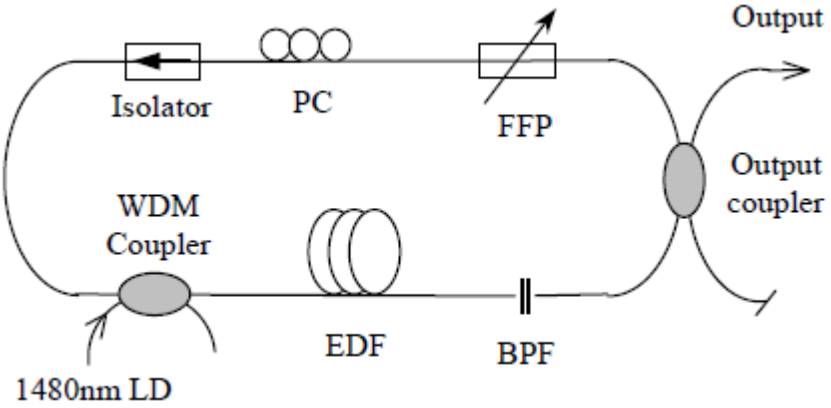

Figure 3.8: High power widely tunable EDFRL [25].

A linear cavity widely tunable EDFL is experimentally demonstrated by X. Dong and *et al.* [26], as shown in Figure 3.9. They demonstrated that short and long band wavelength tuning depends on the EDF length. They showed that short EDF length is not suitable for long band lasing, and long EDF length is not suitable for short band lasing. They reported 100 nm tuning range using an optimized length, where EDF was backwardly pumped through a WDM coupler by a 90 mW laser diode emitting at 1480 nm. They used six band pass filters with 20 nm band width and a tunable FFP with 0.2 nm bandwidth and 40 nm FSR as frequency selective elements.

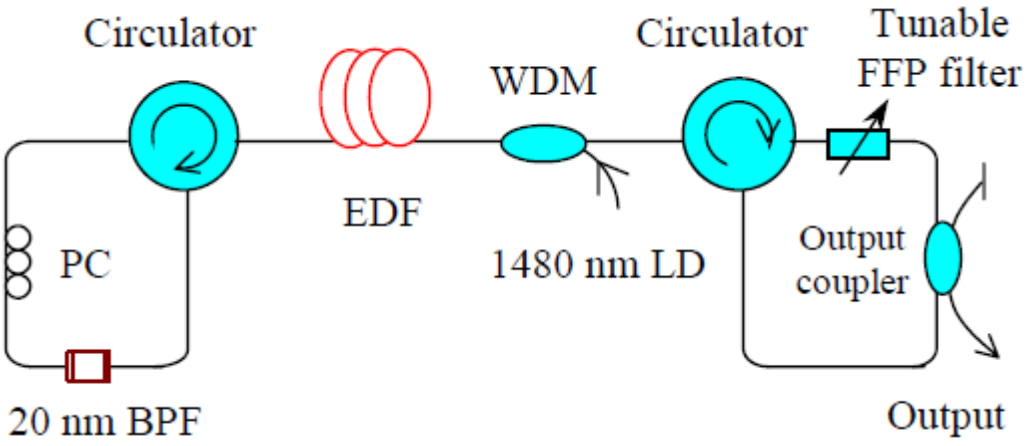

Figure 3.9: Widely tunable EDFL using length optimization and linear cavity [26].

X. Dong and his co-workers numerically and experimentally investigated the effects of active fiber length on the tunability of EDFL. They reported that tuning range shift form C band to L band with the increase of gain media length. They got over 100 nm tuning range by optimizing the EDF length. They also observed that PIQ is favorable for achieving L band lasing though it reduces output power and degrades the power flatness. Based on the findings, they proposed a novel method where active fiber length switching is used to extend tuning range. Their proposed configuration is shown in Figure 3.10 [85].

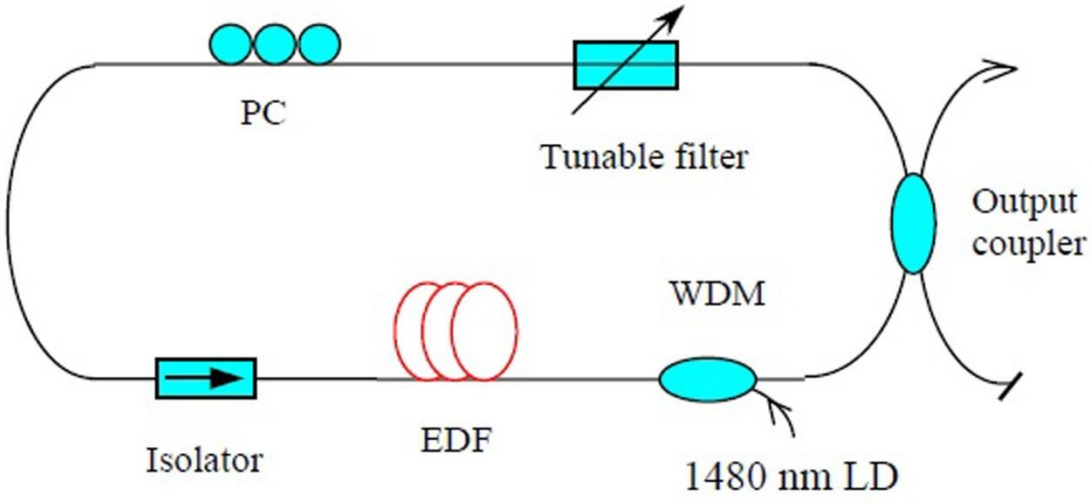

Figure 3.10: Tunable EDFL using active fiber length switching [85].

X. Dong *et al.* reported that the concentration quenching can induce non-uniform power in tunable laser with highly doped EDF. They proposed a theoretical model for a high concentration EDFL considering PIQ. A Ge-Al codoped fiber with an absorption coefficient of α (1530 nm) = 15 dB/m , and α (1480 nm) = 7 dB/m, a doping concentration of 9.2×10^{24} ions/m^3, core diameter of 3.2 µm, paired ion percentage 5.2%, and numerical aperture of 0.27 was used for their experimental investigation. The experimental setup used by X. Dong *et al.* is shown in Figure 3.11. They also used a tuning filter whose bandwidth and tuning range was 0.2 nm and 120 nm, respectively. They observed the emission wavelength for the EDF length of 5, 8 and 12.5 m and concluded that tuning range is sensitive to the length of the gain media. The largest tuning range (104 nm) was obtained using 8 m fiber, which showed a good agreement with the results obtained numerically [86].

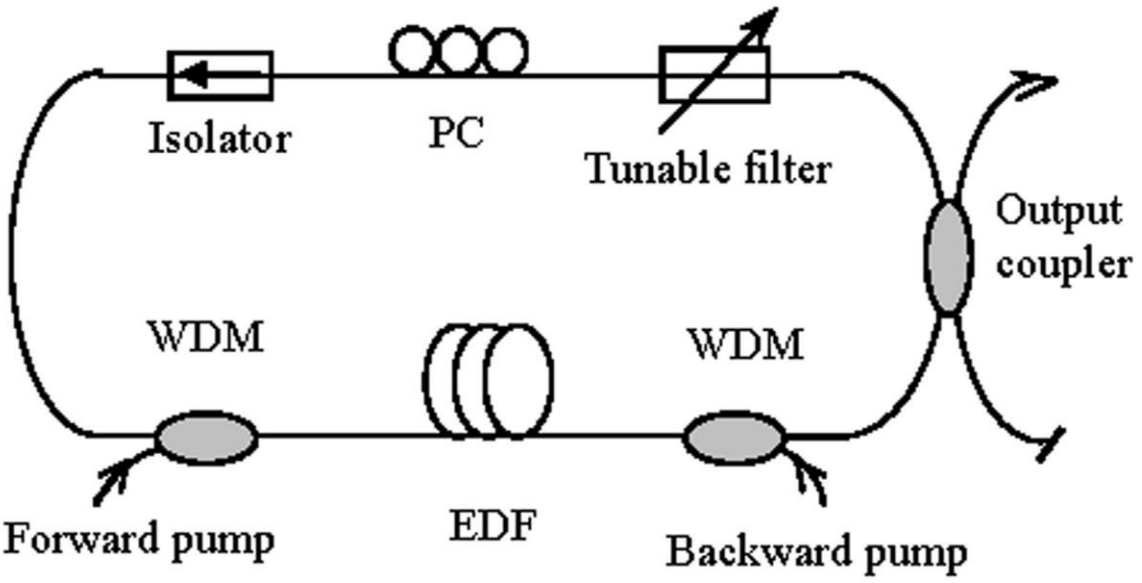

Figure 3.11: Widely tunable EDFRL using high concentration EDF [86].

In this chapter, background literature review of EDFA performance analysis and tuning range analysis of different EDFL configurations were presented. During the review, we identified some advantages, and drawbacks of the existing research. From the existing investigation, we came up with some new idea to enhance the existing system performance. The simulation model and experimental setups that are used in our thesis are presented in the following chapter.

CHAPTER 4

SIMULATION AND EXPERIMENTAL SETUP

It is known that laser performances are significantly affected by the characteristics of the active gain medium. In EDFL design, EDF is used as the active gain media. Therefore, EDFL performances are greatly affected by the EDF performances. In this thesis, EDF performances are investigated based on the doping radius, and erbium ions concentration prior to designing EDFL. Moreover, detrimental effect of ion-ion interaction is simulated by designing EDFA and tunable EDFRL. Following this, EDF performances have again been evaluated in terms of population inversion with an aim to design a widely tunable EDFRL. Then, a widely tunable fiber laser is proposed and simulated based on the pumping configuration and EDF length optimization. After this, tuning range of EDFL is investigated based on the output coupling ratio, intra-cavity loss, and pump power. In this thesis, EDF and EDFL performances are simulated using OptiSystem version 13 and VPIphotonicsComponentMaker version 9.3 (brief information of the simulation tools is given in Appendix A). Finally, EDFRL performances have been demonstrated experimentally based on the coupling ratio and intra-cavity loss. For these experimental setups, available laboratory equipment has been used.

4.1 Performance Analysis of Conventional Band EDF

For analyzing the performances of conventional band EDF, a simple EDFA is designed using OptiSytem version 13. A typical forward pumped EDFA configuration and its corresponding simulation model are shown in Figure 4.1 and Figure 4.2, respectively.

This simulation model is used for determining dopant radius, dopant concentration, and ion-ion interaction effects on the EDFA gain performances.

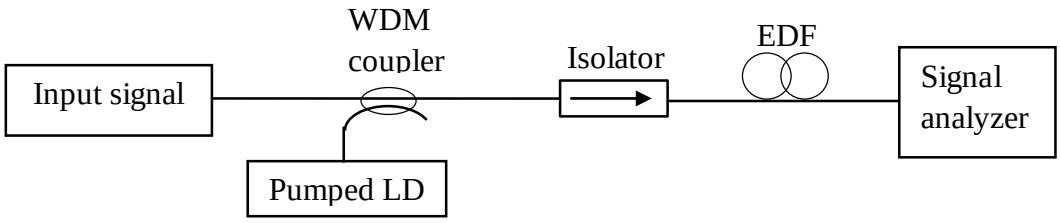

Figure 4.1: Forward pump EDFA configuration

4.1.1 Doping Radius Effects on EDF Performance

In the model, pump and input signal are coupled into the EDF using ideal WDM multiplexer. Here, co-propagating pumping configuration has been used. An ideal isolator has been used to ensure unidirectional operation. For investigating the doping radius effects on the EDF performance, we have used different simulation parameters which are given in Table 4-1, and Table 4-2. The doping radius is varied and EDFA gain performances are monitored in the optical spectrum analyzer (OSA). In the OptiSystem model, all the input terminals should be connected to the appropriate optical sources for providing error free output. Therefore, an optical null signal is used in the EDF terminal to avoid unconnected input terminal.

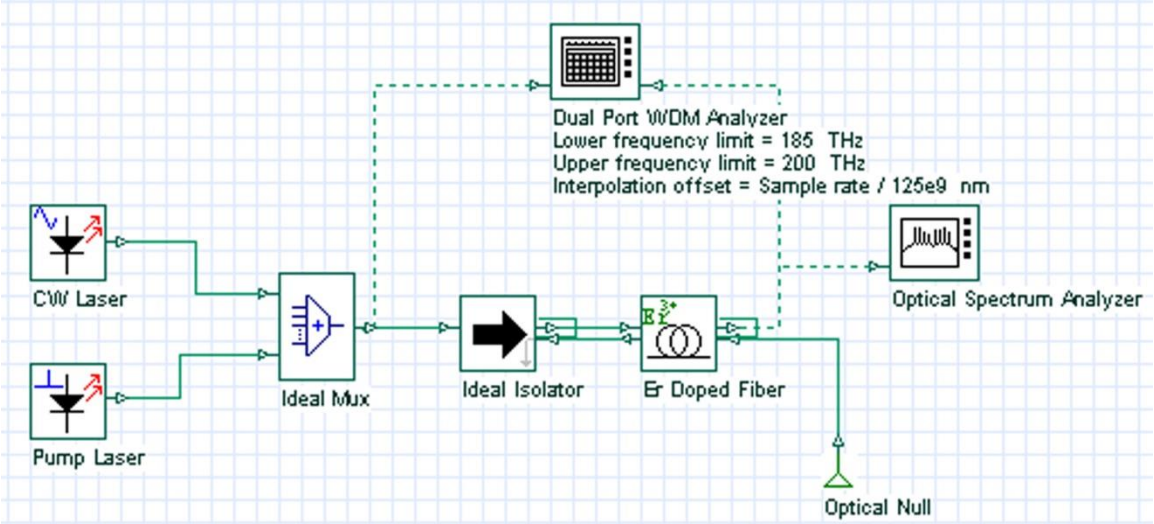

Figure 4.2: Simulation model of forward pumped EDFA.

Table 4-1: Effect of doping radius on EDF performances

Parameters	Value
Pump power	20,25 and 30 mW
Pump wavelength	980 nm
Signal power	-20 dBm
Signal wavelength	1550 nm
Erbium ion concentration	700 ppm
Er metastable life time	10 ms
Saturation parameter	4.4 exp(15) /s.m
Fiber core radius	1.8 µm
Erbium doping radius	0.4-1.8 µm
Numerical aperture	0.32
Erbium doped fiber length	20 m

Table 4-2: Gain spectrum simulation parameters with different doping radius

Parameters	Value
Pump power	20,25 and 30 mW
Pump wavelength	980 nm
Signal power	-20 dBm
Signal wavelength	1530-1570 nm
Erbium ion concentration	700 ppm
Er metastable life time	10 ms
Saturation parameter	4.4 exp(15) /s.m
Fiber core radius	1.8 μm
Erbium doping radius	0.6, 0.8, 1.0 μm
Numerical aperture	0.32
Erbium doped fiber length	20 m

4.1.2 Dopant Ion Concentration Effects on EDF

Parameters, as given in Table 4-3, are used to determine the EDF performances based on the dopant concentration. In the simulation tool, EDFA gain performances have been analyzed by varying the EDF length with different dopant concentrations. It is found that higher dopant concentrations are required for designing shorter length EDF devices. However, higher concentration dopant ions degrade the EDF performances due to ion-ion interaction.

4.1.3 Er^{3+}- Er^{3+} Interaction Effects on the EDFA Performance

The ion-ion interaction effects in the EDF are also simulated by introducing the ion-ion interaction parameters in the simulation model. For the ion-ion interaction effects on the EDF performance, we have set the simulation parameters according to Table 4-4.

From the given data, shortest possible length and best possible ppm concentrations have been selected again to simulate the ion-ion interaction effects.

Table 4-3: Er^{3+} concentration effect in EDF length

Parameters	Value
Pump power	20 mW
Pump wavelength	980 nm
Signal power	-20 dBm
Signal wavelength	1550 nm
Erbium ion concentration	250-400 ppm
Er metastable life time	10 ms
Fiber core radius	1.8 µm
Erbium doping radius	1.6 µm
Numerical aperture	0.32
Erbium doped fiber length	2-30 m

Table 4-4: Er^{3+}- Er^{3+} effects on EDF performances

Parameters	Value
Pump power	20 mW
Pump wavelength	980 nm

Signal power	-20 dBm
Signal wavelength	1530 nm-1570 nm
Erbium ion concentration	350 and 400 ppm
Er metastable life time	10 ms
Fiber core radius	1.8 µm
Erbium doping radius	1.6 µm
Numerical aperture	0.32
Erbium doped fiber length	13 m
Homogenous upconversion coefficient	15 exp (-24) m^{-3}/s
Ions per cluster	2, 6 and 10
Relative number of clusters	10%

4.1.4 EDF Absorption Coefficient and Dopant Ion Concentration

The simulation model for determining the absorption coefficient with different ion concentrations is shown in Figure 4.3. In this model, power of the continuous wavelength (CW) laser is set to -20 dBm, and input wavelengths are varied from 1450 nm to 1650 nm to measure the absorption coefficient with different erbium ion concentrations. To determine the absorption coefficient value, two different EDF lengths (5m and 0.5m) have been chosen and the corresponding output powers are measured for each length. Then the measured output powers are used to determine the EDF absorption coefficient. In OptiSystem simulation tool, the absorption coefficient for the EDF can be measured using a simple relation [87]:

$$\alpha(\lambda) = \frac{P_{out}(\lambda, L = 0.5m) - P_{out}(\lambda, L = 5m)}{5 - 0.5} \quad (4.1)$$

Where,$P_{out}(\lambda, L = 0.5m)$, $P_{out}(\lambda, L = 5m)$ represent the output power measured for 0.5 m and 5 m EDF length, respectively.

During the absorption coefficient measurement, other physical parameters of the EDF (erbium metastable life time, fiber core radius, erbium doping radius, and NA) are kept same, as given in Table 4-3.

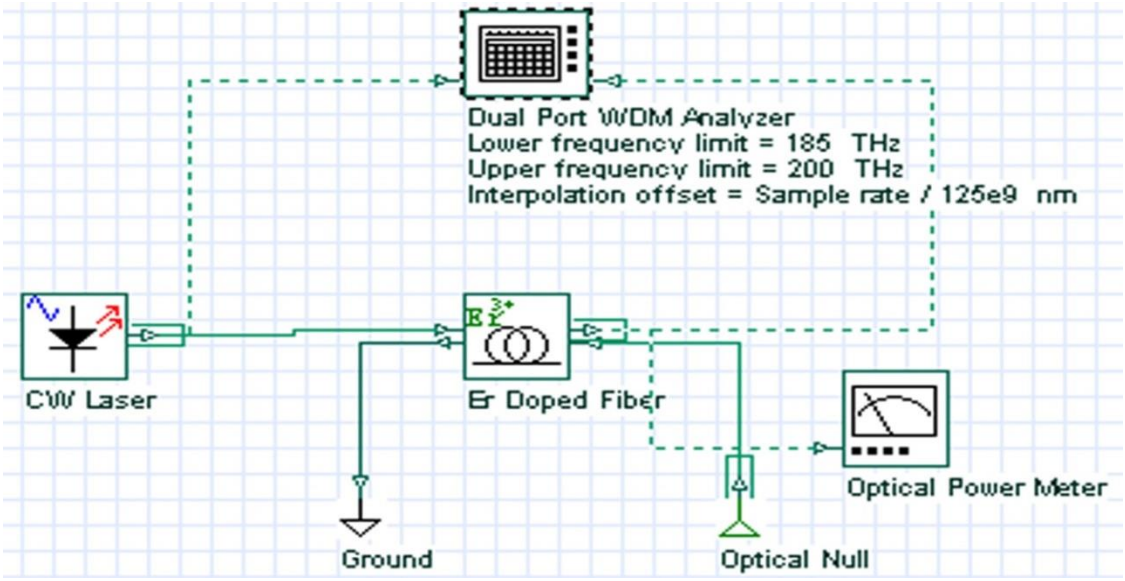

Figure 4.3: Simulation model for determining EDF absorption coefficient [87].

4.1.5 Er^{3+}- Er^{3+} Interaction Effects on EDFRL Performance

A typical forward pumped fiber ring laser configuration is shown in Figure 4.4, and the corresponding simulation model is shown in Figure 4.5. This laser configuration is simulated using OptiSystem Version 13 to observe the Er^{3+} - Er^{3+} interaction effects on the laser tuning performances. Here, a diode pump laser is used to pump the EDF via an ideal WDM multiplexer with pump power of 20 mW emitting at 980 nm. An ideal optical isolator is also used to make unidirectional lasing operation. The lasing wavelength is determined by the intra-cavity transmission type filter with 0.1 nm bandwidth. The lasing

wavelength is varied by changing the central wavelength of the intra-cavity filter and lasing output is observed in Optical Spectrum Analyzer (OSA) via 90: 10 output coupler.

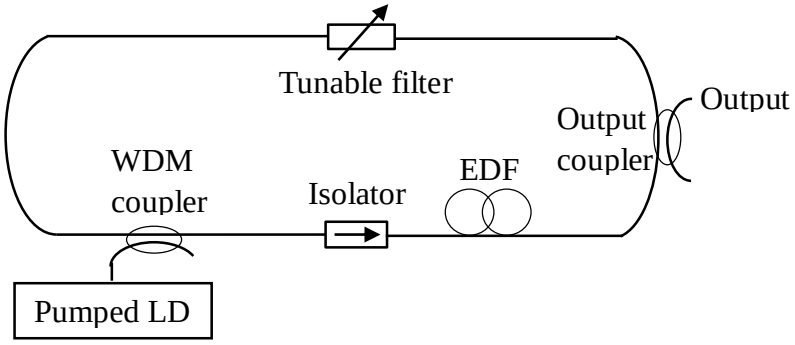

Figure 4.4 Erbium doped fiber ring laser using forward pumping

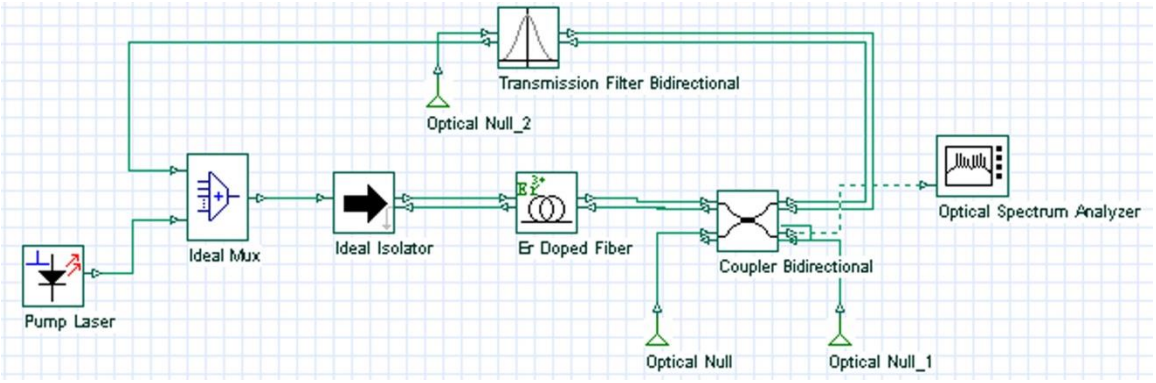

Figure 4.5: Simulation model EDFRL

For determining the ion-ion interaction effects on the lasing performances, different ion-ion interactions parameters have been set in the simulation tool and performances data are recorded via OSA. The parameters used in the EDF performances analysis are kept same for the EDFRL tuning range analysis to make a comparison.

4.2 Simulation Model of EDFA with Different Pumping Configurations and Wavelength

To investigate the effect of pumping wavelength and configuration, a simple erbium doped fiber amplifier (EDFA) is designed with 10 m long EDF, and excited state ions or population inversions distribution are analyzed along the fiber. For this analysis we have chosen VPIphotonicsComponentMaker version 9.3 simulation tool, which offers comprehensive design environment for modeling, optimization, and design of fiber based devices [88]. As for example different EDFA and EDFL configuration can be esaily designed using this simulation tool. It has C+L band EDF, which is required to design widely tunable EDFRL. Moreover, its special singnal analyzer tool allow us to investigate the internal and external behaviour of the components. Therefore, we have chosen this software to investigate the population inversion (internal behavoir of EDF) along the EDF.

4.2.1 Forward Pumped EDFA Configuration

The forward pumped EDFA configuration, as shown in Figure 4.1, is modeled by the VPIphotonicsComponentMaker version 9.3. The corresponding simulation model of Figure 4.1 is presented in Figure 4.6. The main objective of this simulation is to analyze the excited state ion percentage or population inversion. Therefore, input power has been set to 0 mW. To excite the erbium ion to the uper energy level, the pump power is coupled to the EDF via Wavelength Division Multiplexing (WDM) coupler. The excited erbium ion percentage or population inversion is then investigated in the signal analyzer tool of the VPIphotonics.

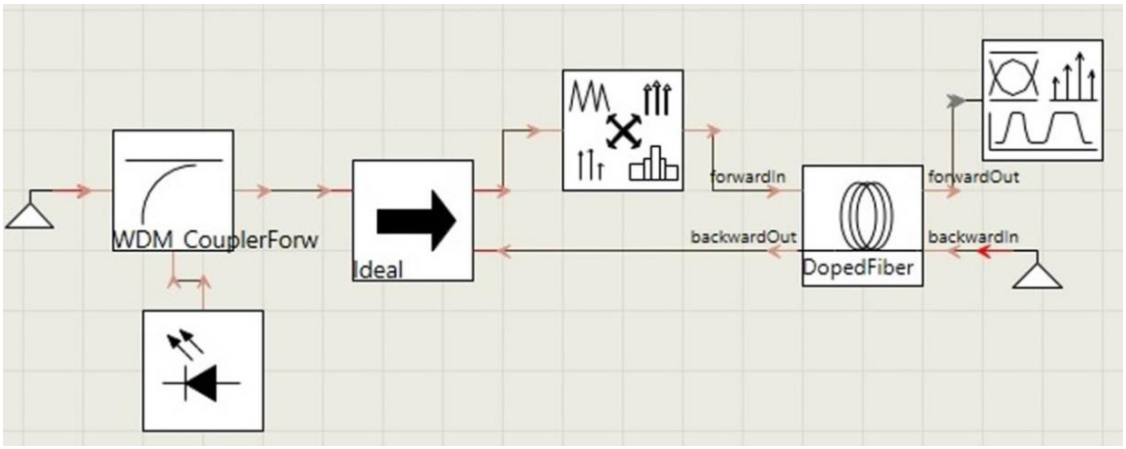

Figure 4.6: Simulation model of forward pumped EDFA to investigate the population inversion.

4.2.2 Backward Pumped EDFA Configuration

Backward pumped EDFA configuration and its corresponding simulation model is shown in Figure 4.7 and Figure 4.8, respectively. The difference between the forward and backward pumped EDFA diagram is the direction of the pumping and signal propagation. In the backward pumped EDFA configuration, pump and input signal are travelled in the opposite direction. Similar to the forward pumping configuration the input signal power is set to 0 mW for population inversion investigation.

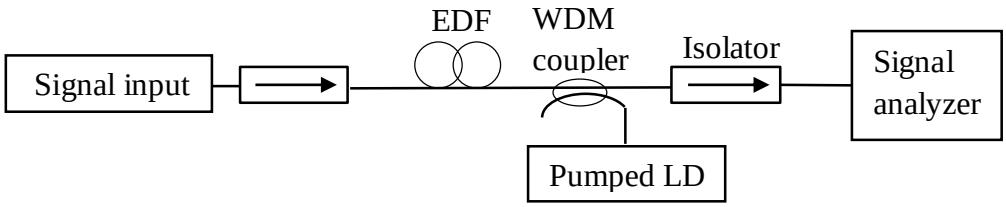

Figure 4.7: Backward pumped EDFA to investigate the population inversion along the EDF

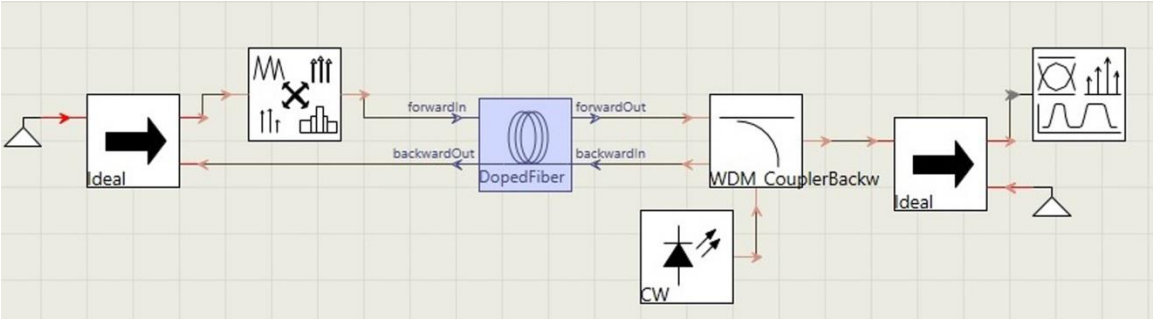

Figure 4.8: Simulation model of backward pumped EDFA to investigate the population inversion along the EDF.

4.2.3 Bi-directionally Pumped EDFA Configuration

Bi-directionally pumped EDFA configuration and its corresponding simulation model is shown in Figure 4.9, and Figure 4.10, respectively. In this case, the pump signal is coupled from the both end of the EDF. Bi-directional pumping or dual pumping configuration combines the forward and backward pumping signals in the EDF.

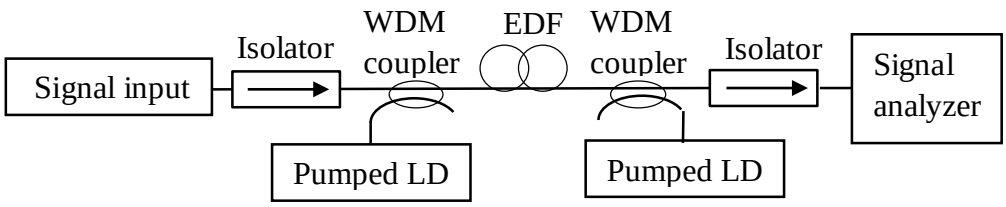

Figure 4.9: Bi-directionally pumped EDFA to investigate the population inversion

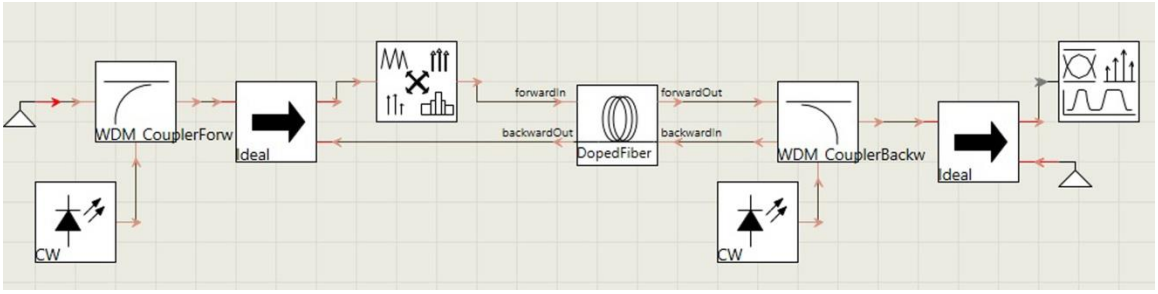

Figure 4.10: Simulation model of bi-directionally pumped EDFA to investigate the population inversion

4.3 Simulation Model of Widely Tunable EDFRL

For the determination of the pumping configuration effect on the tuning range, forward and bidirectionally pumped EDFRL is simulated using VPIphotonicsComponentMaker (version 9.3) simulation tool. Forward pumped erbium doped fiber ring laser configuration, and it coresponding simulation model are shown in Figure 4.4 and Figure 4.11, respectively.

In this configuration, different EDF lengths (20, 30, 50, and 80 m) of (C+L) band have been used to observe the effect of active fiber length on the tuning range. In the simulation model, the EDF is pumped through a WDM coupler by a laser diode (LD) source emitting at 1480 nm. The average pump power of the diode laser is set to 85 mW, and an isolator has been placed in the cavity to ensure unidirectional operation of the ring laser. An intracavity band pass filter is used to determine the lasing wavelength and lasing output is monitored at signal analyzer tool of VPIphotonics, which works as an optical spectrum analyzer (OSA). The lasing output is taken via 10% output coupler.

Then, the central wavelength of the pass band filter is varied and tuning range is observed for the different active fiber length.

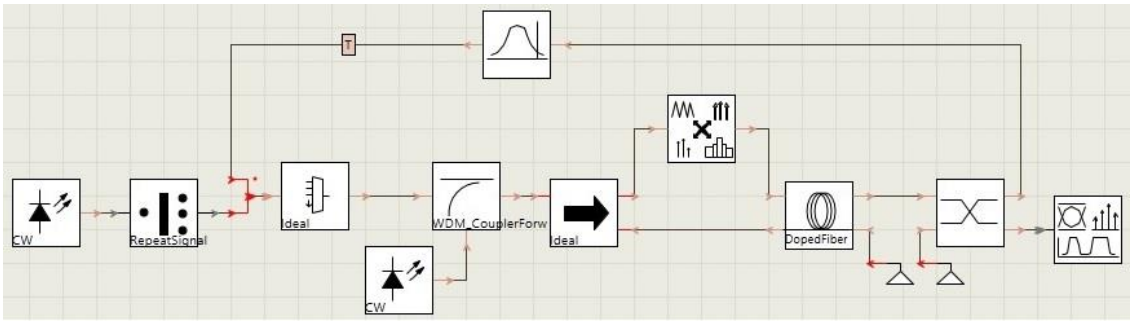

Figure 4.11: Simulation model of forward pump EDFRL.

For analyzing the bidirectional pumping effects on the tuning range, the simulation setup has been modified according to Figure 4.12, and the resultant simulation model is presented in Figure 4.13. Here, two pump laser diodes and isolators are used for bidirectional pumping and unidirectional laser operation, respectively. To determine the optimal EDF length, EDF lengths are varied from 10-80 m. For each EDF length, lasing outputs are monitored in the signal analyzer.

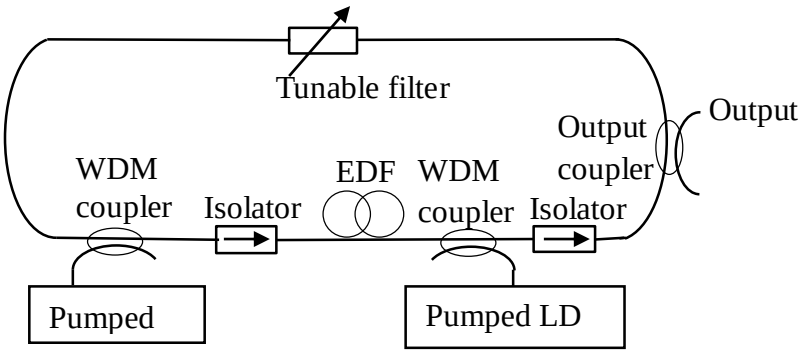

Figure 4.12: Erbium doped fiber ring laser using bidirectional pumping.

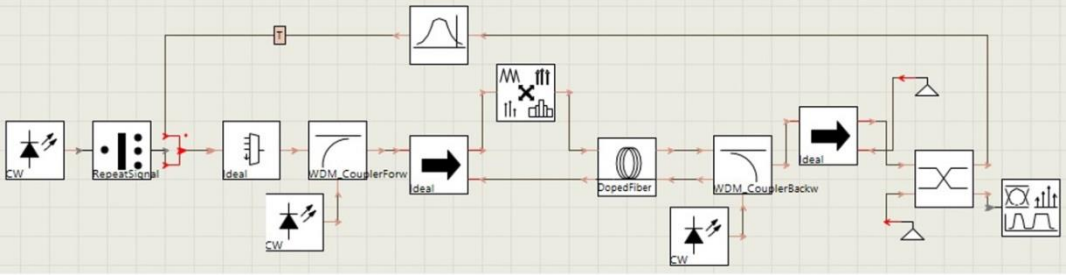

Figure 4.13: Simulation model of bi-directionally pumped EDFRL.

In addition to the tuning range analysis, we also investigated the effect of coupling ratio, intra-cavity loss, and pumping power on the tuning range. For all the investigations, we have used the bidirectional pumping configuration with optimal EDF length (in our case it is 50 m). For coupling ratio effects on the tuning range, we have set the output coupling ratio value to 0.1, 0.3, and 0.6 and observe the lasing output on the signal analyzer. For the intra-cavity loss effects, we have increased the isolator insertion loss from 1 - 4 dB and observe the lasing perfromance. Similarly, the pump power effects are investigated by changing the LD power level. We have set the power level of LD to 40 mW, 50 mW, 85 mW, and 150 mW and observe the tuning range.

4.4 Experimental Configurations of EDFRL

Using the existing lab equipment, we have designed two experimental setups to investigate the coupling ratio, and intra-cavity loss effect on the tunability of EDFRL. In our lab, there is a C-band EDFA (manufactured by Amonics Limited) which is pumped by an atuomated current contolled (ACC) LD emitting at 980 nm. It has two isolator to ensure unidirectional operation. We have used this amplifier to design the EDFRL configuration, which is shown in the Figure 4.14.

4.4.1 Coupling Ratio Effects on the Tuning Range of EDFRL

For investigating the coupling ratio effects, we have used 10% and 50% output coupler in the fiber ring laser cavity and recorded the lasing output using YOKOGAWA (AQ6370C) OSA, which has 0.01 nm resoution. For changing the lasing wavelength of the ring cavity, we have used Micron Optics FFP tunable filter. The transmission wavelength of the tunable filter is changed by applying DC voltage across its terminal. By applying around 18 V the central wavelength can be changed upto one FSR. FSR, and fineness of this filter are 113 nm, and 2176, respectively. As the lasing wavelength and output lasing power is dependent on the polarization of cavity light, therefore we have used a polarization controller to adjust the state of the polarization (SOP) of the cavity light.

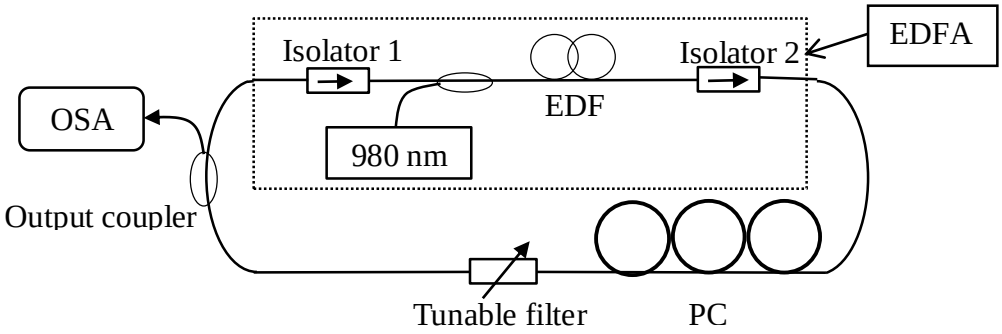

Figure 4.14: Experimental EDFRL configuration

4.4.2 Intra-cavity Loss Effects on The Tunability of EDFRL

For investigating the intra-cavity loss effect, we have used the same configuration as shown in Figure 4.14. Here we have used an aditional digital variable attenuator (VA), manufactured by OZ Optics Limited, in the fiber ring cavity to introduce loss. This VA can introduce loss for 350 nm-2050 nm wavelength range. In our configuration, we have used only the insertion loss of the VA, which is 0.97 dB at 1550 nm wavelength. We have monitored the lasing output for two different conditions: without additional intra-cavity loss, and with aditional cavity loss of 0.97 dB.

CHAPTER 5

RESULTS AND CONCLUSION

In the first part of this chapter, EDF (acts as a gain media of EDFL) performances in terms of doping radius, doping concentrations, and ion-ion intreaction are presentated. Following this, detrimental ion-ion interaction effect on the tuning range of EDFRL are described. Before presenting the widely tunable EDFRL tuning range, EDF perfromances have again been presented in terms of excited state ion percentage or population inversion. Then, widely tuanable EDFRL tuning perfromances have been analyzed in terms of active fiber length for both forward and bidirectional pumping configuration. From these tuning range analysis, we have concluded that bi-directionally pumped EDFRL provide the wider tuning range (about 120 nm for an optimized EDF length). Then coupling ratio, intra-cavity loss, pumping power effects on the tunability are presented. Finally, we have described the experimental results of coupling ratio, and intra-cavity loss effects on the tuning range of EDFRL.

5.1 Simulation Results

5.1.1 Dopant Radius Effects on EDF Performance

For the given data in Table 4-1, The EDFA gain performances have been presented in Figure 5.1 for different doping radius. For the above mentined simulations, three different pump powers (20 mW, 25 mW and 30 mW) have been used for observing the pump power effects in the EDFA gain. For each pump power, gain reaches the maximum value when the doping radius is 0.8 μm, which is the optimal value for the given data. If the

doping radius is increased or decreased further from this optimal point the gain performance decreases. If the doping radius is increased, the pumping power goes below the threshold value in the outer region of the EDF core. Therefore, erbium ions situated around the core-cladding boundary create an absorption region, as explained in Figure 2.9, and degrade the EDFA performance.

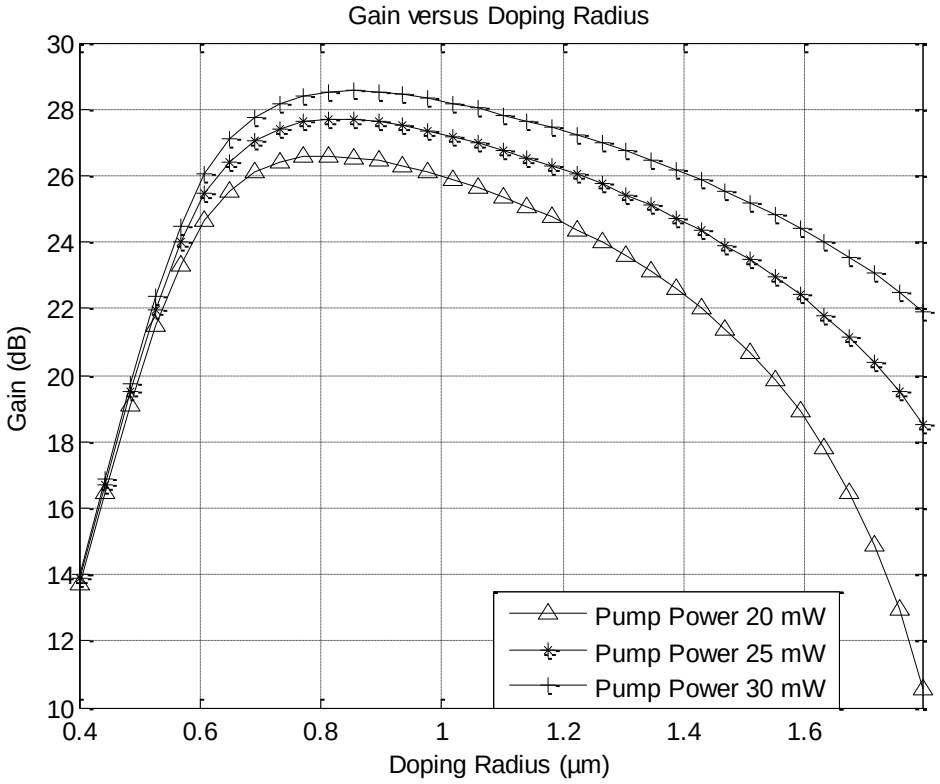

Figure 5.1: EDFA gain with different doping radius

Increasing pump power can reduce the number of absorbing ions from the core-cladding boundary edge and slow down the gain decreasing slope. On the contrary, reducing the doping radius from the optimal value will introduce the up-conversion effects, as explained in section 2.8 and 2.9, and decrease the gain performance.

For the comparison of the EDFA gain spectrum, different doping radius (0.6 μm, 0.8 μm and 1.0 μm) have been set in the simulation tool. For the given data in Table 4-2, the best gain spectrum is achieved for the optimum doping radius (0.8 μm), as shown in Figure 5.2. As the doping radius increases or decreases further, the EDFA gain performance degrades. Increasing the doping radius from the optimal value will increase the number of absorbing ions near the core-cladding interface and reduce the gain performance.

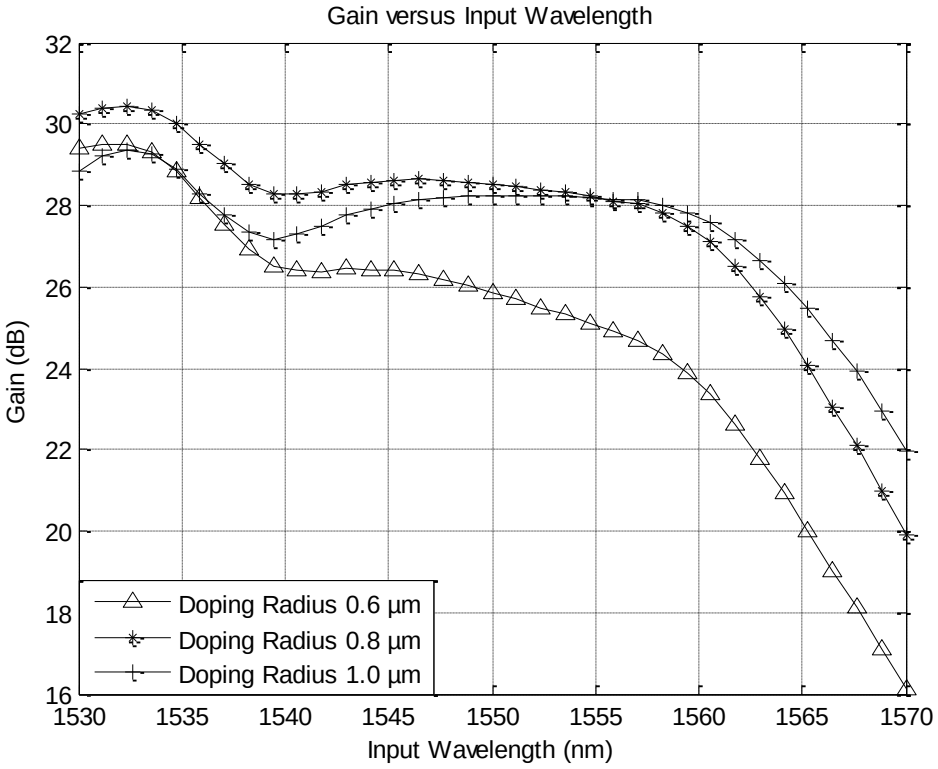

Figure 5.2: EDFA gain spectra with different doping radius

On the other hand, if doping radius is decreased from the optimal value, erbium ions will come closer and interact with each other. Due to this interaction, they will transfer and exchange energy with each other, which will reduce the excited state populations, as

explained in section 2.8 and 2.9. Therefore, gain performance will degrade, if doping radius is decreased from the optimal value.

5.1.2 Dopant Concentration Effect on EDF Length

Here, the EDFA gain performance is presented by varying the Er^{3+} concentrations. The gain performance of the EDFA with different Er^{3+} concentrations is shown in Figure 5.3.

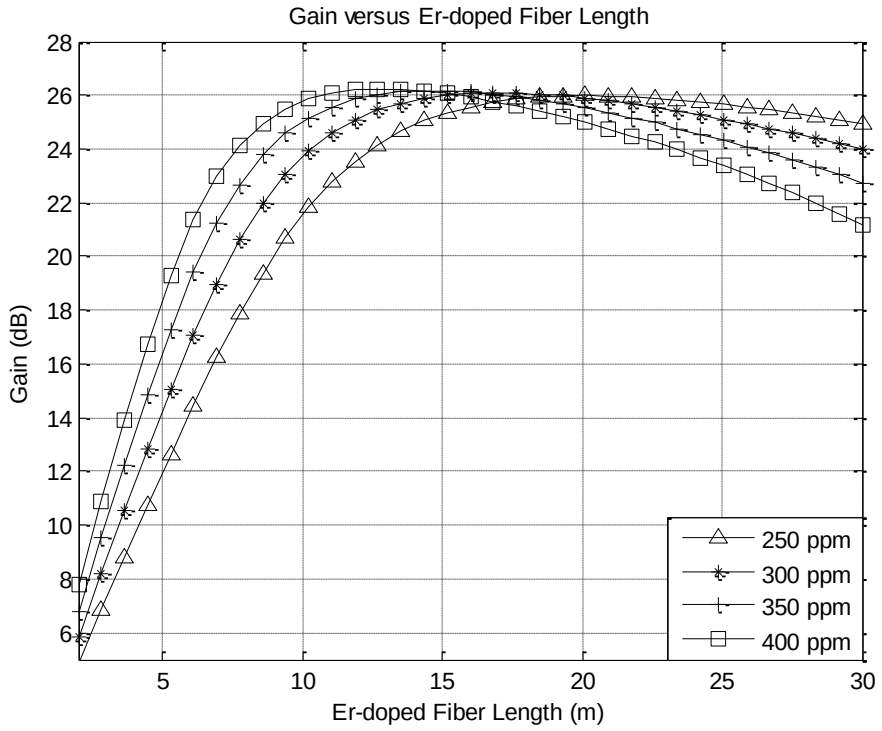

Figure 5.3: EDFA performance for different Er^{3+} ion concentrations

As the concentrations of the dopant ion are increased, shorter length fiber can provide higher gain. However, after a certain length the gain decreases with the increase of EDF length. This happens because the given pump power is not sufficient enough to invert the populations in the far end of the EDF, where the pump power goes below the threshold and Er^{3+} absorbs the signal energy. This problem can be solved by increasing the pump power, but sometimes it crosses the practical limit of pumping laser diode. In addition,

certain application like fiber laser, which have the potential to become compact integrated sources of ultra-fast fiber optic communication systems, requires short length fiber to provide high gain. Though higher dopant concentration is helpful in desiging compact integrated photonic devices but the EDF performance is degraded due to ion-ion interaction process. In the following section, detrimental effects of ion-ion interaction are presented for EDFA and EDFL.

5.1.3 Er^{3+}- Er^{3+} Interaction Effects on the EDFA Performance

Doping concentration beyond a certain limit degrade the EDFA performance via the upconversion mechanisms such as homogenous upconversion (HUC) and inhomogenous upconversion (IUC). For investigating the upconversion effect in the EDFA, we have selected 13 m long EDF with 400 ppm dopant ion concentrations and simulated the gain performances with different upconversion effects. The best performance of the EDFA is obtained when upconversion mechanisms are ignored, as shown in Figure 5.4 by dotted line. As we know, the EDFA performance decreases when the HUC effect is taken into consideration. The HUC effects on EDFA performance is shown by the solid line with plus (+) symbol. For IUC, the performance of EDFA depends on the relative number of clusters and number of ions per cluster. As the numbers of ions in the cluster are increased, the EDFA performances decrease accordingly. In Figure 5.4, we have used dashdot, dashed, and black solid lines to represent IUC interaction effects with 2, 6 and 10 ions per cluster, respectively. The distance between the interacting ions in the IUC process is much closer than the HUC process. Therefore, EDFA shows the much degraded performances in IUC process than the HUC. Combination of both HUC and

IUC in the simulation provides the cumulative effects of upconversion process. The worst performance of the EDFA is obtained, when the combined effects are taken into account.

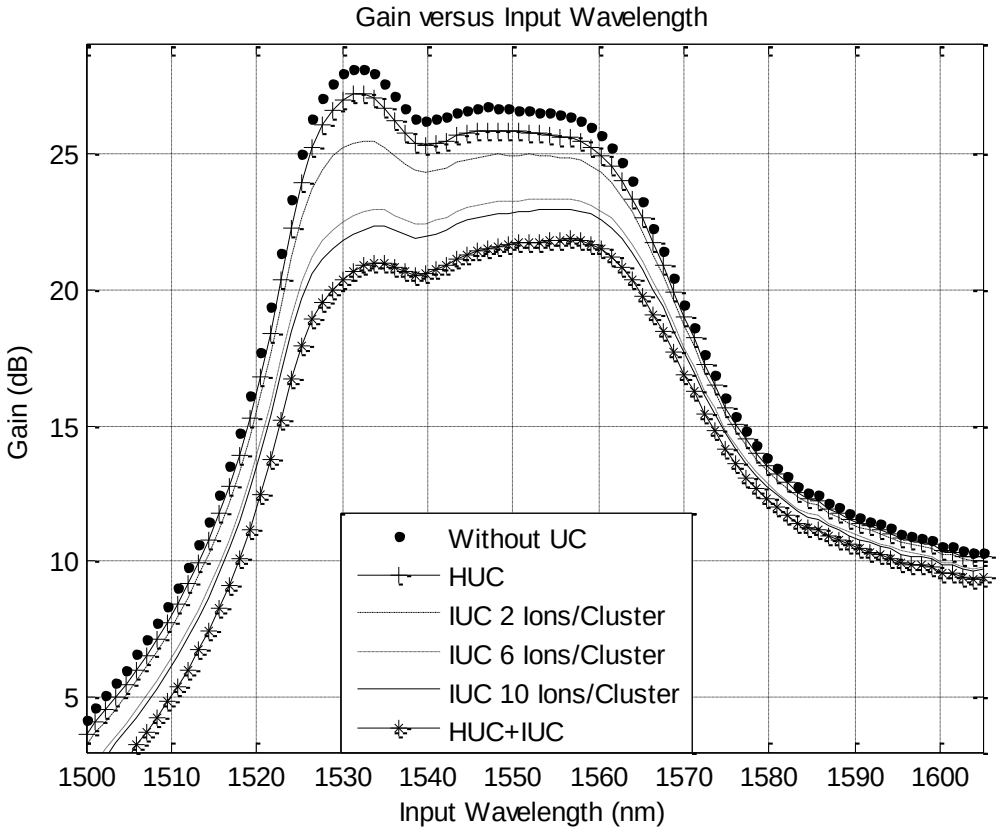

Figure 5.4: EDFA gain profile considering upconversion effects.

The combined effect of upconversion on the EDFA performance is shown by the solid line with asterisk (*) symbol. Here, the effects of IUC with 10 ions per cluster and HUC with upconversion coefficient 15 exp (-24) m^{-3}/s are combined.

5.1.4 EDF Absorption Characteristics

The absorption characteristic of EDF with different ions concentrations is shown in Figure 5.5. As the dopant ion concentrations are increased, the signal absorption increases for the entire wavelength starting from 1450 to 1650. Moreover, there is a

dominant absorption region near 1530 nm, where the EDF absorption is the highest. Therefore, lasing output power will be affected due to high absorption at 1530 nm.

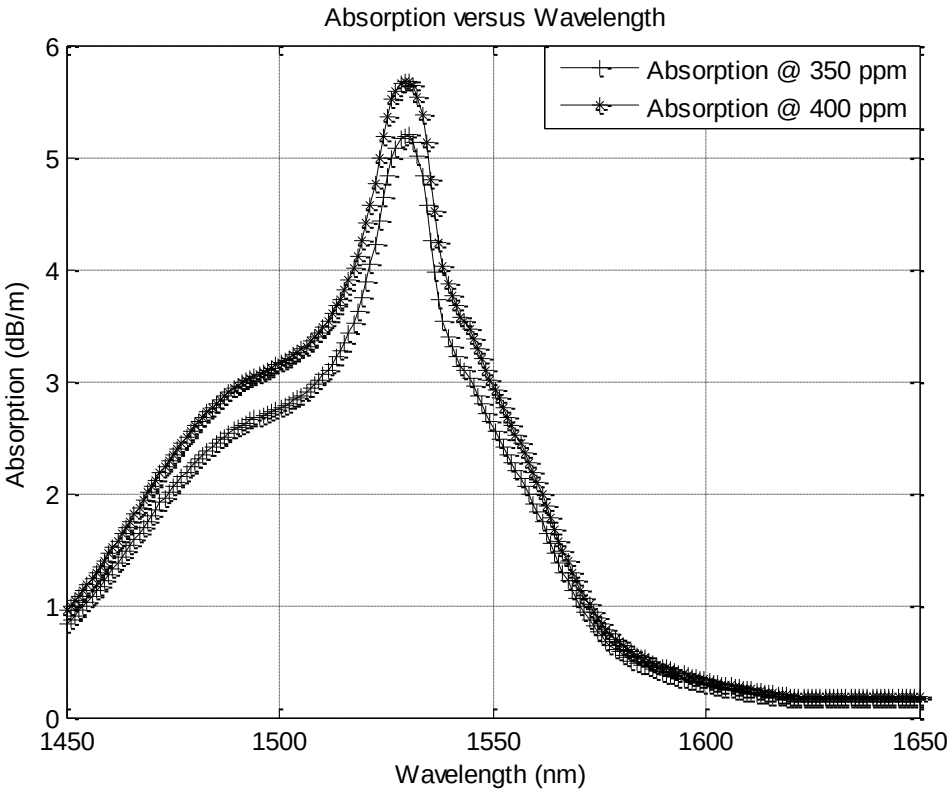

Figure 5.5: EDF absorption characteristics

5.1.5 Er^{3+}- Er^{3+} Interaction Effects on the EDFL

The lasing wavelength versus output power variation is shown in Figure 5.6. Simulation results show that EDFRL provide the best performance, if the ion interaction processes are not considered. However, introduction of ion-ion interaction process decrease the lasing output power. The effect of HUC process on the lasing output power is not that dominant. On the other hand, as the number of ions per cluster is increased the lasing output power decreases accordingly due to ion-ion interaction process, as explained in section 2.8 and 2.9.

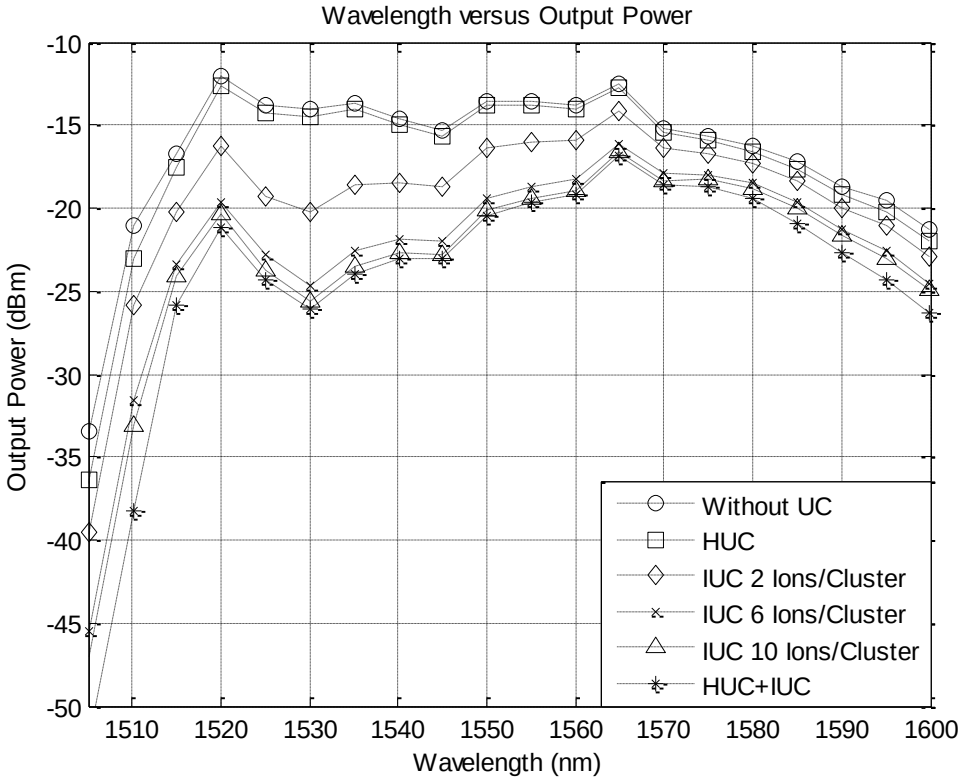

Figure 5.6: EDFL performance with 350 ppm doping concentration

The most dominant effect on the lasing output power is observed in the 1530 nm region. The lasing output power around 1530 nm wavelength region decreases more abruptly than the other wavelength region. This happens due to high absorption around 1530 nm region. From the absorption characteristics of EDF, it is observed that 1530 nm signal is highly absorbed and consequently EDFL provides the low output power at 1530 nm. The worst lasing output power is observed when both HUC and IUC ion interaction process are considered.

For the comparison purpose, the lasing performance has been evaluated for the different dopant ion concentrations. Lasing wavelength versus output power variation for 400 ppm ion concentration is shown in Figure 5.7. As the erbium ion concentrations increases from 350 ppm to 400 ppm, the absorption at 1530 nm increases, as explained in

Figure 5.5. Moreover, comparatively higher number of dopant ions decrease dopant ions separation. Therefore, ion-ion interaction effects are increased and comparatively low output power is observed for high dopant ion concentration. For the detailed comparative analysis, the best and worst performance of 350 ppm and 400 ppm are shown in Figure 5.8.

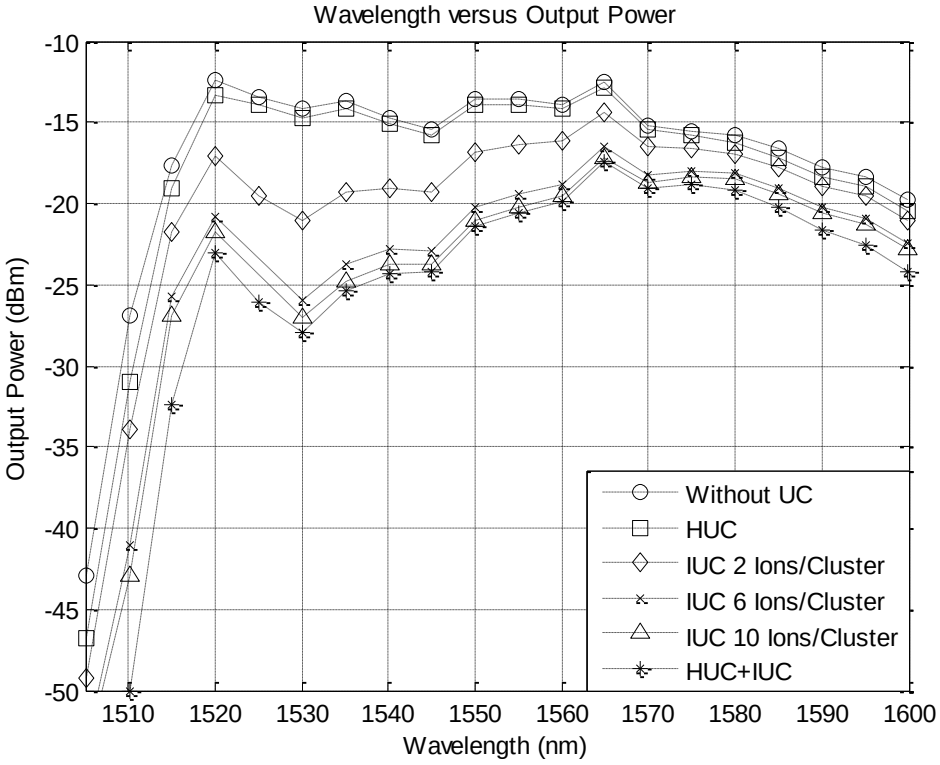

Figure 5.7: EDFL performance with 400 ppm doping concentration

Form the comparative analysis with different ion concentration, it is evident that high dopant concentration is advantageous for L band lasing. However, ion-ion interaction effects reduce the lasing output power around 1530 nm wavelength region due to high absorption. As the erbium ion concentration increases detrimental ion-ion interaction effects increase, which reduce the lasing output power and consequently reduce the tuning range of EDFRL.

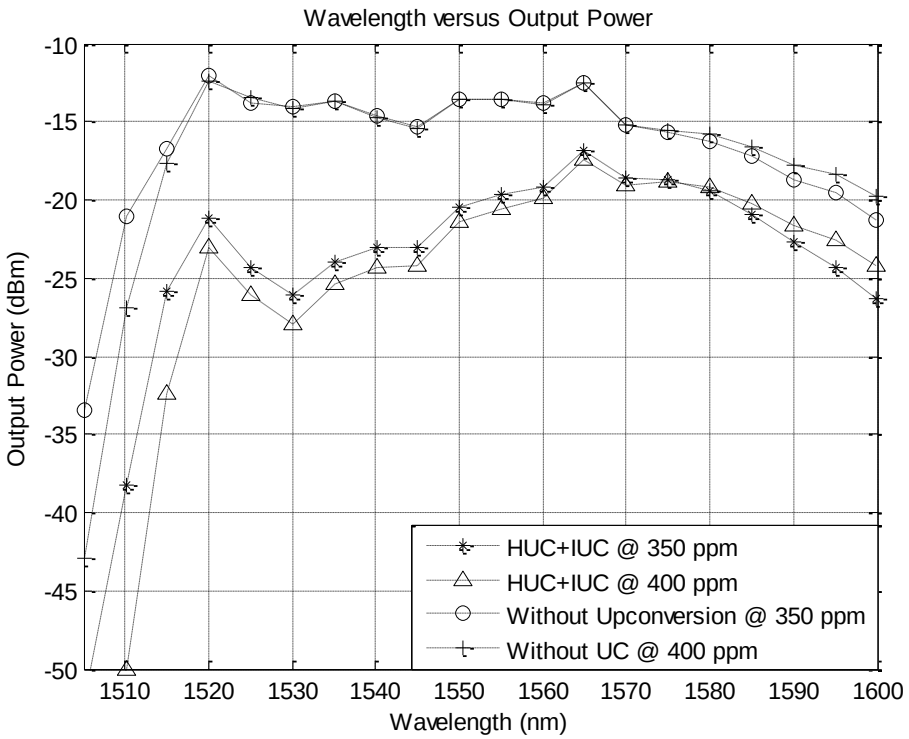

Figure 5.8: Comparative EDFL performance analysis with different ion concentration.

5.2 Population Inversion Simulation in EDF

5.2.1 Forward and Backward Pump Power at 980 nm

In Figure 5.9 and Figure 5.10 excited ions percentage (population inversion) versus EDF length is depicted for 980 nm and 1480 nm pumping, respectively. For the 980 nm pumping case, higher population inversion can be achieved with the shorter EDF length. However, population inversion decreases more rapidly with the increase of EDF length due to high absorption at 980 nm. This consequently reduces the quantum conversion efficiency and increase the threshold value of lasing.

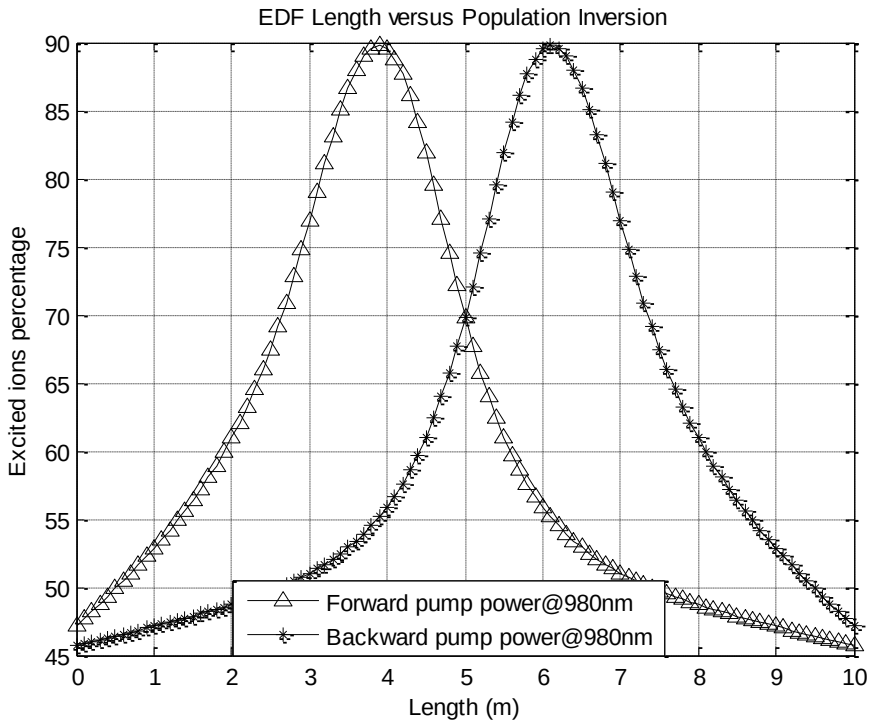

Figure 5.9: EDF length versus excited ions percentage (population inversion) for forward and backward pumping configuration at 980 nm.

5.2.2 Forward and Backward Pump Power at 1480 nm

For 1480 nm pumping case, longer EDF length can be used with equal pump power of 980 nm pumping. The evolution of population inversion for 1480 nm pumping is shown in Figure 5.10. For the same parameter, more than 50% population inversion can be maintained up to 8.5 m of EDF length. However, it is just above 6.5 m in 980 nm pumping. This is true for both forward and backward pumping configurations, but the only difference is shifting of the population inversion according to pumping direction. This characteristic of maintaining higher population inversion for longer EDF length is advantageous for L band amplifier or laser design, which requires comparatively longer EDF length.

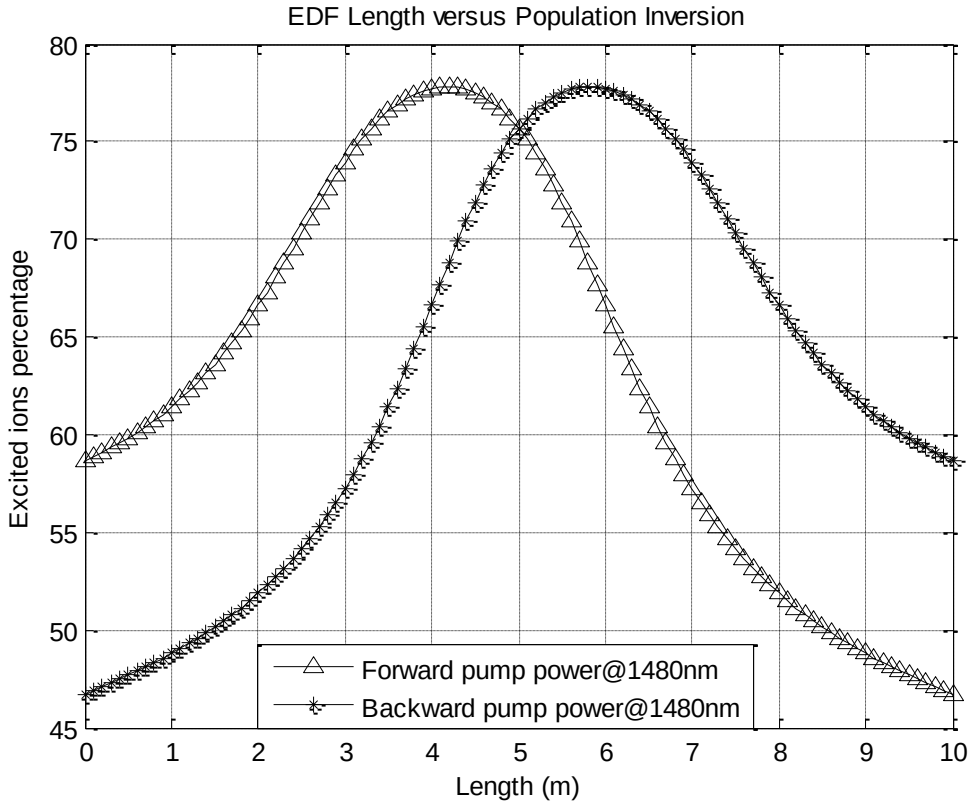

Figure 5.10: EDF length versus excited ions percentage (population inversion) for forward and backward pumping configuration at 1480 nm.

5.2.3 Comparison of Bidirectional and Forward Pump Power at 1480 nm

EDF length versus population inversion for forward and bidirectional pumping configuration is shown in Figure 5.11. For the forward pumping scheme, the population inversion is asymmetrically inverted along the EDF length. For the specific parameters used in the simulation, population inversion decay sharply at the far end of fiber. In general, the population distribution will follow the same trend for the other simulation parameters (i.e. pump power, and EDF length). However, for bidirectional pumping scheme, the population inversion is symmetrically distributed along the EDF. Therefore, it is likely that bidirectional pumping configuration will provide wider tuning range. This

configuration will help in reducing shorter wavelength absorption at the far end of the fiber. Moreover, threshold value, as shown in Figure 5.12, required for bi-directional pumping is smaller than forward pumping.

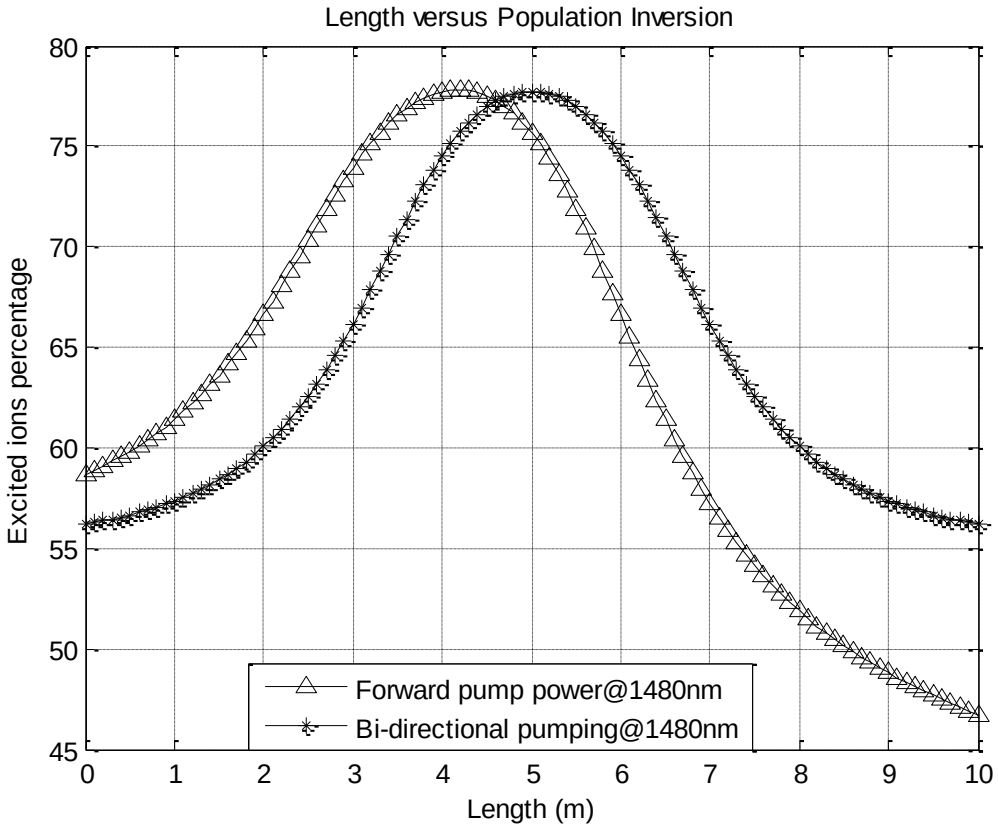

Figure 5.11: EDF length versus excited ions percentage (population inversion) for forward and bidirectional pumping configuration at 1480 nm.

Comparison of lasing threshold value for forward and bidirectional pumping configuration is shown in Figure 5.12. From the comparison it is found that threshold value decreases by around 44.44% for the bidirectional pumping configuration, which is advantageous for the wider tuning range. The threshold value comparison is done for the 1580 nm wavelength. However, the trend will be similar for the other wavelength.

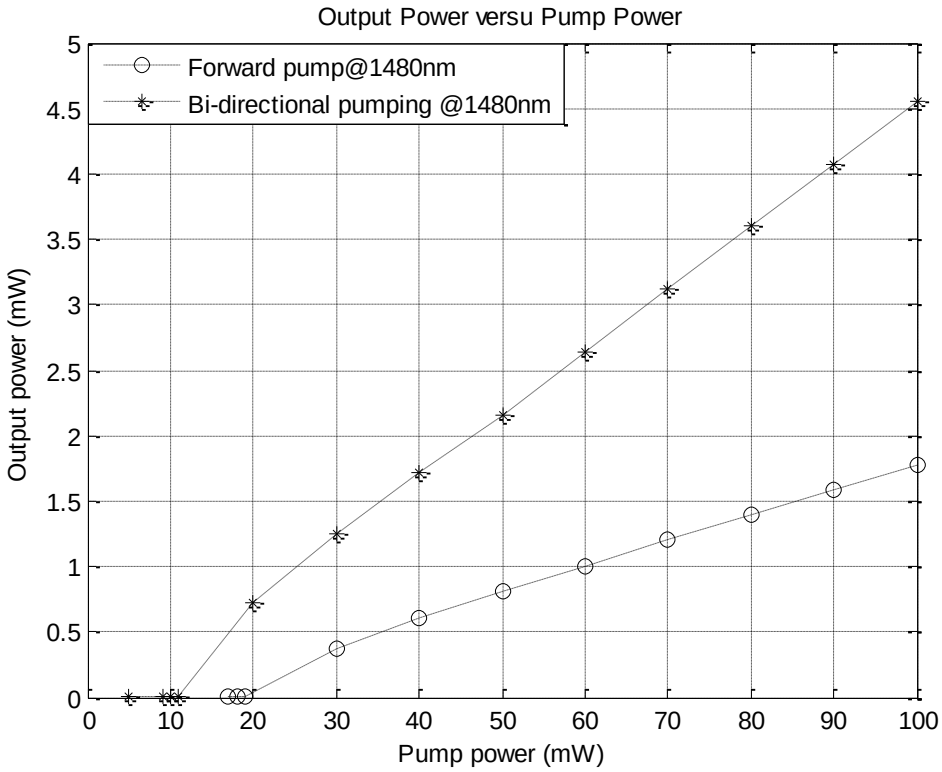

Figure 5.12: Threshold power of forward and bidirectional pumping at 1480 nm.

5.3 EDFRL Simulation Results Based on EDF Length

5.3.1 Forward Pumping and Tuning Range

The lasing wavelength versus output power for the forward pumping configuration is shown in Figure 5.13. Here the tuning range is shown as a function of EDF length. As the EDF length is increased, the tuning range is shifted to the longer wavelength band. This happens because of the gain shifting in the higher wavelength band of the EDF. If the EDF length is too short, it cannot lase in the longer wavelength region. On the other hand, too long EDF fiber cannot provide shorter wavelength lasing due to absorption of the shorter wavelength.

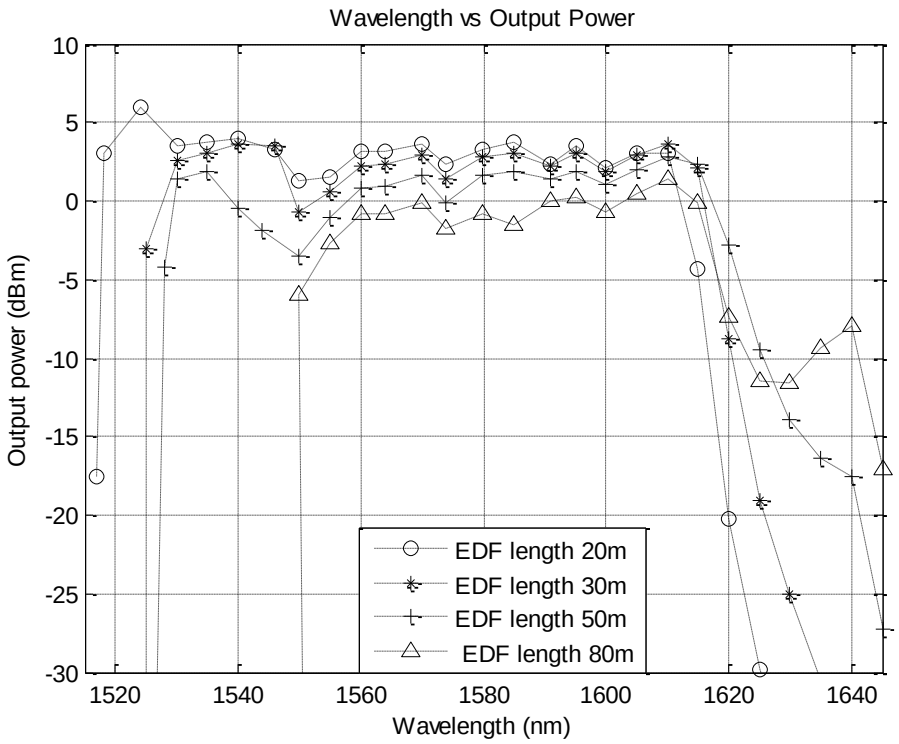

Figure 5.13: Output power versus lasing wavelength for forward pumping EDFRL.

Therefore, an optimized length is required for the wider tuning range. For the forward pumping configuration, 50 m EDF length provides the broadest tuning range 93 nm (1528-1620 nm). Moreover, lasing output power variation with the EDF fiber length is another noticeable point. For the shorter EDF length output power is higher due to high pump power conversion efficiency.

5.3.2 Bidirectional Pumping and Tuning Range

In Figure 5.14, wavelength versus lasing output power is presented as a function of EDF length for bidirectional pumping. In this case, lasing wavelength is also shifted to longer wavelength band with the increase of EDF length, and there is an optimal EDF length for which the tuning range is the widest.

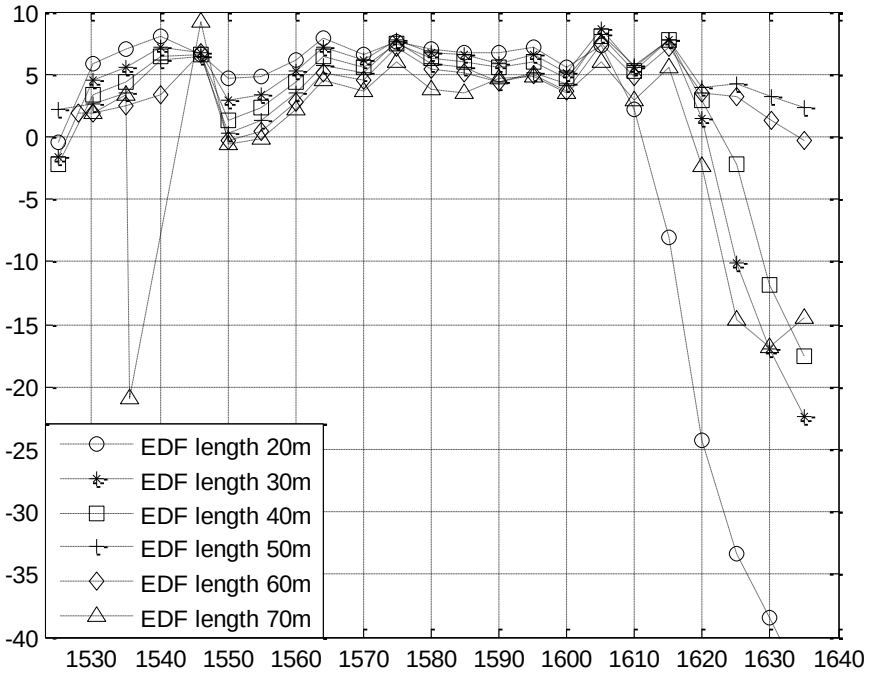

Figure 5.14: Output power versus lasing wavelength for bidirectional pumping EDRFL.

For the chosen parameters in the simulation, the optimal EDF length is 50 m and the corresponding tuning range is around (1525-1645 nm) 120 nm. This widest tuning range is achieved because of considering all the ideal components in the cavity. However, it will not be possible to obtain such wide tuning range with the experimental setup. In experimental setup cavity loss cannot be avoided for different cavity components, and this will reduce the tuning range. In this case lasing output power variation due to the EDF length variation is not that significant due to symmetrical population inversion along the EDF length. Moreover, the shorter lasing wavelengths are not absorbed at far end of the fiber up to certain EDF length. But, comparatively long EDF absorbed the shorter wavelengths and reduce the tuning range.

5.3.3 Tuning Range Comparison for Forward and Bidirectional Pumping Configuration

Finally, a comparison of tuning range for forward pumping and bidirectional pumping tuning is shown in Figure 5.15. The threshold value is smaller for the bidirectional pumping configuration, which provides the wider tuning range. It is clear from the simulation graph that bidirectional pumping provides wider tuning range than the forward pumping.

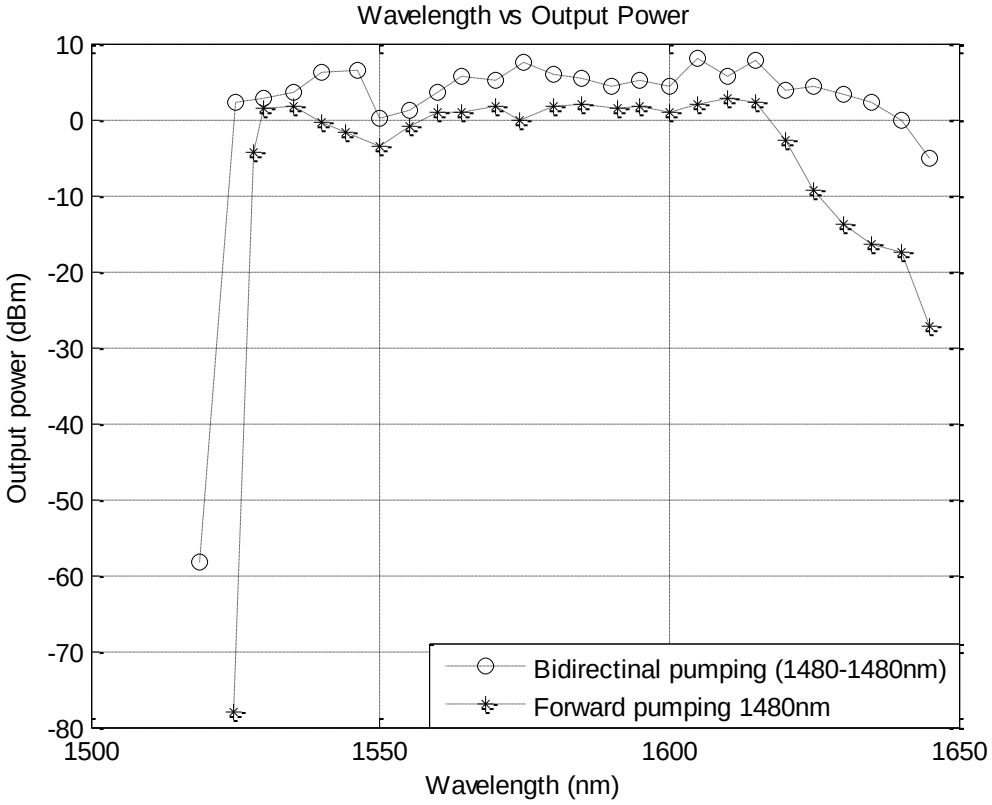

Figure 5.15: Tuning range comparison for forward and bidirectional pumping configurations.

5.4 EDFRL Simulation Results Based on Pump Power

The effect of pump power on the tunability of EDFRL is shown in Figure **5.16**. In this simulation, we have used four different pump powers (40, 50, 85, and 150 mW) to observe the effect of pump power. As the pump power increases the lasing output power increases due to high population inversion along the EDF length. Therefore, high lasing output power can be extracted from EDFRL with the high pump power. However, laser diode has a practical limit of pumping power.

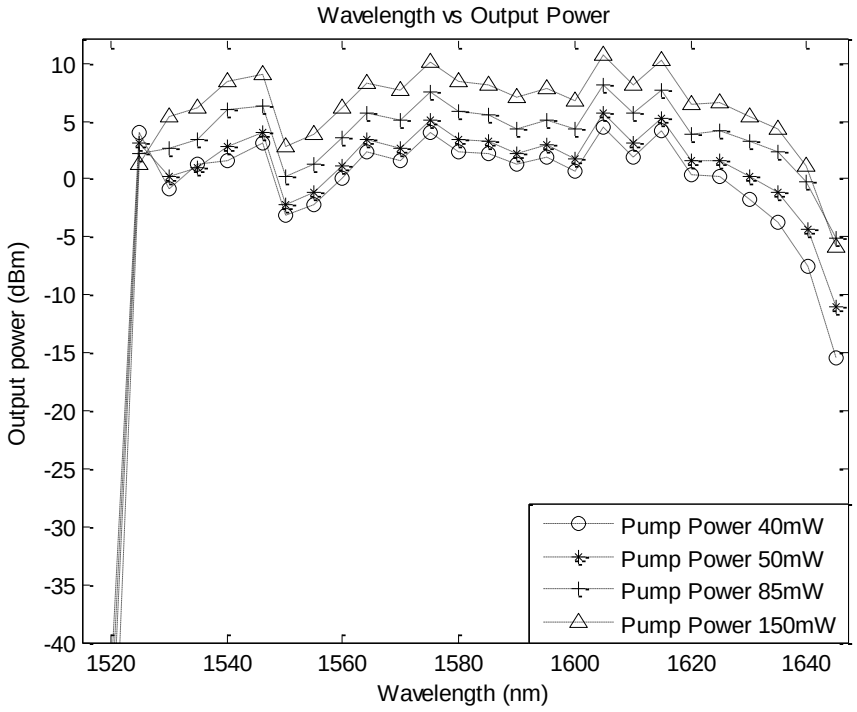

Figure 5.16: Effect of pump power on the EDFRL performance.

5.5 EDFRL Simulation Results Based on Intra-Cavity Loss

The effect of intra-cavity loss on the EDFRL tunability is shown in Figure **5.17**. To observe this effect, intra-cavity loss is varied and lasing output power is monitored on the signal analyzer. With 4 dB increase of the intra-cavity loss, we observe the 40 nm tuning range reduction from the longer wavelength region.

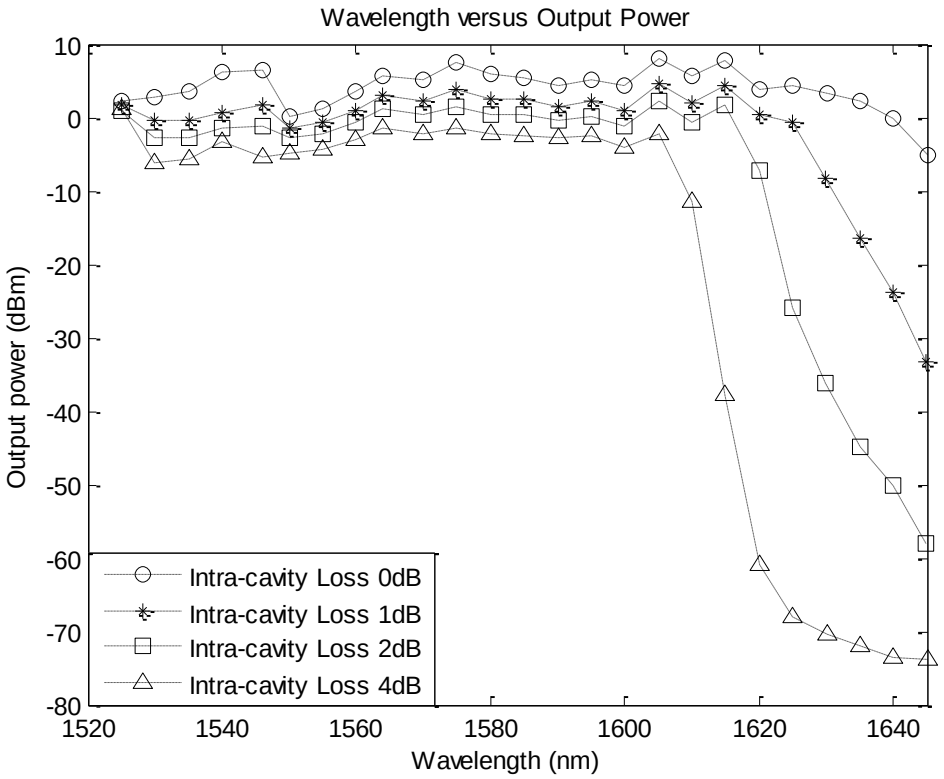

Figure 5.17: Effect of intra-cavity loss on EDFRL tunability.

Increasing the intra-cavity loss is equivalent to decreasing EDF length from the optimal one. Therefore, the long band lasing output power is affected rather than shorter wavelength with the increasing intra-cavity loss. Moreover, the lasing output power is decreased for all lasing wavelengths with the increase of intra-cavity loss. The effect of

intra-cavity loss on the tuning range stresses the need of reducing the intra-cavity loss, if the widest tuning range is desired from the EDFRL.

5.6 Simulation Results of EDFRL Based on Coupling Ratio

Effects of output coupling ratio on the tuning range and output power of EDFRL is shown in Figure 5.18. To investigate effects of output coupling ratio on the laser output power and tuning range , we have used three different output coupling ratio (0.1, 0.3, and 0.6). For this simulation, output pump power and EDF length have been fixed to 85 mW and 50 m, which is the optimal length to provide the widest tuning range, respectively.

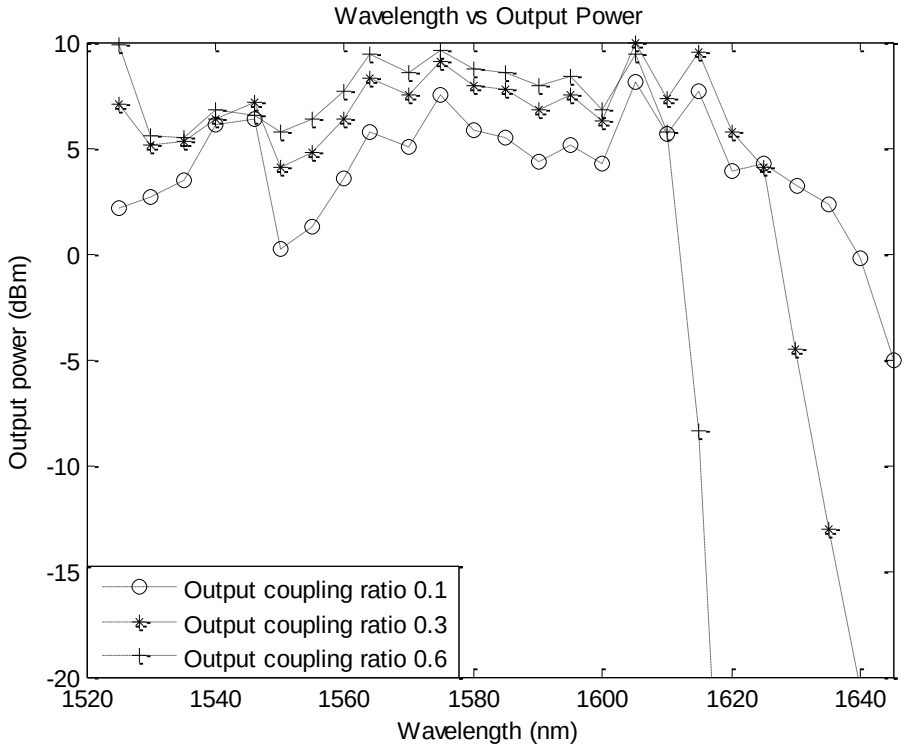

Figure 5.18: Effects of coupling ratio on the tuning range.

The simulation results show that laser output power increases as the output coupling ratio increases from 0.1 to 0.6. However, tuning range decreases with the increase of output

coupling ratio from 0.1 to 0.6. This happens due to smaller emission cross section of EDF at longer wavelength region as compared to the 1330 nm.

5.7 Experimental Results

We have demonstrated the performance of tunable EDFRL using an experimental setup, which is shown in Figure 4.14. The lasing wavelength of the EDFRL is selected by Micron Optics FFP tunable filter. This is done by varying the DC voltage across its terminal. Initially, we have set the central wavelength of tunable filter for the lowest wavelength lasing. Then, we have varied the applied voltage with a step of 0.5 V across its terminal to change the lasing wavelength. The output lasing line is monitored in the YOKOGAWA (AQ6370C) OSA via 10% output coupler. By using the PC, the state of polarization is controlled and lasing output is stabilised. Following this, stabilized lasing output is recored in the OSA. The superimposed lasing spectra of EDFRL is shown in Figure 5.19. We have gone through the following steps to obtain the superimposed lasing spectra of the tunable EDFRL. Firstly, we have selected the lowest lasing wavelength (1522 nm) of the laser cavity by applying appropriate (18 V) dc voltage across the tunable filter terminals. Then, we have changed lasing wavelength of the EDFRL by reducing the applied voltage across the tunable filter terminals with a step of 0.5 V. By doing so, we got the second lasing line (1524 nm). In this way, we have recorded all the possible lasing wavelengths of the tunable EDFRL and measured the tuning range. 1581 nm is the last lasing wavelength recorded using the experimental setup of EDFRL. The overall tuning range of the experimental setup is around 60 nm (1522 nm-1581 nm).

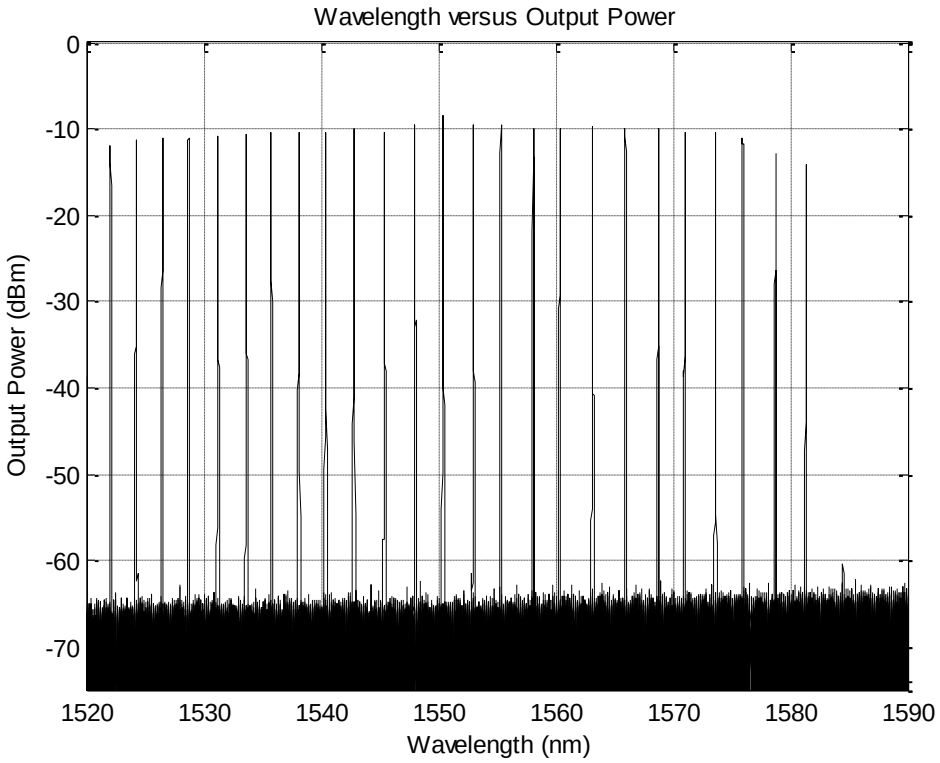

Figure 5.19: Superimposed spectra of EDFRL with 10% output coupling

5.7.1 Coupling Ratio Effects on Tuning Range

For investigating the coupling ratio effects on the tuning range of EDFRL, we have replaced the 10% output coupler by 50% output coupler and recorded the lasing spectra following the steps mentioned in section 5.7. Then, we have picked the maximum output power of each lasing wavelength for both (10% and 50% output coupler) cases. Following this, we have superimposed the tuning range performance of EDFRL with two different coupling ratios, as shown in Figure 5.20. If we increase the output coupling ratio from 10% to 50%, tuning range decreases for the longer wavelength region. The emission cross section of EDF in the longer wavelength region is smaller than the shorter wavelength region; therefore, tuning range decrease for the longer wavelength region. However, the lasing output power increases with the increasing coupling ratio.

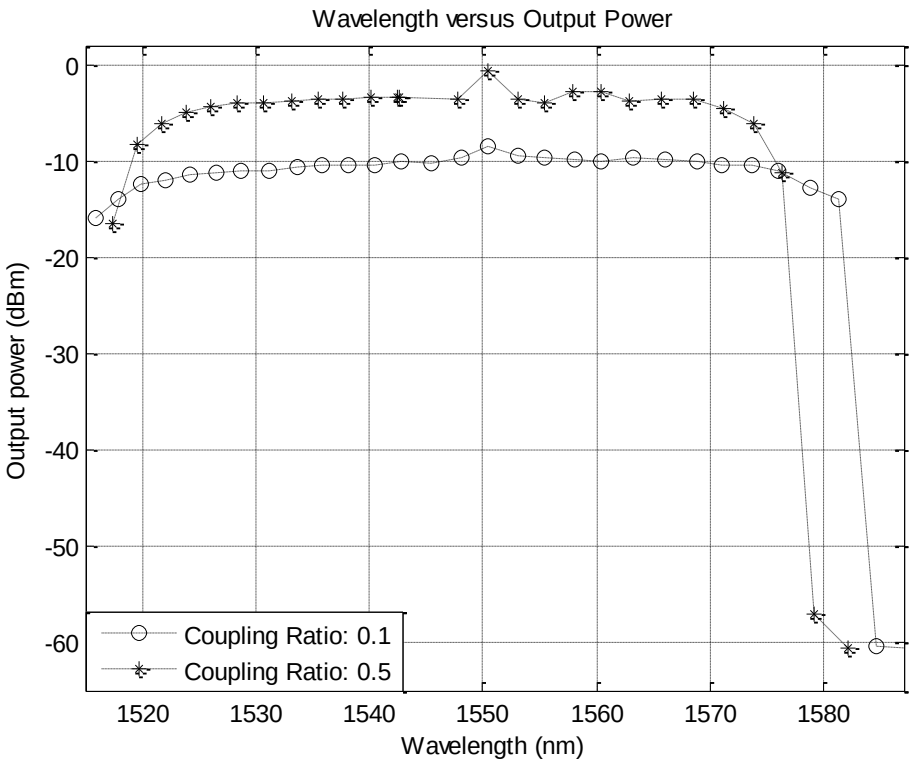

Figure 5.20: Effects of coupling ratio on the tuning range of EDFRL.

5.7.2 Intra-cavity Loss Effects on The Tuning Range

The intra-cavity loss effect on the tuning range is depicted in Figure 5.21. For this investigation, we have used 10% output coupler to monitor the lasing output. A variable digital attenuator is used in the cavity to increase intra-cavity loss and lasing output is recorded in the OSA. Without introducing intra-cavity loss, 60 nm tuning range is achieved with 10% output coupling. However, introduction of 0.97 dB loss in the cavity reduces tuning range by 15 nm.

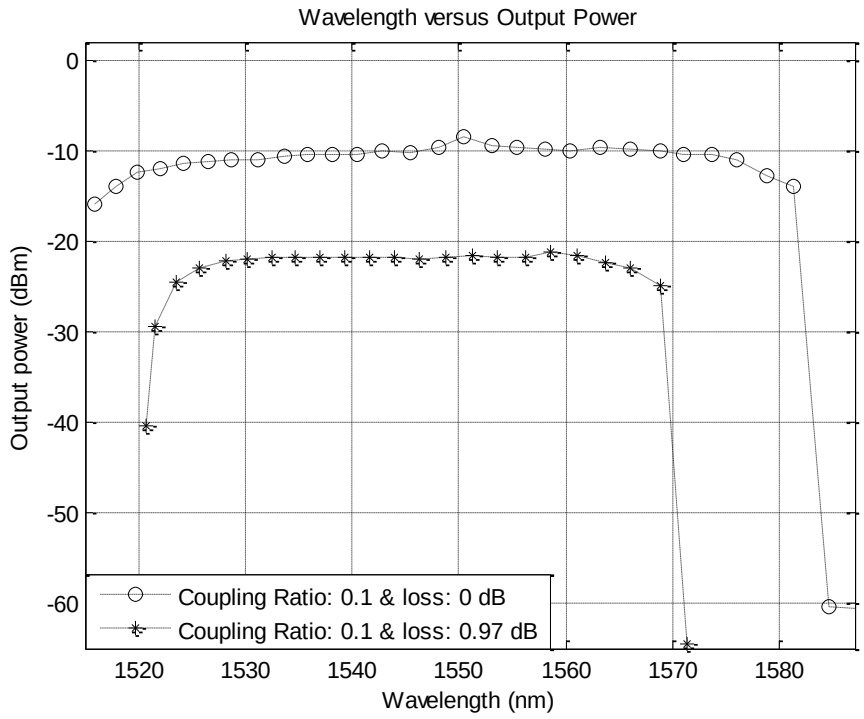

Figure 5.21: Intra-cavity loss effect on the EDFRL tuning range

If the intra-cavity loss is increased, the lasing threshold value will increase for some spectral region of EDFA gain profile. This increased threshold value subsequently reduces the tuning range. EDFA gain profile shows smaller gain in the shorter and longer wavelength region. Therefore, tuning range decreases for the shorter and longer wavelength region.

5.8 Conclusion and Future Research

The erbium doped fiber laser research have witnessed unprecedented growth and now become integral part of many photonic applications. Some distinguishing advantages of this laser such as high gain, compact cavity configuration, excellent heat dissipation capabilities, and compatibility with the communication fiber make them suitable over the solid state lasers. In the erbium doped fiber ring laser, erbium doped fiber act as the gain medium. Therefore, performance affecting factors of erbium doped fiber need to be understood for the efficint erbium doped fiber laser design. In this thesis, we have simulated the effects of doping radius, erbium ion concentrations, and ion-ion interaction effects on the erbium doped fiber pefromances. We have shown that an optimal doping radius is nessceary for the best gain perfromance of erbium doped fiber amplifier. Following this, we have shown the effect of ion concentration on the device length. Subsequently, ion-ion interaction effect is simulated by designing an erbium doped fiber amplifier and a tunable erbium doped fiber ring laser. It is found that erbium doped fiber amplifier and erbium doped fiber ring laser performance is reduced significantly due to ion-ion interaction process. Later, erbium doped fiber perfoamnce has been analyzed in terms of population inversion with an aim to design broadband tunable erbium doped fiber ring laser. From this analysis, we have concluded that 1480 nm pumping with bi-directional pumping configuration will be advantagious for designing widely tunable erbium doped fiber ring laser. Then, we have simulated our proposed wideband tunable erbium doped fiber ring laser. We have shown around 120 nm tuning range with erbium doped fiber length optimization. Finally, we have shown the effects of intracavity loss, coupling ratio, and pump power on the tunability via simulation and experimental setups.

However, we could not comapare our simulation and experimental results due to the limitations of our laboratory equipment.

During the study of this thesis, a number of points had been identified which could not be investigated due to the time constrain and limited laboratory facilities. The following points can be investigated for the future research.

1. Design experimental setups to analyze the ion-ion interaction effects on EDFA performances, and EDFRL tunability.
2. Design an experimental setup to validate our claim, bi-directionally pumped EDFRL provides the widest tuning range with 1480 nm pumping wavelength.

Appendix A

SIMULATION SOFTWARES

Fiber based photonic device design using experimental setups requires the access of latest components. Moreover, experimental design method is time consuming and costly. On the other hand, simulation tools provide the flexibilities of accessing the latest components. Moreover, different combinations of amplifier topologies and laser configurations can be designed to investigate the EDFA and EDFL performances. As for example, fiber with different doping concentrations, amplifier with different pumping configurations, lasers with different intra-cavity components can be designed. Therefore, use of an appropriate simulation tool before designing experimental setups would be an efficient method. In our thesis, we have used two optical communication system design softwares:

1. OptiSystem (version 13)
2. VPIphotonics (version 9.3)

A.1 OptiSystem

OptiSystem can be used in access network, dispersion management, optical amplifier, fiber laser, optical receiver, and optical transmitter design [87]. In this thesis, we have used this simulation tool for designing and analyzing EDFA and EDFRL performances. Graphical User Interface (GUI) of OptiSystem allows us to design almost any fiber amplifier and laser topology by using the wide range of doped and passive fibers, active

and passive components. GUI, as shown in Figure A.1, of this software contains the following three main windows:

1. Project layout
2. Dockers
3. Status bar

A.1.1 Project Layout

Project layout is the main working area where discrete components are inserted to design a specific simulation model. After inserting the discrete components, they are connected according to the proposed EDFA or EDFL configurations.

A.1.2 Dockers

Dockers provide the information of the current projects. It consists of three elements such as component library, project browser, and description.

A.1.2.1 Component Library

Component library contains the different group of components like optical sources and detectors, universal transmission fibers and doped optical fibers, optical amplifiers, signal visualizers, and passive devices. For designing a simulation model, different components are chosen from the component library and connected according to proposed configuration. Simulation parameters of the components can be changed by double clicking the component symbols. For each component, parameters are organized by categories. As for example, CW diode laser has five parameter categories such as:

1. Main (frequency, power, line width, and initial phase)

2. Polarization
3. Simulation
4. Noise
5. Random numbers

A.1.2.2 Project Browser

Project browser is used for organizing and navigating through the current project more efficiently. This browser also provides the list of components used in the current project.

A.1.2.3 Description

Status bar displays the useful hints of using OptiSystem. It is located just below the project layout window.

A.1.3 Simulation Run

To run the simulation, OptiSystem calculation dialog box need to be opened from the file menu. There is a run button in the calculation dialog box to start the simulation. The calculated simulation data will appear in a dialog box. Moreover, the simulation data can be saved in the data monitor from where we can visualize the simulation results in the visualizer tools.

A.1.4 Results Visualization

Simulation results can be visualized in a number of ways. According to the type of input signal, visualizer can be categorized as an optical or electrical visualizer. As for example, an oscilloscope visualizer is needed to visualize the electrical signal generated by the non- return to zero (NRZ) pulse generator.

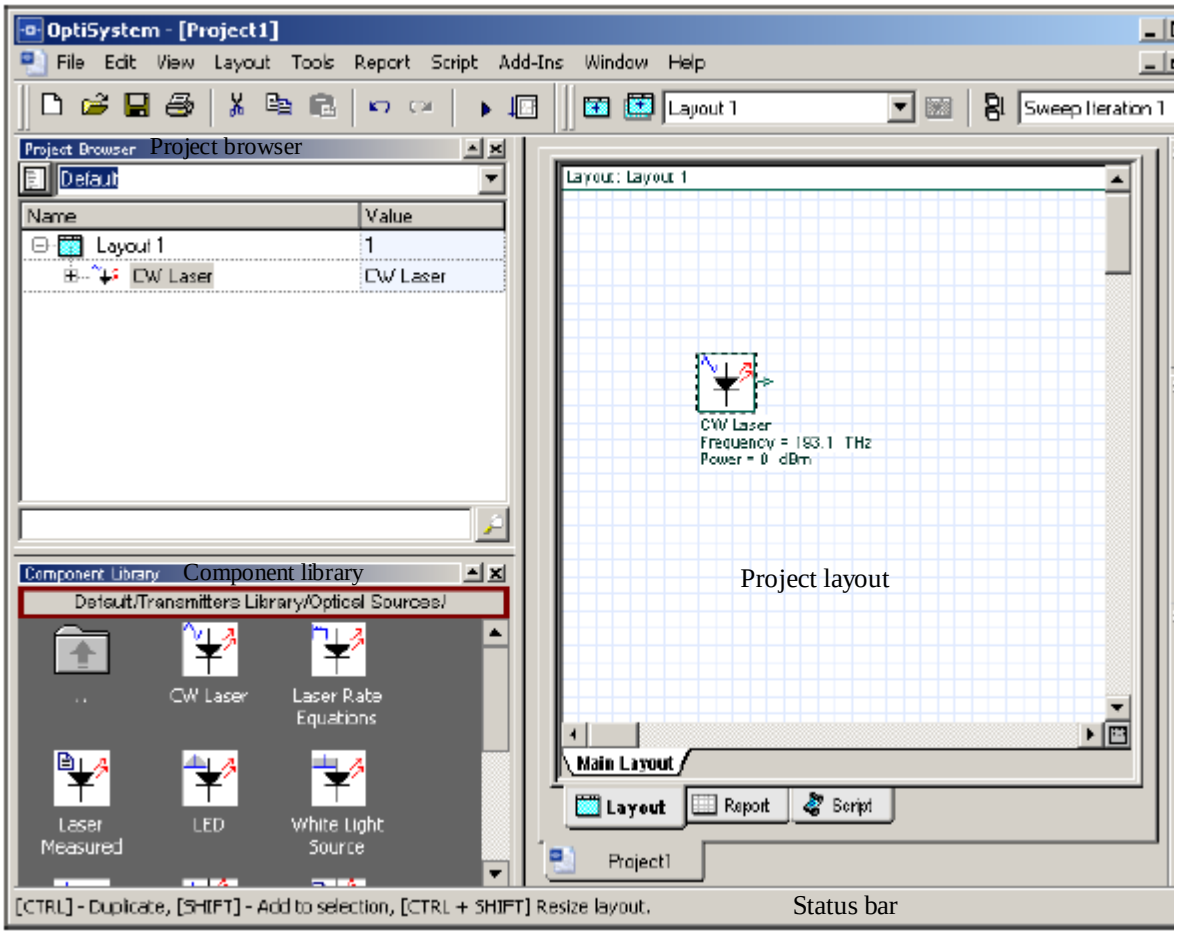

Figure A.1: Graphical user interface of OptiSystem

On the other hand, optical spectrum analyzer is needed to monitor the optical signal output. If a visualizer is connected to the components output port, OptiSystem insert a default data monitor to the same output port, where the simulation data are saved. As the simulation data are stored in the data monitor, multiple visualizers can be connected with the component output. Moreover, the simulation data can be saved in a spread sheet for the post processing of simulation data.

A.2 VPIphotonics

VPIcomponentMaker fiber optics version 9.3 is a product of VPIphotonics, which is used to design, and optimize fiber based photonic devices. By using this tool, we can design doped fiber amplifiers; Raman and parametric amplifiers; continuous wave and pulsed optical fiber sources. In addition, it can be used in optical signal processing for telecommunication, high power, and ultra-fast applications [88]. The GUI of this simulation tool is almost similar to the OptiSystem, as shown in Figure A.2 . Here, individual component is identified as module and accessed from the module library. Due to the modular nature, complex topology of EDFA and EDFL is possible, simply interconnecting the modules. Form the component modules; different components are inserted into the main working layout to design the proposed simulation configuration. In this thesis, we have modeled EDFA and EDFRL by interconnecting different modules such as pump laser, WDM coupler, doped fiber, isolator, signal analyzer, signal converter, and optical filter. The parameters of the different components can be changed by double clicking the component symbols. There is a run button in the manu bar to run the simulation. Simulation data can be monitored and recorded in the signal analyzer tool.

A.3 Comparison of OptiSystem and VPIphotonics

The complexity of building a simulation model is almost same in the both tools (i.e. model design, parameter selection, running simulation are similar in nature). Therefore, any of the simulation tools can be selected for designing EDFA and EDFRL model. However, each tool has some distinct features, which make them suitable for some specific investigations.

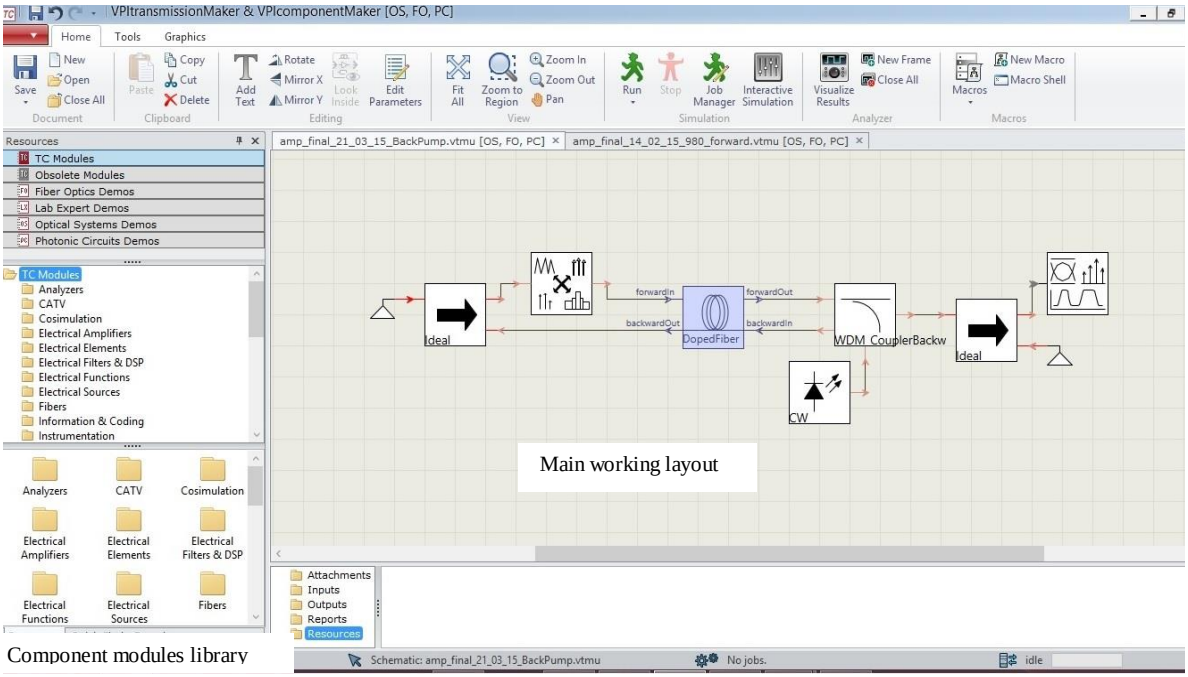

Figure A.2: Graphical user interface of VPIcomponentMaker

As for example, homogenous and inhomogeneous upconversion investigation is easier in OptiSystem because different cluster size can be considered in the EDF model. But it has no C+L band EDF. Therefore, we could not investigate the wide tuning range using OptiSystem. On the other hand, VPIphotonics simulation has C+L band EDF, which enable us to design widely tunable EDFRL. Moreover, it has a special signal analyzer tool, which allows displaying the internal and external characteristics of the model components. Due to this special displaying property, we were able to investigate the population inversion characteristics of EDF.

References

[1] K. C. Kao and G. A. Hockham, "Dielectric-fibre surface waveguides for optical frequencies," in *Proceedings of the Institution of Electrical Engineers*, 1966, pp. 1151–1158.

[2] A. Werts, "Propagation de la lumiere coherente dans les fibres optiques," *L'Onde Electr.*, vol. 46, pp. 967–980, 1966.

[3] F. P. Kapron, D. B. Keck, and R. D. Maurer, "Radiation Losses in Glass Optical Waveguides," *Appl. Phys. Lett.*, vol. 17, pp. 423–425, 1970.

[4] G. Keiser, *Optical Fiber Communications*, Fourth. McGraw-Hill Science, 2010.

[5] J. M. Senior, *Optical Fiber Communications Principles and Practice*, Third. Prentice Hall, 2008.

[6] R. J. Sanferrare, "Terrestrial Lightwave System," *Bell Labs Tech. J.*, vol. 66, no. 1, 1987.

[7] F. Idachaba, D. U. Ike, and O. Hope, "Future Trends in Fiber Optics Communication," in *Proceedings of the World Congress on Engineering*, 2014.

[8] V. S. Bagad, *Optical Fiber Communications*, First. Technical Publication Pune, 2009.

[9] O. Takaaki, "Recent Status and Trends in Optical Submarine Cable Systems," *NEC Tech. J.*, vol. 5, no. 1, pp. 4–7, 2010.

[10] H. Suzuki, M. Fujiwara, N. Takachio, K. Iwatsuki, T. Kitoh, and T. Shibata, "12.5-GHz spaced 1.28-Tb/s (512-channel2.5 Gb/s) super-dense WDM transmission over 320-km SMF using multiwavelength generation technique.," *IEEE Photonics Technol. Lett.*, vol. 14, pp. 405–407, 2002.

[11] Y. Sun, J. W. Sulhoff, A. K. Srivastava, S. L. Zyskind, T. A. Strasser, J. R. Pedrazzani, C. Wolf, J. Zhou, S. B. Judkins, R. P. Espindola, and A. M. Vengsarkar, "80 nm ultra-wideband erbium-doped silica fibre amplifier," *Electron. Lett.*, vol. 33, no. 23, pp. 1965–1967, 1997.

[12] H. B. Choi, J. M. Oh, D. Lee, S. J. Ahn, B. S. Park, and S. B. Lee, "Simple and efficient L-band erbium-doped fiber amplifiers for WDM networks," *Opt. Commun.*, vol. 213, no. 1–3, pp. 63–66, 2002.

[13] S. Yamashita and M. Nishihara, "L-Band Erbium-Doped Fiber Amplifier Incorporating an Inline Fiber Grating Laser," *IEEE J. Sel. Top. Quantum Electron.*, vol. 7, no. 1, pp. 44–48, 2001.

[14] X. Dong, P. Shum, N. Q. Ngo, H. Tam, and X. Dong, "Output Power Characteristics of Tunable Erbium-doped Fiber Ring Lasers," *J. Light. Technol.*, vol. 23, no. 3, pp. 1334–1341, 2005.

[15] K. K. Qureshi, "Fiber Ring Lasers and All-Optical Signal Processing Devices For Wavelength-Division Multiplexing Systems," Hong Kong Polytechnic University, 2006.

[16] S. Yamashita and M. Nishihara, "Widely Tunable Erbium-Doped Fiber Ring Laser Covering Both C-Band and L-Band," *IEEE J. Sel. Top. Quantum Electron.*, vol. 7, no. 1, pp. 41–43, 2001.

[17] H. Tabuchi and H. Ishikawa, "External Grating Tunable MQW Laser with Wide Tuning Range 240 nm," *Electron. Lett.*, vol. 26, no. 11, pp. 742–743, 1990.

[18] Y. Nakazaki and S. Yamashita, "Fast and wide tuning range wavelength-swept fiber laser based on dispersion tuning and its application to dynamic FBG sensing," *Opt. Express*, vol. 17, no. 10, pp. 8310–8318, 2009.

[19] H. Y. Ryu, W. K. Lee, H. S. Moon, and H. S. Suh, "Tunable erbium-doped fiber ring laser for applications of infrared absorption spectroscopy," *Opt. Commun.*, vol. 275, pp. 379–384, 2007.

[20] F. W. Sheu, C. Y. Chiou, and S. C. Yang, "Performance of a wavelength-tunable erbium-doped fiber laser using a Sagnac interferometer," *Opt. Commun.*, vol. 281, pp. 4719–7422, 2008.

[21] K. J. Zhang, "Compound Ring Erbium-Doped Fiber Lasers," University of Waterloo, 1994.

[22] P. Urquhart, "Review of rare earth doped fibre lasers and amplifiers," in *IEE Proceedings*, 1988, pp. 385–407.

[23] D. C. Hanna, M. J. McCarthy, and P. J. Suni, "Thermal considerations in longitudinally pumped fiber and miniature bulk lasers," in *Proc. SPIE 1171, Fiber Laser Sources and Amplifiers*, 1990.

[24] R. J. Mears and S. R. Baker, "Erbium fibre amplifiers and lasers," *Opt. Quantum Electron.*, vol. 24, no. 5, pp. 517–538, 1992.

[25] X. Dong, H. Y. Tam, B. O. Guan, C. Zhao, and X. Dong, “High power erbium-doped fiber ring laser with widely tunable range over 100 nm,” *Opt. Commun.*, vol. 224, pp. 295–299, 2003.

[26] D. Xinyong, N. Q. Ngo, S. Ping, H. Y. Tam, and X. Dong, “Linear cavity erbium-doped fiber laser with over 100 nm tuning range.,” *Opt. Express*, vol. 14, no. 11, pp. 1689–94, 2003.

[27] E. Snitzer, “Optical Maser Action of Nd+3 in a Barium Crown Glass,” *Phys. Rev. Lett.*, vol. 7, no. 12, pp. 444–446, 1961.

[28] E. Snitzer, “Proposed fiber cavities for optical masers,” *J. Appl. Phys.*, vol. 32, no. 01, pp. 36–39, 1961.

[29] C. J. Koester and E. Snitzer, “Amplification in a fiber laser,” *Appl. Opt.*, vol. 3, no. 10, pp. 1182–1186, 1964.

[30] J. Stone and C. A. Burrus, “Neodymium-Doped Fiber Lasers: Room Temperature cw Operation with an Injection Laser Pump,” *Appl. Opt.*, vol. 13, no. 6, pp. 1256–1258, 1974.

[31] T. M. Valerii, *Fundamentals of Fiber Lasers and Amplifiers*. Springer International Publishing, 2014.

[32] M. Shimizu, H. Suda, and M. Horiguchi, “High efficiency Nd doped fiber lasers using direct coated dielectric mirrors,” *Electron. Lett.*, vol. 23, no. 768–769, pp. 768–769, 1987.

[33] W. J. Barnes, S. B. Poole, J. E. Townsend, L. Reekie, D. J. Taylor, and D. N. Payne, “Er3+-Yb3+ and Er3+ doped fiber laser,” *J. Light. Technol.*, vol. 7, pp. 1461–1465, 1989.

[34] R. J. Mears, L. Reekie, S. B. Poole, and D. N. Payne, “Neodymium-doped silica single-mode fibre lasers,” *Electron. Lett.*, vol. 21, no. 17, pp. 738–740, 1985.

[35] R. J. Mears, L. Reeki, S. B. Poole, and D. N. Payne, “Low-threshold tunable CW and Q-switched fibre laser operating at 1.55 μm,” *Electron. Lett.*, vol. 22, no. 3, pp. 159–160, 1986.

[36] F. R. Karl, *Basics of Laser Physics: For Students of Science and Engineering*. Springer-Verlag Berlin Heidelberg, 2012.

[37] R. S. Quimby, *Photonics and lasers*. John Wiley & Sons, 2006.

[38] J. Hecht, “Fiber lasers: The state of the art,” 2012.

[39] K. Thyagaraji and A. Ghatak, *Lasers Fundamentals and Applications*, Second. Springer, 2010.

[40] T. Rosadiuk, "Tunable Erbium Fiber Lasers," University of Alberta, 1994.

[41] M. J. F. Digonnet, *Rare-Earth-Doped Fiber Lasers and Amplifiers*, Second. CRC Press, 2001.

[42] V. Hughes, "Experimental Study of Modelocked Fiber Lasers," University of Alberta, 2005.

[43] M. Csele, *Fundamental of Light Sources and Lasers*. New Jersey: John Wiley & Sons, 2004.

[44] P. C. Becker, N. A. Olsson, and J. R. Simpson, *Erbium-Doped Fiber Amplifiers Fundamental and Technology*, First. Academic Press, 1999.

[45] A. W. Synder and L. J, *Optical Waveguide Theory*, First. Springer US, 1984.

[46] A. Hassani, E. Arzi, and F. E. Seraji, "Intensity based erbium distribution for erbium doped fiber amplifiers," *Opt. Quantum Electron.*, vol. 39, no. 1, pp. 35–50, Mar. 2007.

[47] E. Delevaque, T. Georges, M. Monerie, P. Lamouler, and J. F. Bayon, "Modeling of pair-induced quenching in erbium-doped silicate fibers," *IEEE Photonics Technol. Lett.*, vol. 5, no. 1, pp. 73–75, 1993.

[48] J. B. Blixt, P. Nilsson, J. Carlnäs, "Concentration-Dependent Upconversion in Er3+- Doped Fiber Amplifiers: Experiments and Modeling," in *IEEE Transactions Photonics Technology letters*, 1991, vol. 3, no. 11, pp. 996–998.

[49] A. V Kir, Y. O. Barmenkov, G. E. Sandoval-romero, and L. Escalante-zarate, "Er 3 + Concentration Effects in Commercial Erbium-Doped Silica Fibers Fabricated Through the MCVD and DND Technologies," *IEEE J. Quantum Electron.*, vol. 49, no. 6, pp. 511–521, 2013.

[50] J. A. Vallés, V. Berdejo, M. Á. Rebolledo, A. Díez, J. A. Sánchez-martín, and M. V Andrés, "Dynamic Characterization of Upconversion in Highly Er-Doped Silica Photonic Crystal Fibers," *IEEE J. Quantum Electron.*, vol. 48, no. 8, pp. 1015–1022, 2012.

[51] P. Myslinski, D. Nguyen, and J. Chrostowski, "Effects of concentration on the performance of erbium-doped fiber amplifiers," *J. Light. Technol.*, vol. 15, no. 1, pp. 112–120, 1997.

[52] S. Berkdemir, Cüneyt Ozsoy, "The Effects of Complex Energy Transfer Dynamics and Gaussian Profiles on the Performance of High-Concentrations EDFAS," *J. Light. Technol.*, vol. 27, no. 21, pp. 4642–4649, 2009.

[53] N. I. Razaki, U. S. Jais, A. Chiasera, M. Ferrari, and M. K. Abd-rahman, "Preparation and Characterization of SiO2 - ZrO2 : Er 3 + / Yb 3 + Planar Waveguides for Optical Amplifier," in *International Conference on Photonics*, 2010, pp. 4–7.

[54] D. Boivin, T. Föhn, E. Burov, A. Pastouret, C. Gonnet, O. Cavani, C. Collet, and S. Lempereur, "Quenching investigation on new erbium doped fibers using MCVD nanoparticle doping process," in *Proc. of SPIE*, 2010, vol. 7580, no. 0, p. 75802B–75802B–9.

[55] J. Myslinski, P. Fraser, J. Chrostowski, "Nanosecond Kinetics of upconversion process in EDF and its effect on EDFA performance," *proc. Opt. Amplifiers Their Appl*, vol. ThE3–1, pp. 100–103, 1995.

[56] C. R. Giles and E. Desurvire, "Modeling Erbium-Doped Fiber Amplifiers," *J. Light. Technol.*, vol. 9, no. 2, 1991.

[57] P. Myslinski, C. Barnard, G. Cheney, J. Chrostowski, B. Syrett, and J. Glinski, "Nanosecond all-optical gain switching of an erbium-doped fibre amplifier," *Opt. Commun.*, vol. 97, no. 5–6, pp. 340–346, Apr. 1993.

[58] R. I. Laming and D. N. Payne, "Progress in the optimisation of erbium doped fiber amplifiers (EDFAs)," in *Optical Fiber Communication Conference*, 1991, pp. 177–178.

[59] M. N. Zervas, R. I. Laming, and D. N. Payne, "Trade-off and design considerations of the erbium-doped fiber amplifier," in *Optical amplifiers for communications*, 1999.

[60] J. R. Armitage, "Three-level fiber laser amplifier: a theoretical model," *Appl. Opt.*, vol. 27, no. 23, pp. 4831–4836, 1988.

[61] B. J. Ainslie, J. R. Armitage, S. P. Craig, and B. Wakefield, "Fabrication and Optimization of The Erbium Distribution in Silica Based Doped Fibers," in *ECOC'88*, 1989, pp. 62–65.

[62] M. Ohashi, "Design Considerations for an Er3+ -Doped Fiber Amplifier," *J. Light. Technol.*, vol. 9, no. 9, pp. 1099–1104, 1991.

[63] Y. Kimura, M. Nakazawa, and K. Suzuki, "Ultra-efficient erbium-doped fiber amplifier," *Appl. Phys. Lett.*, vol. 57, no. 25, pp. 2635–2537, 1990.

[64] S. P. Craig-Ryan, J. F. Massicott, M. Wilson, B. J. Ainslie, and R. Waytt, "Optical study of low concentration Er3+ fibres for efficient power amplifiers," in *16th ECOC, Amsterdam*, 1990, pp. 571–574.

[65] R. I. Laming, J. E. Townsend, D. N. Payne, F. Meli, G. Grasso, and E. J. Tarbox, "High-Power Erbium-Doped Amplifiers Operating in the Saturated Regime," *IEEE Photonics Technol. Lett.*, vol. 3, no. 3, pp. 253–255, 1991.

[66] M. Shimizu, M. Yamada, M. Horiguchi, and E. Sugita, "Concentration Effect on Optical Amplification of Er-Doped Silca Single Mode Fibers," *IEEE Photonics Technol. Lett.*, vol. 2, no. 1, pp. 43–45, 1990.

[67] P. F. Wysocki, J. l. Wagener, M. J. F. Digonnet, and H. J. Shaw, "Evidence and modeling of paired ions and other loss mechanisms in erbium-doped silica fibers," *Fiber Laser Sources amplifiers IV*, vol. SPIE-1789, pp. 66–79, 1992.

[68] J. Nilsson, B. Jaskorzynska, and P. Blixt, "Implications of pair-induced quenching for erbium-doped fiber amplifiers," *Opt. Amplifiers Their Appl. Tech. Dig*, vol. MD19–1, pp. 222–225, 1993.

[69] H. Masuda, A. Takada, and K. Aida, "Modeling the Gain Degradation of High Concentration Erbium-Doped Fiber Amplifiers by Introducing Inhomogenous Cooperative Up-Conversion," *J. Light. Technol.*, vol. 10, no. 12, pp. 1789–1799, 1992.

[70] O. Lumholt, T. Rasmussen, and A. Bjarklev, "Modelling of Extremely High Concentration Erbium-Doped Silica Waveguides," *Electron. Lett.*, vol. 29, no. 5, pp. 1992–1993, 1993.

[71] J. Nilsson, B. Jaskorzynska, and P. Blixt, "Performance reduction and design modification of erbium-doped fiber amplifiers resulting from pair-induced quenching," *IEEE Photonics Technol. Lett.*, vol. 5, no. 12, pp. 1427–1429, Dec. 1993.

[72] R. S. Quimby, W. J. Miniscalco, and B. Thompson, "Clustering in erbium-doped silica glass fibers analyzed using 980 nm excited-state absorption," *J. Appl. Phys.*, vol. 76, no. 8, p. 4472, 1994.

[73] M. Shimizu, M. Yamada, M. Horiguchi, T. Takeshita, and M. Okayasu, "Erbium-Doped Fiber Amplifiers with an Extremly High Gain Coefficient of 11.0 dBl/ mW," *Electron. Lett.*, vol. 26, no. 20, pp. 1641–1643, 1990.

[74] B. Pedersen, M. L. Dakss, B. A. Thompson, W. J. Miniscalco, T. Wei, and L. J. Andrews, "Experimental and Theoretical Analysis of Efficient Erbium-Doped Fiber Power Amplifiers," *IEEE Photonics Technol. Lett.*, vol. 3, no. 12, pp. 1085–1087, 1991.

[75] L. Reekie, R. J. Mears, S. B. Poole, and D. N. Payne, “Tuneable Single-Mode Fiber Lasers,” *J. Light. Technol.*, vol. 4, no. 7, pp. 956–960, 1986.

[76] R. J. Mears, L. Reekie, S. B. Poole, and D. N. Payne, “Low-Threshold Tunable CW and Q-Switched Fiber Laser Operating at 1-55 μm,” *Electron. Lett.*, vol. 22, no. 3, pp. 159–160, 1986.

[77] L. Reekie, I. M. Jauncey, S. B. Poole, and D. N. Payne, “Diode laser pumping operation of an Er3+ doped singlemode fibre laser,” *Electron. Lett.*, vol. 23, pp. 1076–1078, 1987.

[78] P. L. Scrivener, E. J. Tarbox, and P. D. Maton, “Narrow Linewidth Tuneable Operation of Er3+ Doped Single-Mode Fiber Laser,” *Electron. Lett.*, vol. 25, no. 8, pp. 549–550, 1989.

[79] C. Y. Chen, M. M. Choy, M. j. Andrejco, M. A. Saifi, and C. Lin, “A Widely Tunable Erbium Doped Fiber Laser Pumped at 532 nm,” *IEEE Photonics Technol. Lett.*, vol. 02, no. 01, pp. 18–20, 1990.

[80] J. L. Zyskind, J. W. Sulhoff, J. Stone, D. J. Digiovanni, L. W. Stulz, H. M. Presby, A. Piccirilli, and P. E. Pramayon, “Electrically Tunable, Diode-Pumped Erbium-Doped Fiber Ring Laser with Fiber Fabry-Parot Etalon,” *Electron. Lett.*, vol. 27, no. 21, pp. 1950–1951, 1991.

[81] P. D. Humphrey and J. E. Bowers, “Fiber-Birefringence Tuning Technique for an Erbium-Doped Fiber Ring Laser,” *IEEE Photonics Technol. Lett.*, vol. 5, no. 1, pp. 32–34, 1993.

[82] Y. T. Chieng and R. A. Minasian, “Tunable Erbium-Doped Fiber Laser with a Reflection Mach-Zender Interferometer,” *IEEE Photonics Technol. Lett.*, vol. 6, no. 2, pp. 153–156, 1994.

[83] A. Bellemare, M. Karásek, C. Riviere, F. Babin, G. He, V. Roy, and G. Schinn W., “A Broadly Tunable Erbium-Doped Fiber Ring Laser: Experimentation and Modeling,” *IEEE J. Sel. Top. Quantum Electron.*, vol. 7, no. 1, pp. 22–29, 2001.

[84] X. Dong, H.-Y. Tam, B.-O. Guan, C. Zhao, and X. Dong, “High power erbium-doped fiber ring laser with widely tunable range over 100 nm,” *Opt. Commun.*, vol. 224, pp. 295–299, 2003.

[85] X. Dong, P. Shum, N. Ngo, C. Chan, B.-O. Guan, and H.-Y. Tam, “Effects of active fiber length on the tunability of erbium-doped fiber ring lasers,” *Opt. Express*, vol. 11, no. 26, p. 3622, Dec. 2003.

[86] X. Dong, N. Q. Ngo, P. Shum, B.-O. Guan, H.-Y. Tam, and X. Dong, "Concentration-induced nonuniform power in tunable erbium-doped fiber lasers," *Opt. Lett.*, vol. 29, no. 4, p. 358, 2004.

[87] "OptiSystem Tutorials - Volume 1," 2014.

[88] "User's Manual on VPIcomponentMaker Fiber Optics," 2014.

]

Vitae

Name : Md. Ziaul Amin

Nationality : Bangladeshi

Date of Birth : 1/1/1984

Email : ziaulece@gmail.com

Address : Village: Banishwar, Post Office: Jalsin, Police Station: Dhamrai, District: Dhaka, Bangladesh

Academic Background :

Md. Ziaul Amin attended Khulna University, Khulna, Bangladesh from where he obtained B. Sc engineering degree in Electronics and Communication in 2007. After graduation, he joined in a local telecom company, Rankstel Bangladesh Ltd, as a system Engineer. Then, He joined at Electronics and Communication Engineering Discipline, Khulna University, Bangladesh as a faculty member in September 2008. After that, he completed his M.Sc degree from King Fahd University of Petroleum and Minerals, Saudi Arabia in September 2015